Characterization of cardiac progenitor cell activity in engineered heart muscle

Doctoral Thesis

In partial fulfillment of the requirements for the degree

“Doctor rerum naturalium (Dr. rer. nat.)”

in the Molecular Medicine Study Program

at the Georg-August University Göttingen

Submitted by

Elif Levent

born in Karabük, Turkey

Göttingen 2016

Members of the Thesis Committee:

Prof. Dr. med. Wolfram-Hubertus Zimmermann (Supervisor)

Email: w.zimmermann@med.uni-goettingen.de

Phone: +49 (0) 551 39 5781

Postal Address: Institute of Pharmacology and Toxicology
University Medical Center Göttingen
Georg-August University Göttingen
Robert-Koch-Str. 40
37075 Göttingen
Germany

Prof. Dr. Dörthe Katschinski (Second member of thesis committee)

Email: doerthe.katschinski@med.uni-goettingen.de

Phone: +49 (0) 551 39 5896

Postal Address: Institute of Cardiovascular Physiology
Humboldtallee 23
37073 Göttingen
Germany

Prof. Dr. Viacheslav O. Nikolaev (Third member of thesis committee)

Email: v.nikolaev@uke.de

Phone: +49 (0) 40 7410 51391

Postal Address: Institute of Experimental Cardiovascular Research
University Medical Center Hamburg-Eppendorf (UKE)
Martinistr. 52
20246 Hamburg

Date of disputation: 13.06.16

AFFIDAVIT

Here I declare that my doctoral thesis entitled:

"**Characterization of cardiac progenitor cell activity in engineered heart muscle**"

has been written independently with no other sources and aids than quoted.

Elif Levent

Göttingen, April 2016

List of poster presentations

- Elif Levent, Malte Tiburcy, Amke Hesse, Dörthe Katschinski, Mark Sussman and Wolfram-H Zimmermann (2013). Hypoxia/Reoxygenated engineered heart muscle as an injury model system to investigate cardiac progenitor cell function in heart repair *in vitro*. Cardiorepair European multidisciplinary initiative (CARE-MI) annual meeting Lisbon, Portugal.

- Elif Levent, Malte Tiburcy, Mark Sussman and Wolfram-H Zimmermann (2013). Engineered heart muscle as a model system to investigate cardiac progenitor cell function and heart regeneration *in vitro*. Deutsche Gesellschaft für Kardiologie (DGK) annual meeting, Mannheim, Germany.

- Elif Levent, Malte Tiburcy, Alberto Izarra, Antonio Bernad and Wolfram-H Zimmermann (2012). Engineered heart tissue to investigate cardiac progenitor cell function and heart regeneration *in vitro*. Cardiorepair European multidisciplinary initiative (CARE-MI) annual meeting, Leuven, Belgium.

List of publications

- Vogler M, Zieseniss A, Hesse AR, **Levent E**, Tiburcy M, Heinze E, Burzlaff N, Schley G, Eckardt KU, Willam C, Katschinski DM. (2015). Pre- and post-conditional inhibition of prolyl-4-hydroxylase domain enzymes protects the heart from an ischemic insult. Pflugers Arch. 467:2141-9.

- Izarra A, Moscoso I, **Levent E**, Cañón S, Cerrada I, Díez-Juan A, Blanca V, Núñez-Gil IJ, Valiente I, Ruíz-Sauri A, Sepúlveda P, Tiburcy M, Zimmermann WH, Bernad A. (2014). mir-133a enhances the protective capacity of cardiac progenitors cells after myocardial infarction. Stem Cell Reports. 3:1029-42.

- Hesse AR*, **Levent E***, Zieseniss A, Tiburcy M, Zimmermann WH, Katschinski DM. (2014). Lights on for HIF-1α: genetically enhanced mouse cardiomyocytes for heart tissue imaging. Cell Physiol Biochem. 34:455-62. (*equal contribution)

Table of Contents

Acknowledgements

I would like to present my gratitude firstly to my supervisor Prof. Wolfram-Hubertus Zimmermann for giving me the opportunity to work on this project and the valuable advices which he has given during the data discussions throughout my PhD.

I would like to furthermore thank my thesis committee members Prof. Dr. Dörthe Katschinski and Prof. Dr. Viacheslav Nikolaev for their persistent support and guidance during my study.

I am especially grateful to Dr. Malte Tiburcy for the continuous and firsthand support and advice he has given me throughout my project. I would like to also thank him for giving me the freedom to develop my own ideas and continuously being open to my questions. I will also not forget our warm and friendly group meetings in the Christmas market. Moreover, I would like to thank Andreas Schraut for generating cardiomyocyte specific antibiotically selectable ODD-Luc expressing mESC cell line, Dr. Claudia Noack for establishing the ODD-Luc construct, Mrs. Krasimira Sharkova for her help in the generation of the ODD-Luc expressing hES2 cell line as well as her sincere friendship and Dr. Sebastian Zeidler for his patience and support with the analysis of RNAseq data. Also, I thank to Daria Reher for constantly providing very valuable cardiomyocytes.

I have spent this long period together with my very nice and valuable friends that I feel really lucky to have met them. Foremost, I would like to express my sincere gratitude for having my close friend, Eriona Heta nearby. She shared all my moods and kept me alive with her support. I especially thank her for having the door of her home always open to me, no matter what time it is. I felt warmer and relieved with the support of her presence. Furthermore, I thank to my lab mates; Satish Galla, Farah Raad, Sumon Sur, Elena Pavlova and Dr. Poh Loong Soong for their sincere friendships. I enjoyed the lab and the office a lot more together with them. Having many years past together, I am very thankful for their presence and giving the spiritual support.

I think it was magic to have spent four years of my PhD with my old friend, Mine Bakar. Her presence was very important and a big support for me throughout the

duration of my PhD. I became free from all the concerns and enjoyed my time here a lot more together with her.

Lastly, I would like to express my special gratitude to my family. My parents and my brother were all the time nearby me. I would like to thank them a lot for supporting me to come here and their constant belief in me throughout all these years.

Summary

The heart has been considered a post-mitotic organ incapable of regeneration upon injury. Recent findings suggest that the heart contains cardiac progenitor cells (CPCs) with the potential to give rise to cardiovascular cells. CPCs are currently under clinical investigation aiming at cell-based induction of heart regeneration in patients with myocardial infarction related injury. The mechanisms of action underlying the reported beneficial effects of CPCs remain for the most part elusive. This study was designed to enhance our knowledge on CPC biological activity. By making use of engineered heart muscle (EHM) constructed from cardiomyocytes, fibroblasts and CPCs in a collagen type 1 hydrogel the aim was to simulate a three-dimensional heart muscle environment as closely as possible. Different types of mouse and human CPCs were investigated and found to be mesenchymal cells distinct from fibroblasts. Transcriptome profiling suggested a pericyte phenotype within the human CPC population. Despite the apparent differences in cell phenotype, CPCs and fibroblast supported the assembly of cardiomyocytes into macroscopically contracting EHM. Evidence for CPC transdifferentiation in EHM could not be obtained. Novel EHM models of hypoxia/reoxygenation and chronic hypoxia damage were developed and used to study potential cardio-protective effects of CPCs. Surprisingly, these experiments revealed that hypoxia/reoxygenation damage could be attenuated by fibroblasts, but not by CPCs. This effect appeared to be mediated by the release of cell protective growth factors and cytokines from fibroblasts. Conversely, transcriptome profiling suggested angiogeneic and immune modulatory activity in CPCs, which may not be effective in a vascular and leukocyte-free EHM. The cell context specific biological activity of CPCs was further exemplified by studies in EHM tri-cultures composed of cardiomyocytes, fibroblasts and CPCs. Only tricultures with CPCs were protected from chonic hypoxia. Finally, to in the future be able to visualize the oxygenation level in cardiomyocytes, a transgenic hypoxia reporter was established. In summary, CPCs exhibited a distinct phenotype from fibroblasts. It appeared that CPCs require a specific mutlicellular context to exhibit protective effects upon hypoxia. EHM-hypoxia injury tools and a transgenic hypoxia reporter were developed to facilitate future organoid studies on cardio-protection.

List of Figures

List of Tables

Abbreviations

ACE	Angiotensin converting enzyme
APS	Ammonium persulfate
ACTA2	Actin, alpha 2, smooth muscle
ALCADIA	Autologous human cardiac-derived stem cell to treat ischemic cardiomyopathy
ARHGAP26	Rho GTPase Activating Protein 26
ARHGEF2	Rho/Rac Guanine Nucleotide Exchange Factor (GEF) 2
BrdU	Bromodeoxyuridine
BM	Bone marrow
BM-MSC	Bone marrow-derived mesenchymal stem cell
BM-MNC	Bone marrow-derived mononuclear cells
BSA	Bovine serum albumin
CPC	Cardiac progenitor cell
CADUCEUS	Cardiosphere-derived autologous stem cells to reverse ventricular dysfunction
CDC	Cardiosphere-derived cell
CM	Cardiomyocytes
C	Carbon
cDNA	Complementary DNA
CDH5	Cadherin 5, type 2 (Vascular endothelium)
CHIR	Glycogen synthase kinase 3β inhibitor
CMR	Custom made replacement
Cacl2	Calcium chloride
cTnT	Cardiac troponin T

DNA	Dioxyribonucleic acid
DEG	Differentially expressed gene
DDR2	Discoidin domain-containing receptor 2
DMSO	Dimethyl sulfoxide
EHM	Engineered heart muscle
ECM	Extracellular matrix
EB	Embryoid body
EDTA	Ethylenediaminetetraacetic acid
FA	Formaldehyde
FGF-2	Basic fibroblast growth factor
FOC	Force of contraction
GATA4	GATA binding protein 4
GFP	Green fluorescent protein
HGF	Hepatocyte growth factor
HIF-1α	Hypoxia Inducible Factor 1, Alpha Subunit (Basic Helix-Loop-Helix Transcription Factor)
hCM	Human cardiomyocyte
H/R	Hypoxia/Reoxygenation
HEK	Human embryonic kidney
hCPC	Human cardiac progenitor cell
hEHM	Human engineered heart muscle
IGF-1	Insulin-like growth factor-1
IWP4	Wnt/β-catenin pathway antagonist

IFN-γ	Interferon-gamma
ITS-X	Insulin-Transferrin-Selenium-Ethanolamine
Ki67	Marker of proliferation Ki-67
KIT (CD117 or c-kit)	V-Kit Hardy-Zuckerman 4 Feline Sarcoma Viral Oncogene Homolog
KDR	Kinase insert domain receptor
KSR	Knockout serum replacement
KO	Knockout
KCl	Potassium chloride
LVAD	Left ventricular assist device
LV	Left ventricular
Luc	Firefly luciferase
LDH	Lactate dehydrogenase
LIF	Leukemia inhibitory factor
MADM	Mosaic analysis with double markers
MEF2	Myocyte enhancer factor 2
MDR1	Multi drug resistance protein 1
MSC	Mesenchymal stem cell
MAPK	Mitogen activated protein kinase
mCPC	Mouse cardiac progenitor cell
MEF	Mouse embryonic fibroblast
MHC	Myosin heavy chain
mCM	Mouse cardiomyocyte

MYH11	Myosin heavy chain 11, smooth muscle
mCF	Mouse cardiac fibroblast
MAPK	Mitogen activated protein kinase
MgCl2	Magnesium chloride
Nkx2.5	NK2 transcription factor related, locus 5
NM	Non-myocyte
NRCM	Neonatal rat cardiomyocyte
NADH	Nicotinamide adenine dinucleotide
NES	Nestin
NEAA	Non-essential amino acid
NaHCO3	Sodium bicarbonate
NaH2PO4	Sodium phosphate monobasic
ODD	Oxygen dependent degradation domain of HIF-1α
PDGFRA	Platelet-derived growth factor receptor, alpha polypeptide
PECAM1	Platelet enodethelial cell adhesion molecule-1
PHD2	Prolyl-hydroxylase domain-containing protein 2
PFA	Paraformaldehyde
POSTN	Periostin, Osteoblast specific factor
PDGFRB	Platelet-derived growth factor receptor, beta polypeptide
PHD2	Prolyl-hydroxylase domain-containing protein 2
PBS	Phosphate buffered saline
PDGFA	Platelet-derived growth factor, alpha polypeptide

PDGF	Platelet-derived growth factor
RFP	Red fluorescent protein
RoT	Room temperature
ReT	Resting tension
RNA	Ribonucleic acid
Rho	Ras homology
RAC2	Rho Family, Small GTP Binding Protein
Sca-1	Stem cells antigen -1
SMA	Smooth muscle actin
SF	Serum free
SDS	Sodium dodecyl sulfate
TLN1	Talin 1
TGF-B1	Transforming growth factor-beta 1
tdRFP	Tandem dimer red fluorescent protein
T3	Triiodothyronine
TAGLN	Transgelin
TCF21	Transcription factor 21
TEMED	Tetramethylethylenediamine
vWF	Von Willebrand factor
VEGFA	Vascular endothelial growth factor a
WIPF1	WAS/WASL interacting protein family, member 1
WT1	Wilms tumor 1

1 Introduction

Myocardial infarction causes the loss of approximately 1 billion cardiomyocytes, which are not regenerated, but replaced by non-contractile scar tissue (Gerbin and Murry 2015). The associated loss of function is typically at first compensated by a hypertrophic response, which finally results in additional cardiomyocyte death and whole organ failure (Mill et al. 2011, Zangi et al. 2013). Therapeutic strategies to reduce cardiomyocyte death, regenerate the infarcted myocardium and prevent progression to heart failure are clearly needed in light of the high mortality in affected patients (Yancy et al. 2013).

1.1 Evidence for cardiomyocyte renewal in the postnatal heart

The embryonic heart grows through proliferation of cardiomyocytes. Fetal cardiomyocytes in the human heart start to withdraw from the cell cycle. Shortly after birth, most of the cardiomyocytes are considered post-mitotic; subsequent cardiomyocyte growth is by hypertrophy (Laflamme and Murry 2011). Over the recent years, a number of studies suggested *de novo* cardiomyogenesis challenging the view that the heart is a static organ (Raphael Rubin 2008). Elegant carbon dating studies in human hearts identified very low DNA-replication (lifetime average of <1%/year), arguing against significant self-renewal of the heart (Bergmann et al. 2009, Bergmann et al. 2015). Cardiomyocytes shortly after birth showed the highest cell cycle activity, which then decreases with age (Bergmann et al. 2015, Senyo et al. 2013).

1.2 Origin of new cardiomyocytes in the postnatal heart

Identification of cycling cardiomyocytes or progenitors with cardiomyogenic potential in the adult heart would open the door for targeted stimulation of these cells. In lower vertebrates, such as zebrafish and neonatal mice (1-day old), the heart is capable of fully regenerating, which is mediated by the proliferation of pre-existing cardiomyocytes (Porrello et al. 2011). Given the fact that the regenerative response declines in the adult mammalian heart (**Figure 1**) (Laflamme and Murry 2011), reactivation of proliferation in endogenous cardiomyocytes appears attractive to

achieve myocardial remuscularization (Bersell et al. 2009, Engel et al. 2006, Hassink et al. 2008, Kuhn et al. 2007).

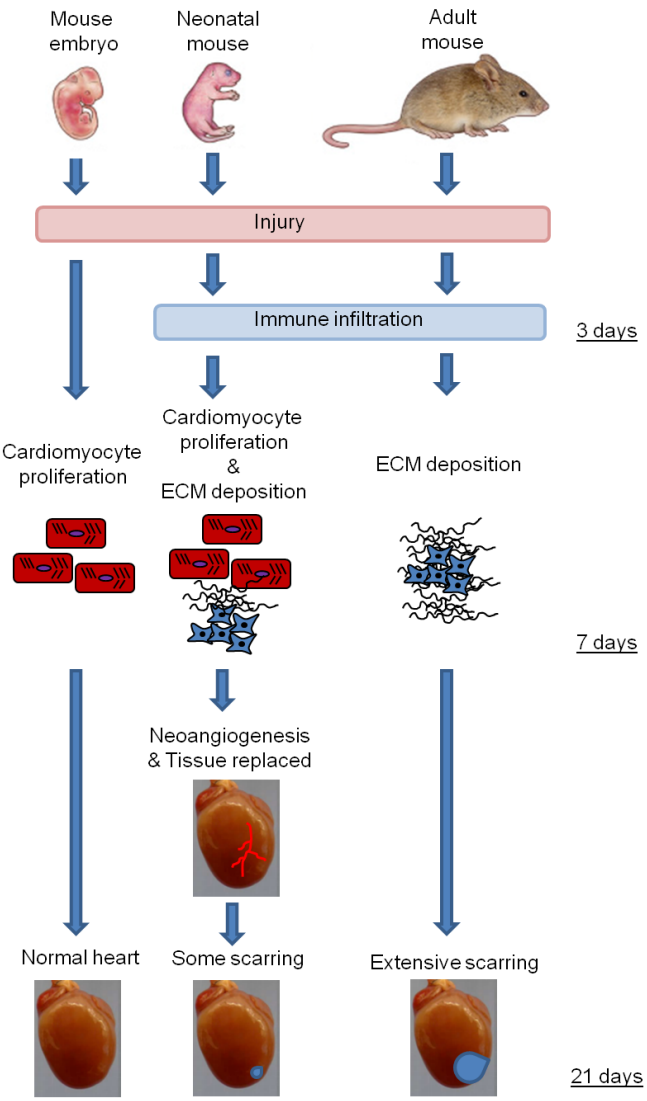

Figure 1. Heart regenerative response in mammalian heart. Embryonic stage: cardiomyocytes undergo cell-cycle entry and repopulate the heart. Neonatal stage: cardiomyocyte proliferation and angiogenesis as the two main mechanisms involved in complete regeneration of neonatal mouse heart following injury. Adult stage: insufficient cardiomyocyte proliferation and extracellular matrix deposition after injury. Schematic adapted from Uygur et al. (2016).

Genetic fate mapping strategies based on the expression of fluorescence reporter genes in specific cell types are powerful tools to track the origin of new cardiomyocytes formed during physiological and pathological conditions (Hsieh et al. 2007). Differential labeling of endogenous cardiomyocytes at a given time point indicated no change in the percentage of pre-existing cardiomyocytes during physiological aging, suggesting that non-cardiomyocytes do not contribute to heart development under normal conditions (Hsieh et al. 2007). Evidence for DNA-replication and cell cycle activity in resident adult cardiomyocytes (genetically labeled) (Malliaras et al. 2013, Senyo et al. 2013) and unambiguously labeling of dividing cardiomyocytes with alternative fate-mapping approaches, such as *mosaic analysis with double markers* (MADM) (Ali et al. 2014), supported the hypothesis that endogenous cardiomyocytes are the main source of cardiomyocyte turnover under physiological conditions, albeit in a very low amount (0.1% of total cardiomyocytes) (Ali et al. 2014, Malliaras et al. 2013, Senyo et al. 2013). Collectively, there is

compelling evidence for postnatal cardiomyogenesis via proliferation of endogenous cardiomyocytes; however, these rare events cannot be considered of relevance for myocardial regeneration after injury of the adult heart.

Whether endogenous cardiomyocyte proliferation or remuscularization via progenitor cell activation is enhanced under pathological conditions remains a matter of debate. Studies, which utilized fate-mapping strategy to label pre-existing cardiomyocytes as previously described, demonstrated a dilution in the percentage of labeled pre-existing cardiomyocytes in the infarcted region of the heart after myocardial infarction (Ellison et al. 2013, Hsieh et al. 2007). In addition, Malliaras et al. reported that although adult cardiomyocyte cycling increases after myocardial injury, the majority of likely proliferating cardiomyocytes are from another cell source, so called progenitor cells. Thus, both endogenous cardiomyocytes and cardiac progenitors appeared to be involved in the replacement of lost cardiomyocytes (Malliaras et al. 2013). Although these studies provided some indirect evidence for new myocyte formation from a progenitor source, there is no consensus in the literature on the involved mechanisms. For example, in a recent study mass spectrometric analysis of cardiomyocytes labeled with ^{15}N-stable isotope revealed that new myocytes were mostly originating from adult cardiomyocytes after myocardial infarction, although a minor contribution of progenitors could not be excluded (Senyo et al. 2013).

The discrepancies between different studies might be due to technical reasons. Fate-mapping strategies of resident cardiomyocytes (Ellison et al. 2013, Hsieh et al. 2007, Malliaras et al. 2013) can only provide indirect evidence for cardiac differentiation of endogenous progenitor cells. In addition, the number of the cells analyzed by multi-isotope imaging mass spectrometry (Senyo et al. 2013) may have been too small to define the contribution of progenitor-derived cardiomyocytes. The limitation of these different techniques could only be addressed by direct and unambiguous labeling of specific progenitors and their progeny *in vivo*.

1.3 Stem/progenitor cell markers in the heart

c-Kit, also known as v-kit hardy-zuckerman 4 feline sarcoma viral oncogene homolog receptor function has been shown to play a crucial role for the migration, proliferation and survival of primordial germ cells, neural-crest-derived melanoblasts and hematopoietic precursors during embryo development. Many other organs and systems (e.g. skeleton, tooth, brain and neural tube, sensory organs, the respiratory system, the digestive system, endocrine organs, the genitoexcretory system and circulatory system) have been also found to express c-Kit, but without being essentially required for their development (Bernex et al. 1996).

c-Kit receptor belongs to the family of type III receptor tyrosine kinase (RTK), which also includes platelet-derived growth factor receptor (PDGFR), the macrophage colony stimulating factor receptor (CSFR) and fms related tyrosine kinase 3 (FLT3). c-Kit receptor tyrosine kinase structure is characterized by extracellular domain comprised of five immunoglobulin-like domains, spanning transmembrane region followed by an intracellular part that contains juxtamembrane, tyrosine kinase domain 1 and 2, which is split by a kinase insert sequence and carboxyterminal tail (**Figure 2**) (Lennartsson and Ronnstrand 2012).

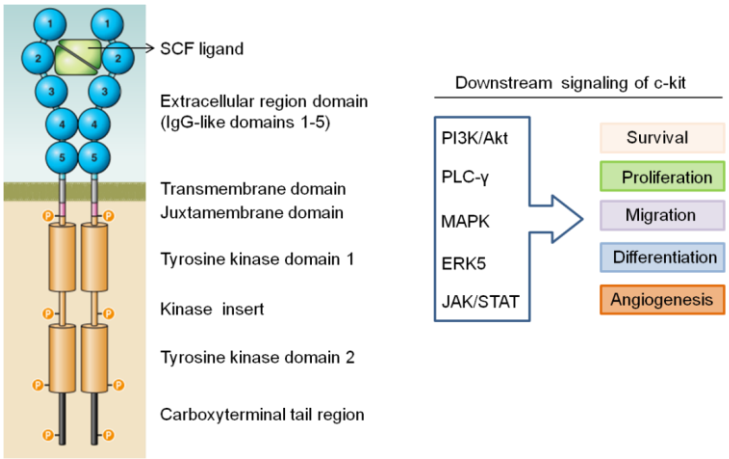

Figure 2. Schematic representation of c-Kit receptor structure and activation. Stem cell factor (SCF) ligand binding and dimerization of c-Kit followed by autophopshorylation on tyrosine residues and activated downstream signaling pathways. Schematic adapted from Lennartsson et al. (2012).

Binding of c-Kit ligand, stem cell factor (SCF) triggers dimerization of c-Kit receptor followed by autophosphorylation of the receptor. Highly phosphorylated tyrosine residues on the activated c-Kit receptor interact with different Src homology domain 2 (SH2) or SH3 domain containing adaptor proteins which subsequently coordinate the activation of downstream signaling pathways including phosphotidylinositol 3-kinases (PI3K)/AKT, phospholipase C (PLC)-γ, mitogen-activated protein kinases (ERK1/2, p38, JNK), ERK5 and Janus kinase (JAK)/Signal tansducer and activator of transcription (STAT) signal transduction pathways that are involved in cell survival, proliferation, migration, differentiation, and angiogenesis (Liang et al. 2013).

Stem cells antigen-1 (Sca-1) is a member of lymphocyte activation protein-6A (Ly-6A) gene family and is a glycosylphosphatidylinositol-anchored cell surface protein (GPI-AP) (van de Rijn et al. 1989). The ligand for Sca-1 has been not characterized yet; however there is evidence that Sca-1 is associated with Src family kinase members suggesting that Sca-1 functions as a receptor (Stefanova et al. 1991). Sca-1 expression has been detected in several organs; mostly restricted to endothelial cells or vasculature in the heart, brain and liver, in cortical tubes of kidney as well as in thymus and spleen (van de Rijn et al. 1989). It is important to note that although Sca-1 protein has been reported in mouse, a human Sca-1 analogue has not been identified yet. Sca-1^+ cells in human are considered Sca-1^+-like cells that have been isolated from the adult human heart based on an anti-mouse Sca-1 antibody (Valente et al. 2014).

c-Kit and Sca-1 are two surface proteins reported to be expressed on hematopoietic stem cells (HSCs) that show the capacity of self-renewing, giving rise to committed progenitors and differentiating into all cell lineages of blood system (Ikuta and Weissman 1992, Ito et al. 2003). HSCs are mainly found inside specific microenvironments, so called endosteal niche in the bone marrow within the trabecular bone. The c-Kit receptor ligand, SCF and C-X-C motif chemokine 12 (CXCL12; also known as stroma cell-derived factor 1 [SDF-1]) are secreted by osteoblasts, mesenchymal stromal cells/fibroblasts and CXCL12-abundant reticular (CAR) cells within the endosteal niche to support long-term maintenance of HSCs (**Figure 3**). Furthermore, c-Kit and Sca-1 expression on HSCs and their multipotent progenitors (e.g. myeloid and lymphoid progenitors) suggest that these receptors are

important for self-renewal, motility and differentiation of the stem/progenitor cells during hematopoiesis (Ito et al. 2003, Wilson et al. 2007).

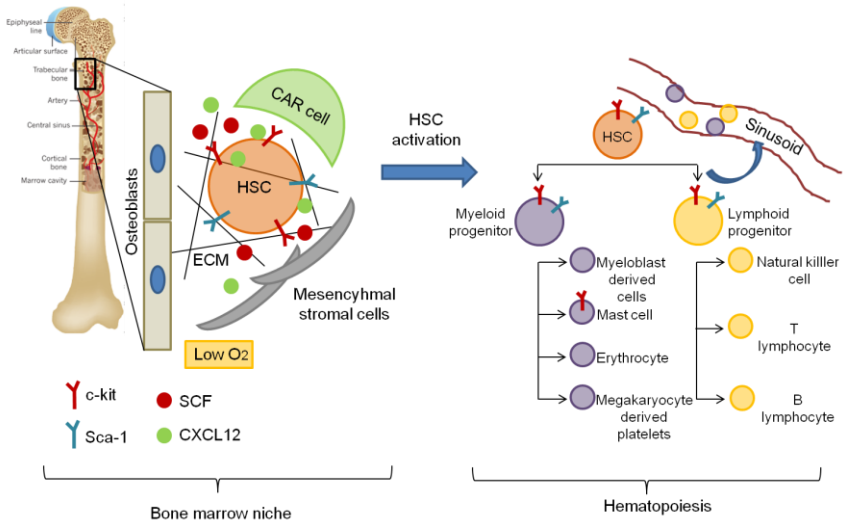

Figure 3. Hematopoietic stem cells in bone marrow niche and their activation. Schematic adapted from Morrison et al. (2014).

1.4 Evidence for cardiac progenitors in the adult heart

The first evidence for the existence of stem cells in the adult heart was obtained two decades ago in the rat heart with isolation of cells that display mesenchymal stem cell (MSC) characteristics differentiating into mesodermal lineages (Warejcka et al. 1996). Subsequently, cells decorated with c-Kit and Sca-1 protein were identified in the heart as putative cardiac stem/progenitor cells from the adult heart (Beltrami et al. 2003, Oh et al. 2003). Resident cardiac progenitor cells (CPCs) were firstly identified based on the expression of tyrosine kinase receptor, c-Kit. Isolated c-Kit$^+$ cardiac cells showed partial expression of cardiac transcription factors NK2 homeobox 5 (Nkx2.5), GATA binding protein 4 (GATA4) and myocyte enhancer factor 2 (MEF2), suggesting the presence of a small proportion (7-10%) of cardiac committed progenies. They displayed stem cell characteristics, i.e., clonogenic growth, self-renewing capacity and multipotency with evidence presented for their differentiation into cardiomyocytes (α-sarcomeric actin$^+$, cardiac myosin heavy chain$^+$), smooth muscle cells (α-smooth muscle actin$^+$), and endothelial cells (von Willebrand factor$^+$) within 7-10 days under defined medium conditions *in vitro* (Beltrami et al. 2003). In

addition, direct fluorescence labeling of isolated and *in vitro* expanded CPCs demonstrated that they were able to contribute new myocardium formation upon injection into the infarcted region of the heart, giving rise to all three cardiac cells mentioned above (Beltrami et al. 2003).

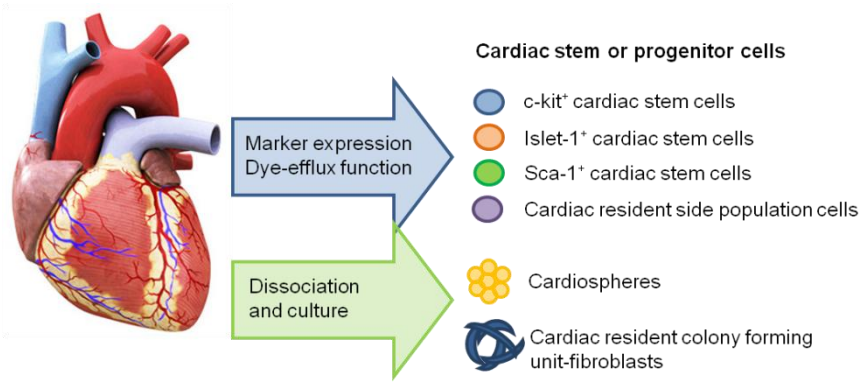

Figure 4. Cardiac progenitor cells residing in the adult heart. Cardiac progenitors cells identified based on the cell surface marker expression (e.g. c-Kit, Sca-1), genetic marker expression of transcription factors Islet-1 and functional properties such as dye-efflux function (cardiac side population cells), cardiosphere formation (cardiosphere cells or cardiosphere derived cells) and colony formation (colony forming unit-fibroblasts). Schematic adapted from Kikuchi et al. (2012).

Following this first study demonstrating the presence of endogenous progenitors in the adult heart with the capacity to differentiate into cardiac cells *in vitro and in vivo*, c-kit$^+$ CPCs (Bearzi et al. 2007, Miyamoto et al. 2010, Tallini et al. 2009, Zaruba et al. 2010) as well as other cardiac progenitors were isolated by several groups based on the expression of different stem cell-associated surface markers such as Sca-1 (Noack et al. 2012, Oh et al. 2003, Uchida et al. 2013, Wang et al. 2006), platelet derived growth factor receptor, alpha polypeptide (PDGFRα) (Chong et al. 2013, Noseda et al. 2015) or functional characteristics (e.g. cardiosphere formation, efflux of DNA binding dye and colony forming unit-fibroblasts) (Davis et al. 2009, Pfister et al. 2005) or origin (e.g. epicardium) (Limana et al. 2007) (**Figure 4**). However, it is still ambiguous whether these identified CPCs represent subsets of a common stem cell source in the heart with a transiently different phenotype or distinguishable stem cell types. The list of some of the defined CPCs so far is represented with their phenotypic characterization in **Table 1**.

	Stem cell markers (c-kit/Sca-1/PDGFRα)			Mesenchymal markers	Vascular cell markers	Hematopoietic markers	References
Surface marker selected CPCs	c-kit+					CD34-, CD45-, Lin-	(Beltrami et al. 2003)
	c-kit+	Sca-1+				CD34+, CD45+	(Matsuura et al. 2004)
		Sca-1+			Flk-1-, CD31+	CD34-, CD45-	(Oh et al. 2003)
	c-kit-	Sca-1+		CD90+, CD105+, CD29+, CD44+, CD73+	CD31-	CD34-	(Tateishi et al. 2007)
		Sca-1+	PDGFRα+	CD90+, CD105+, CD29+, CD44+	Flk-1-, CD31-	CD45-	(Chong et al. 2011)
	c-kit-	Sca-1+		CD29+	CD31-	CD34-, CD45-	(Takamiya et al. 2011)
	c-kit-	Sca-1+	PDGFRα+	CD90-, CD105+, CD29+, CD44+	Flk-1-, CD31-	CD34-, CD45-	(Freire et al. 2014)
Side population CPCs	c-kit-	Sca-1+		CD44-	CD31-, Tie2+	CD34-, CD45-	(Pfister et al. 2005)
	c-kit+	Sca-1+		CD29+, CD44+	Flk-1+	CD34+, CD45-	(Tomita et al. 2005)
	c-kit+	Sca-1+			CD31-	CD34+, CD45+	(Martin et al. 2004)
Epicardial progenitors	c-kit-	Sca-1+			Flk-1-, CD31-		(Smart et al. 2011)
Cardiospheres/ Mesoangioblast	c-kit+	Sca-1+		CD29+	Flk-1+, CD31+	CD34+	(Messina et al. 2004)
	c-kit-	Sca-1+			Flk-1-, CD31-	CD34-, CD45-, CD133-	(Ye et al. 2012)

Table 1. Putative CPCs and their phenotype in the adult heart.

1.5 Cardiogenic potential of endogenous CPCs

Utilizing direct genetic labeling strategies, based on the putative stem cell markers aforementioned (e.g. c-Kit and Sca-1), helped to clarify whether these markers only label stem or progenitor cells in the heart. Furthermore, it provided insight on cardiomyogenic potential of these endogenous CPCs through lineage tracing studies.

1.5.1 c-Kit CPCs

During embryogenesis in mice, c-Kit$^+$ cells appear as early as at embryonic day (E) 6.5 in the cardiogenic mesoderm (Ferreira-Martins et al. 2012), endocardial cells at E8.5 and 9.5, and exhibit a broad distribution in the developing and adult heart including the inner layers of atrial and ventricular chambers with a preferential localization in the endothelium of vessels as well as subepicardium region (Bernex et

al. 1996, Limana et al. 2007, Sultana et al. 2015, van Berlo et al. 2014). Pulse-chase labeling of c-Kit$^+$ cells during embryonic development in a tamoxifen inducible MerCreMer mouse model demonstrated the contribution of c-Kit$^+$ cells to the different compartments of the adult heart (**Figure 5**) (Sultana et al. 2015, van Berlo et al. 2014). In contrast to other studies, suggesting the existence of c-Kit as CPCs in the myocardial interstitium (Bearzi et al. 2007, Beltrami et al. 2003, Urbanek et al. 2003), evidence for a broad distribution of c-Kit$^+$ cells was demonstrated (**Figure 5B**).

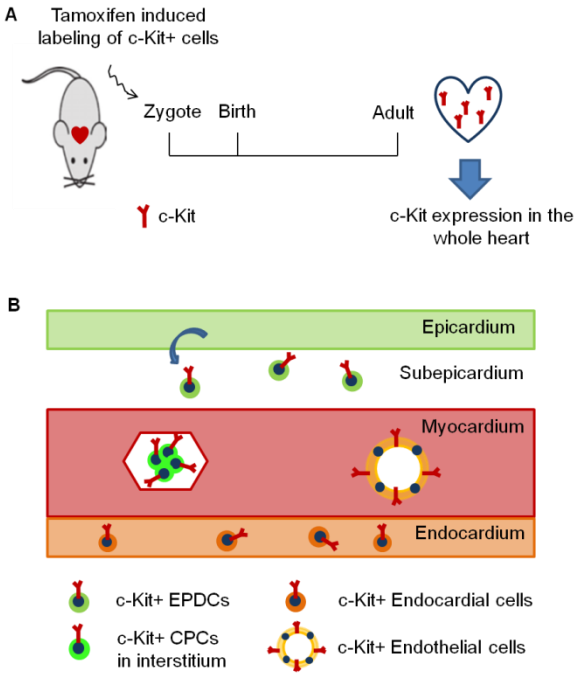

Figure 5. c-Kit cell progeny in the adult heart. A Lineage tracing of c-Kit$^+$ cells in the developing heart in transgenic MerCreMer mice. **B** Spatial distribution of c-Kit$^+$ cells in the adult heart. EPDC: Epicardium-derived progenitor cells.

Embryonic c-Kit$^+$ cells appeared to have contributed mainly to blood vessel associated endothelial cells in the adult heart (~80% of c-Kit$^+$ cells co-labeled with CD31$^+$) with rare differentiation into cardiomyocytes (<0.1% of total cardiomyocytes) (Sultana et al. 2015, van Berlo et al. 2014). This limited cardiomyogenic potential of c-Kit$^+$ CPCs was also supported in the aging heart and under pathological conditions using the same transgenic mouse model and postnatal reporter activation (Sultana et al. 2015, van Berlo et al. 2014).

A 3-fold increase in cardiomyogenic activity of c-Kit$^+$ CPCs was reported after infarction; however, the amount of newly generated cardiomyocytes by c-Kit$^+$ CPCs remained too low for a palpable endogenous cardioregenative response (van Berlo et al. 2014). Conversely, Ellison et al. proposed that c-Kit$^+$ CPCs are indispensable for cardiac regeneration (Ellison et al. 2013). Using lentiviral labeling of endogenous c-Kit$^+$ CPCs, they demonstrated that 10% of the newly formed myocytes in the injury site after myocardial infarction stemmed from c-Kit$^+$ CPCs. These CPC-derived cardiomyocytes appeared functional and contained sarcomeric structures, but in immature state (Ellison et al. 2013).

1.5.2 Sca-1 CPCs

Sca-1$^+$ CPCs were first identified by Matsuura et al. reporting that Sca-1$^+$ cells isolated from the adult mouse heart were able to differentiate into beating cardiomyocytes *in vitro* (Matsuura et al. 2004). Moreover, Sca-1$^+$ CPCs had the ability to differentiate into adipocytes and osteocytes, showing MSC-like characteristics. Although a human Sca-1 epitope has not been identified so far, antibody selection for mouse Sca-1 was applied successfully to isolate Sca-1$^+$-like progenitors from the human heart (Smits et al. 2009). Recent studies in the mouse demonstrated that the majority of Sca-1$^+$ cells in the heart were endothelial cells (>70%) and included a small fraction of smooth muscle cells (<5%) (Uchida et al. 2013). Additional Sca-1$^+$ cells in the myocardial interstitium were most likely comprised of cardiac fibroblasts (Furtado et al. 2014) and Sca-1$^+$ progenitors closely associated with the cardiomyocyte basal lamina, expressing stem cell surface markers: c-Kit, CD34 and Abcg2 (ATP-binding cassette, sub-family G, member 2) (Uchida et al. 2013). In other studies, Sca-1$^+$ CPCs that share some of the stem/progenitor cell markers (c-Kit, CD34) have been found in epicardial progenitor cells in the adult epicardium (Limana et al. 2007). In addition, Sca-1$^+$ CPCs have been found to express the epicardium-derived progenitor cell marker, PDGFRα (Chong et al. 2011). Together, these findings suggest a epicardial origin of Sca-1$^+$ cells.

Given the specificity of PDGFRα as a marker for epicardial progenitors (Chong et al. 2011, Chong et al. 2013) and the role of epicardium in the formation of

cardiovascular compartment and stromal cells in the developing heart, Sca-1^+/PDGFRα^+ CPCs were suggested to have the potential to differentiate into interstitial and smooth muscle cells, but not endothelial cells (Chong et al. 2011). This finding was contrary to recent findings, where most of the Sca-1^+ CPCs were shown to differentiate into endothelial cells during physiological development (Uchida et al. 2013). This contradiction regarding the differentiation potential of Sca-1^+ cells might be explained either with the existence of two subtypes of Sca-1^+ progenitors (Sca-1^+/PDGFR$^+$ and Sca-1^+/PDGFR$^-$), as demonstrated in the aorta (Cho et al. 2013), giving rise to different cell types in the heart or the heterogeneity of Sca-1^+ cells, composed of mainly endothelial cells which could mask the fate tracking of actual of Sca-1^+ progenitors in the heart (Uchida et al. 2013). Nevertheless, with respect to cardiomyogenic potential of Sca-1^+ CPCs, lineage tracing of Sca-1^+ cells continuously labeled from embryonic stage to postnatal development revealed that Sca-1^+ cells were able to contribute to cardiomyocyte renewal continuously under normal aging, but in a very low amount suggesting for their limited cardiomyogenic potential. Furthermore, they did not actively contribute to new cardiomyocyte formation even after injury (Uchida et al. 2013).

1.5.3 Vessel resident progenitor cells

So far, different types of blood vessel associated progenitors were identified based on their localization and specific marker expression, such as pericytes, mature vessel medial and adventitial progenitor cells (Kovacic and Boehm 2009). Pericytes have been discussed as mesenchymal stem cell (MSC)-like cells in the heart (**Figure 6**), with similar surface marker expression profile (e.g. Sca-1), the ability to undergo tri-lineage differentiation into osteoblasts, chondrocytes, and adipoyctes (Crisan et al. 2008) and the competency for self-renewal (Sacchetti et al. 2007, Wong et al. 2015).

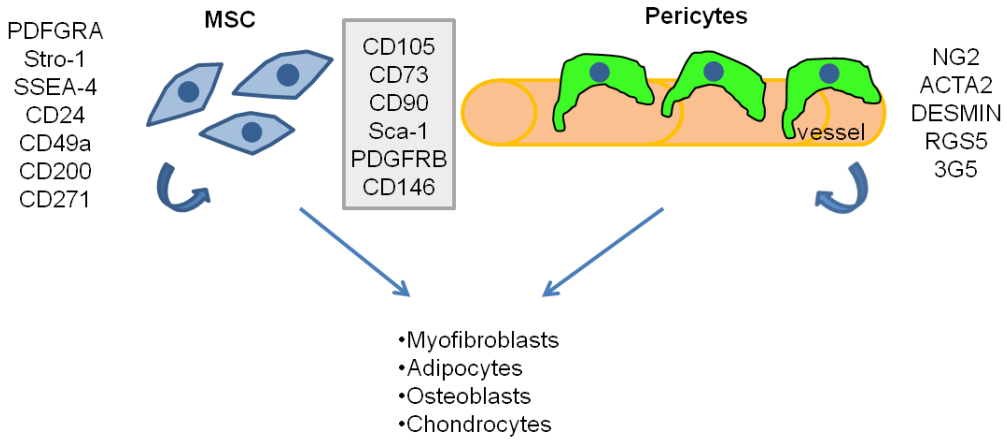

Figure 6. Unique and shared properties of pericytes and mesenchymal stem cells. Schematic adapted from Wong et al. (2015).

Pericytes have been recently defined as progenitors for smooth muscle cells, arising from epicardium during embryonic heart development. In addition, pericytes that are clonally related to smooth muscle cell are able to remain around the coronary arteries or tunica adventitia as cardiac progenitors, if they do not develop into smooth muscle cell (Volz et al. 2015). Consistent with this, the possibility that there are progenitor cells localizing in the *tunica media* or *adventitia* of mature vessels was suggested by several studies. Progenitor cells expressing stem cell markers including c-Kit, Sca-1, CD34 and residing in the *tunica adventitia* with the potential to differentiate into smooth muscle cells were recently identified (Hu et al. 2004). Another study reported that there are also progenitor cells, so called side population cells located in the *tunica media* that express Sca-1 and CD34, being capable of giving rise to smooth muscle and endothelial cells (Sainz et al. 2006). In addition to pericytes and adventitial cells, Kramann et al. reported another type of perivascular progenitors residing in pericyte niche (Kramann et al. 2015), GLI family zinc finger 1 $(Gli1)^+$ cells around the vasculature in close proximity to pericytes. These pericyte niche-associated cells do not show pericyte-specific markers such as CD146 and NG2 (CSPG4; chondroitin sulfate proteoglycan 4). Additionally, these cells display MSC properties and markers including Sca-1 and PDGFRα, suggesting a epicardium-derived progenitors origin (Smith et al. 2011). Given the fact that virtually all the organs contain MSCs with subendothelial localization, it is likely that vasculature in the heart serve as a niche that hosts a number of MSC-like stem or progenitor cells

(Kovacic and Boehm 2009, Wong et al. 2015). However, due to the limited understanding on the origin of cardiac progenitor cells and the heterogeneous expression profile of stem cell surface markers (e.g. c-Kit and Sca-1) in the heart, it is still not clear if these progenitors simply originate from the vasculature or are descendants of a common stem cell source (e.g. epicardium) or remnants of cardiovascular progenitors from embryonic development (Valente et al. 2014). The spatial distribution of putative cardiac stem/progenitor cells in the heart is schematically displayed in **Figure 7**; the relationship between these progenitors still remains to be defined.

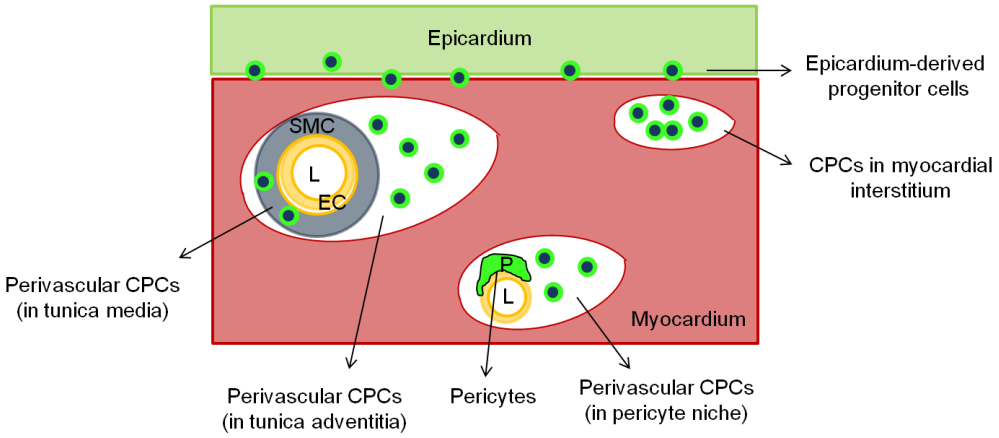

EC: Endothelial cell, L: Lumen, P: Pericye, SMC: Smooth muscle cell

Figure 7. Schematic overview of the spatial distribution of putative CPCs.

1.6 Exogenous regeneration by CPCs

Endogenous cardiac repair by resident CPCs is limited in the adult heart. Thus, implantation of CPCs into the myocardium or their pharmacological activation has been proposed as therapeutic strategies in heart disease (Beltrami et al. 2003). Accordingly, small and large animal models (e.g. rat and pig) were utilized to assess the cardio-regenerative potential of c-Kit$^+$ CPCs and also to develop strategies to enhance their retention rate upon delivery into the myocardium. *In vitro* expanded and growth factor (e.g. HGF and IGF-1) stimulated c-Kit$^+$ CPCs displayed robust engraftment and survival within 2 days after intramyocardial injection and gave rise to

vascularized myocardium, attenuating left ventricular dysfunction after myocardial infarction (Tillmanns et al. 2008). Similarly, autologous c-Kit$^+$ CPC implants induced functional myocardial tissue regeneration within chronically scarred myocardium in rat and pig heart (Bolli et al. 2013, Rota et al. 2008, Tang et al. 2010).

Although the potential mechanisms underlying the cardio-supportive effects of c-Kit$^+$ CPCs still needs to be defined, it is unlikely that differentiation of transplanted CPCs can explain the observed improvements. Instead, paracrine mediated effects initiating endogenous repair through recruitment of endogenous CPCs are discussed as alternative mechanism. Collectively, available animal studies provided convincing evidence for feasibility and safety of c-Kit$^+$ CPC implantation with additional hints for efficacy (van der Spoel et al. 2011).

1.7 Cardiac stem cell based therapy

Various cell types from different sources have been tested experimentally and clinically for their capacity to regenerate the heart using different routes of administration into the myocardium. Cell sources used in direct intracoronary or intramyocardial transplantations include; autologous bone marrow (BM)-derived cells (unselected BM-derived mononuclear and –mesencyhmal stem cells) (Bartunek et al. 2013, Lunde et al. 2006, Meyer et al. 2009, Mushtaq et al. 2014, Perin et al. 2012, Roncalli et al. 2011), skeletal muscle progenitors (satellite cells) (Menasche et al. 2008), peripheral blood cells (Assmus et al. 2007), adipose tissue-derived MSCs (Houtgraaf et al. 2012), heart-derived stem/progenitor cells (c-Kit$^+$ and cardiosphere progenitors) (Bolli et al. 2011, Chugh et al. 2012, Makkar et al. 2012). Besides direct intramyocardial delivery of exogenous cells, mobilization of endogenous progenitors from bone marrow by systemic administration of defined cytokines (e.g. erytropoieitn [EPO] and granulocyte-colony stimulating factor [G-CSF]) were also evaluated as alternative strategies (Achilli et al. 2010, Taniguchi et al. 2010). Candidate cell populations to induce myocardial regeneration and their delivery routes to the heart are summarized in **Figure 8**.

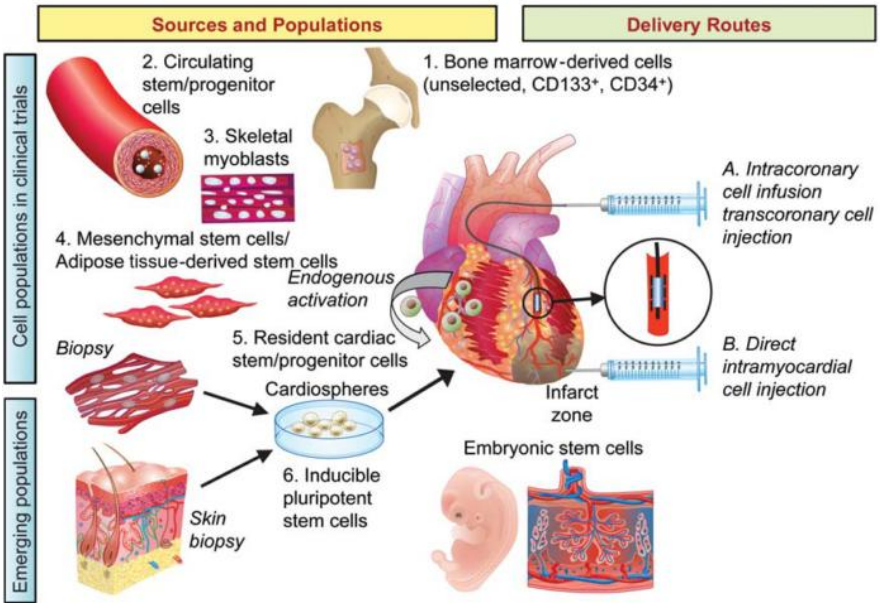

Figure 8. Clinically tested cell sources for heart regeneration. Schematic adapted from Doppler et al. (2013).

Being easy to harvest and apparently immune privileged, BM-derived stem/progenitor cells have been considered feasible and safe to be applied in clinical therapies without adverse effects so far, although it is also speculated that MSCs can transform into malignant tumors (Miura et al. 2006, Rubio et al. 2005). Unselected BM-derived mononuclear cells containing a mixture of endothelial progenitors, angioblasts and hematopoietic stem cells were thought to be an ideal cell source to induce neovascularization and new cardiomyocyte formation (Pavo et al. 2014). These cells, however, displayed a low abundance of relevant progenitors, modest clinical results and lack of convincing evidence for hematopoietic stem cells to differentiate into cardiomyocytes. Hence, the mode of action remains, despite the in some studies clinically observed beneficial effects and a suggested paracrine activity, elusive (Suzuki 2015).

The discovery of the heart containing endogenous cardiac progenitors with the capability to differentiate into vascular cells and cardiomyocytes initiated the isolation and *in vitro* expansion of these cells to be tested in several Phase IIa/b human clinical trials. These include the (1) cardiosphere-derived autologous stem cells to reverse ventricular dysfunction (CADUCEUS; (Makkar et al. 2012)), (2) cardiac stem

cells in patients with ischemic cardiomyopathy (SCIPIO; (Bolli et al. 2011)) and (3) autologous human cardiac-derived stem cell to treat ischemic cardiomyopathy (ALCADIA; (Takehara et al. 2012)) trials. In addition, another clinical trial, so called safety and efficacy evaluation of intracoronary infusion of allogeneic human cardiac stem cells in patients with acute myocardial infarction (CARE-MI) is ongoing in Phase I and II under the sponsorship of Coretherapix company, Spain (CARE-MI trial; Clinical Trial Identifier: NCT02439398).

In the CADUCEUS trial, patients were treated with 25 million autologous cardiosphere-derived progenitor cells (CDCs) isolated from right ventricular endomyocardial biopsies and injected through intracoronary infusion into the infarct related artery 1.5-3 months after myocardial infarction. The hypothesis was that scar tissue would be converted into viable myocardium (Makkar et al. 2012). Injection of CDCs significantly reduced the infarct size, increased the amount of viable myocardium as well as thickness in the peri-infarct zone at 6-12 months follow up, although there was no difference detected in left ventricular (LV) ejection fraction (Makkar et al. 2012). The SCIPIO trial was performed in patients with heart failure due to ischemic cardiomyopathy injecting 0.5-1 million of autologous c-Kit$^+$ CPCs derived from the atrial appendage. A reduction in infarct size and improvement in ejection fraction were reported after one and four year follow-up (Bolli et al. 2011). The ongoing ALCADIA trial differs from these previous studies in that stem cell delivery is combined with a biodegradable gelatin hydrogel scaffold for sustained FGF-2 release and enhanced cell retention (ALCADIA trial; Clinical Trial Identifier: NCT00981006). Taken together, these first clinical trials revealed that autologous transplantation of CPCs is feasible and safe.

More recently and as a consequence of the failure of autografts to form new cardiomyocytes there is a paradigm shift from autologous to allogenic implantations (CARE-MI trial; Clinical Trial Identifier: NCT02439398). Lauden et al. showed that allogeneic c-Kit-selected human CPCs (hCPCs) might exhibit a beneficial immunomodulatory effect. hCPCs express programmed death ligand 1 (PD-L1) protein which plays an important role in immunesuppression via acting as an inhibitory signal on the proliferation and activation of CD8$^+$ T-cells and activating regulatory T-cells. In addition, the immunomodulatory capacity of hCPCs was not

altered upon treatment with interferon gamma (IFN-γ), which is a pro-inflammatory cytokine secreted during myocardial infarction and infarct remodelling. This phenotype of hCPCs and the possibility for cryopreservation suggest that cell banks with allogeneic c-Kit-selected hCPCs may find an application in patients with acute myocardial infarction (Lauden et al. 2013).

Although there is first evidence of clinical efficacy, the main mechanisms for these cardio-supportive effects of transplanted c-Kit$^+$ CPCs are not yet fully understood. There are, however, several mechanisms proposed for these beneficial effects (Lauden et al. 2013), that can be summarized as direct and indirect effects of exogenously transplanted CPCs on the maintenance of heart structure and function. CPCs delivered into the infarcted myocardium may directly contribute to cardiomyogeneis and angiogenesis either via paracrine signaling (e.g. growth factors and cytokines) enhancing proliferation and survival of endogenous cardiomyocytes and vascular cells or giving rise to new cardiomyocytes and vascular cells (smooth muscle cells and endothelial cells). Besides this direct effect of CPCs on cardiac regeneration, they may also indirectly mediate cardio-supporting activity through regulating heart injury responses (e.g. reduced inflammation, fibrosis and remodeling) and activating endogenous CPCs to differentiate into cardiac cells. All these mechanisms are schematically summarized in **Figure 9**.

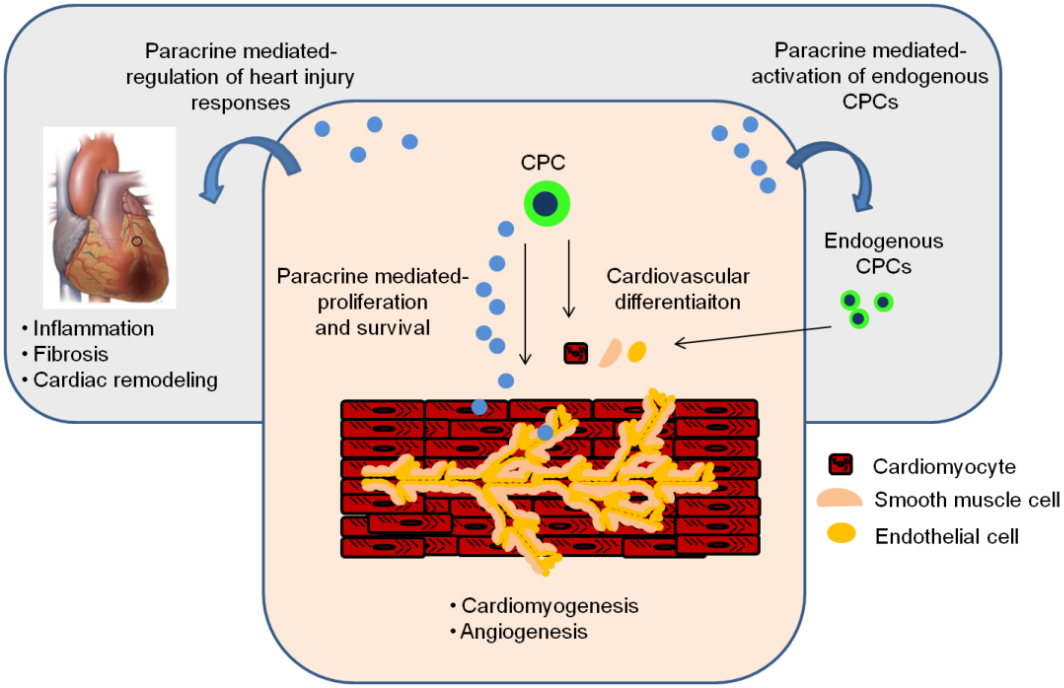

Figure 9. Schematic overview of potential mechanisms involved in heart repair upon CPC transplantation *in vivo*. Core panel (pink-colored): Direct contribution of CPCs to heart regeneration either by direct transdifferentiation or paracrine signaling. Outer panel (grey-colored): Indirect contribution of CPCs to heart regeneration and function through activating endogenous CPCs and regulating heart injury responses (e.g. reduced inflammation, fibrosis and remodeling).

1.8 EHM as an *in vitro* cardiac muscle model

Cardiac tissue engineering focuses on the development of biomimetic artificial cardiac muscle constructs. Engineered heart muscle (EHM) shows structural and physiological characteristics of native heart muscle, which renders it a high-fidelity *in vitro* platform to also study cell-cell interactions within a three-dimensional heart muscle context (Naito et al. 2006, Tiburcy et al. 2011, Zimmermann et al. 2002). Characteristic properties of EHM comprise: 1) the formation of a functional syncytium; 2) terminal differentiation of cardiomyocytes; 3) organotypic maturation with structural and functional properties of the postnatal heart (Christalla et al. 2012). Stromal cells play an essential role in this process by providing and maintaining a cardio-instructive extracellular matrix (ECM) milieu and paracrine support to guide heart muscle development *in vitro* (Naito et al. 2006, Tiburcy et al. 2011).

1.9 Aims of the study

A better understanding of the biological activity of CPCs may help to refine therapeutic strategies aiming at the regeneration of the failing heart. We hypothesized that EHM could be used as an *in vitro* heart surrogate platform to scrutinize and define the cardio-supportive effects of CPCs.

This study tested the following specific hypotheses:

1) CPCs support functional heart muscle formation *in vitro*.

2) CPCs elicit cardioprotective effects upon hypoxic injury.

The hypotheses were investigated in EHM from rat, mouse, and human cells as indicated. A new transgenic reporter model was established to study the role of hypoxia.

2 Materials and Methods

2.1 Preparation of cardiomyocytes

Cardiomyocytes were harvested from neonatal rat heart (section 2.1.1) as well as mouse (section 2.1.2) and human (section 2.1.3) embryonic stem cells. Organ harvest was approved by the responsible animal protection authorities (LAVES - AZ: 10.13/10.14). The use of human embryonic stem cells was approved by the Robert-Koch-Institute (AZ: 1710-79-1-4-16) according to §6 Stammzellgesetz (StZG).

2.1.1 Neonatal rat cardiomyocytes

Neonatal rat hearts (day 0-3) were dissociated by using a digestion protocol based on trypsin/DNAse I (Zimmermann et al. 2000). Cells were thereafter pre-plated for 1 hour at 37 °C, 5% CO_2 on plasma treated cell culture dishes. The non-attached cell suspensions were harvested as myocyte fraction and designated as neonatal rat cardiomyocytes (NRCMs). The purity of cardiomyocytes was determined by flow cytometry (BD LSR II; BD Biosciences) of cells stained for α-sarcomeric actinin (Sigma-Aldrich, see Appendix A3 for antibody dilution and section 2.6.2 for immunostaining protocol).

2.1.2 Mouse embryonic stem cell-derived cardiomyocytes

Upon mating of transgenic ROSA26 ODD-Luc/+ (heterozygous for ODD-Luc knock-in in the ROSA26 locus; see Appendix A4 for detailed background of the mice strain), zygotes at blastocyst stage were harvested and cultured on inactivated mouse embryonic fibroblasts (mEFs). Inner cell mass outgrowths from blastocysts were isolated and cultured on mEFs to give rise to ODD-Luc mouse embryonic stem cell (mESC) colonies. Subsequently, ODD-Luc mESCs were electroporated with a DNA construct expressing a neomycin resistance gene (neoR) under the transcriptional control of cardiomyocyte restricted alpha-myosin heavy chain (αMHC) promoter and a hygromycin resistance gene (hygroR) under ubiquitiously active phosphoglycerate (PGK) promoter (Klug et al. 1996) and selected under hygromycin (500 µg/ml for 7 days). The establishment of bitransgenic ODD-Luc x αMHC-neoR mESC line was

performed by Andreas Schraut (Institute of Pharmacology and Toxicology, University Medical Center Göttingen). ODD-Luc x αMHC-neoR mESCs were expanded on feeder layers composed of mitotically arrested MEFs (γ-irradiated with 30 Gy in Biobeam 8000, STS GmbH) cultivated in mESC culture medium (Appendix A1).

Cardiac differentiation was performed in 100 ml spinner flask cultures (0.1 x 10^6/ml seeding density) for 11 days, followed by additional 7 days of cardiomyocyte selection with G418 (400 µg/ml) in mESC differentiation medium (Appendix A1) as shown in **Figure 10**. Spontaneously beating cardiac bodies (CBs) were dissociated with a digestion protocol based on collagenase type I solution (Appendix A1) and trypsin-EDTA (0.25%). The purity of cardiomyocytes was detected by flow cytometry analysis of sarcomeric α-actinin staining (see Appendix A3 for antibody dilution and section 2.6.2 for immunostaining protocol). Cardiomyocyte yield per input mESCs was in the range between 1:1 and 1:2 after spontaneous differentiation and selection. Purity of cardiomyocytes is represented as a result in section 3.2.1.

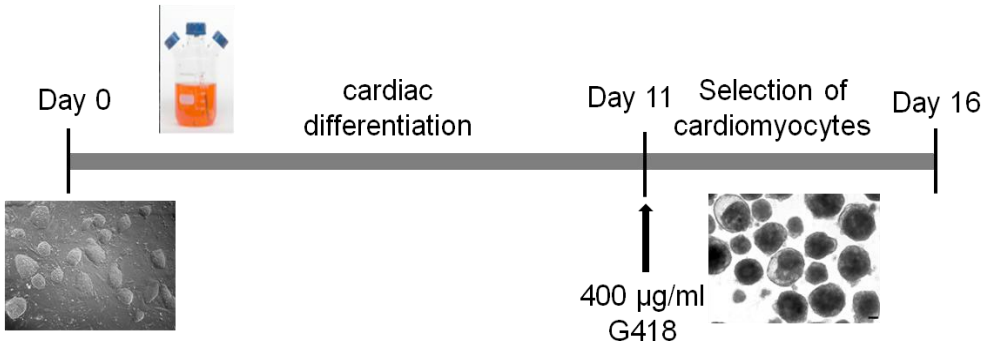

Figure 10. Cardiac differentiation of mESCs. Schematic representation of mouse cardiac differentiation: suspension culture of mESCs cultivated in spinner flasks for 11 days to induce spontaneous cardiac differentiation, followed by 7 days of selection of spontaneously beating cardiac bodies (CBs) with the addition of G418 (400 µg/ml).

2.1.3 Human embryonic stem cell-derived cardiomyocytes

The human embryonic stem cell line “HES2” (Embryonic Stem Cell International, Singapore), genetically modified to stably and ubiquitously express a tandem dimer red fluoresence protein (tdRFP) from the ROSA26 locus (finally designated hES2.R26) was kindly provided by Gordon Keller (Irion et al. 2007). hES2-RFP cells were maintained and differentiated under serum free conditios (Hudson et al. 2012) with minor modifications. Briefly, hESCs were initially cultured on irradiated hFFs in hESC culture medium (Appendix A1) and passaged using EDTA digestion solution (0.5 mol/L, pH 8, AppliChem) for expansion and single cell adaptation. Thereafter, hES2.R26 cells were plated on feeder free, Matrigel™ (Corning, 1:30 diluted in 1x PBS)-coated flasks in hESC-conditioned medium (Appendix A1) with every day medium change. Upon plating of hESCs on Matrigel-coated plates with a seeding density of 5 x 10^4-1 x 10^5 cells/cm² in hESC-conditioned medium for one day, hESCs were rinsed with hCM medium (Appendix A1) and cultured in mesoderm-induction medium (Appendix A1) for 3 days. After another washing step with hCM medium, cells were cultured in cardiac specification medium (Appendix A1) for the following 10 days. After two weeks of differentiation, cardiomyocytes were metabolically selected (Tohyama et al. 2013) in hCM selection medium (Appendix A1) for 5 days to obtain a highly enriched cardiomyocyte population.

Following the purification step, cardiomyocytes were washed two times with 1x PBS at room temperature (RoT) and subsequently, incubated in hCM digestion solution (Appendix A1) for 4 minutes at RoT and 10 minutes at 37 °C for digestion. Harvested cardiomyocytes were either seeded on cell culture flasks pre-coated with Matrigel™ (Corning, 1:30 diluted in 1x PBS) or directly used to generate human engineered heart muscle (hEHM). The purity of cardiomyocytes was detected by flow cytometry analysis of sarcomeric α-actinin staining (see Appendix A3 for antibody dilution and section 2.6.2 for immunostaining protocol).

2.2 Preparation of non-myocytes

Cardiac progenitor cells (CPCs) from mouse (mCPC; section 2.2.1) and human (hCPC; section 2.2.2) heart were used. Fibroblasts were isolated from mouse embryos (MEF; section 2.2.3) and human foreskin (hFF; section 2.2.4). Human cardac fibroblasts (hCF) were acquired from Lonza.

2.2.1 Mouse CPCs

We used two different types of murine cardiac progenitor cells (mCPCs); Sca-1-CPCs and c-Kit-CPCs isolated from adult mouse heart. GFP-labeled Sca-1-mCPCs overexpressing micro RNA 133a (miR-133a-CPCs) and micro RNA control (miR-control-CPCs) were kindly provided by Antonio Bernad (Izarra et al. 2014). GFP-labeled c-Kit-mCPCs (GFP^+ mCPCs) were kindly provided by Mark Sussman (Fischer et al. 2009). CPCs were maintained in mCPC medium (Appendix A1) under 21% O_2 and passaged with 0.05% Trypsin-EDTA (phenol red, #25300-054, Gibco) at 80% confluency.

2.2.2 Human CPCs

Human CPCs (hCPCs) isolated based on the c-Kit surface protein from right atrial appendages of patients were kindly provided by Coretherapix Biomedicine, Spain (Lauden et al. 2013). hCPCs (wild type or GFP-labeled; see Appendix A4) were delivered in frozen aliquots and directly used after thawing to generate hEHM without being cultured in our laboratory.

2.2.3 Mouse embryonic fibroblasts

Mouse embryonic fibroblasts (mEFs) were harvested at days post coitum (d.p.c) 12.5-13.5 by Andreas Schraut. mEFs were maintained in mEF medium (Appendix A1). For passaging, mEFs were enzymatically digested with 0.25% Trypsin-EDTA (#25200056, Gibco) at 80% confluency and split at a 1:3 ratio for further expansion.

2.2.4 Human foreskin fibroblasts

Human foreskin fibroblasts (hFFs) were purchased from the American Type Culture Collection (ATCC). hFFs were passaged with TrypLE (Tryple™ Express Enzyme 1X, no phenol red, #12604-013, Gibco) and cultured in hFF medium (Appendix A1). hFFs were lentivirally transduced to generate a stable cell line expressing GFP. Lentiviral particles were generated by co-transfecting pGIPZ with pMD26 and pSPAX2 helper plasmids into human embryonic kidney (Sagoo et al.) 293-T cells using the FuGENE HD transfection protocol (Promega). After a medium change, virus-containing medium was harvested every 24 hours for 72 hours. Viral particles were pooled and concentrated by centrifugation using Amicon® Ultra Centrifugal Filters (Millipore). Concentrated virus was stored at -80 °C. To transduce hFFs, cells were treated with polybrene (10 µg/ml) in culture medium containing 0.5% fetal bovine serum (FBS; #10270, Gibco) at 37 °C for 10 minutes. Thereafter, virus containing medium was added drop wise on top of the cells and incubated at 5% CO_2, 37 °C for 24 hours. Finally, the medium was exchanged with fresh hFF medium and transduced hFFs were selected with 1 µg/ml puromycin for 5 days.

2.3 EHM

Engineered heart muscle (EHM) was generated from neonatal rat heart and mouse or human embryonic stem cell-derived cardiomyocytes with CPCs or fibroblasts as indicated below.

2.3.1 Rat EHM

NRCMs were mixed with adult mouse heart-derived miR-control CPCs or miR-133a-CPCs in a 70/30% ratio (2.5 x 10^6 cell/EHM) and mixed with a master mix containing collagen type I from rat tail according to the amounts mentioned in **Table 2**. Rat EHMs (rEHMs) were made as previously described (Godier-Furnemont et al. 2015, Zimmermann et al. 2000). Briefly, the rEHM reconstitution mixture was cast into circular molds (inner/outer diameter: 8/16 mm) (Naito et al. 2006) and supplemented with rEHM medium (Appendix A1) following incubation for 1 hour at 37 °C. rEHMs were allowed to condense for 7 days in the casting mold. Subsequently, rEHMs were

transferred and maintained on phasic stretchers from culture day 7 to day 12 to induce functional maturation under mechanical loading (**Figure 11**).

Number of rEHMs	4x rEHMs
	Volume (µl)
Rat collagen (3.4 mg/ml)	940
2x rEHM DMEM (Appendix A1)	940
0.1 N NaOH	182
Matrigel™	400
Cell suspension (2.75 x 10^6/EHM)	1738
Total volume	4200
	900 µl/EHM

Table 2. rEHM master mix.

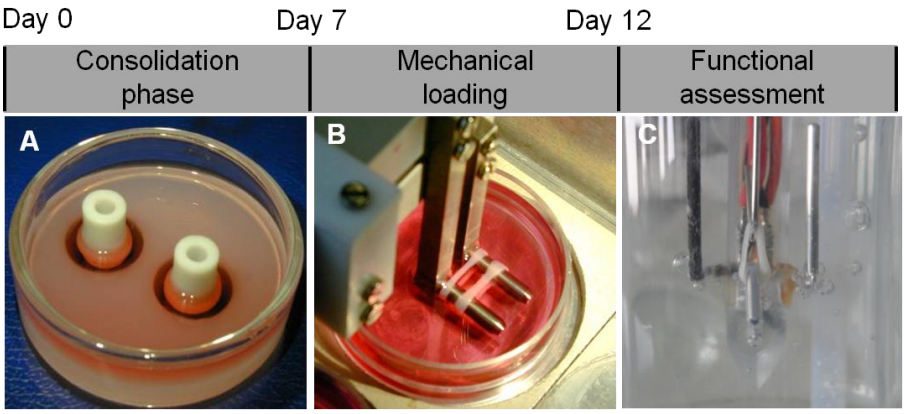

Figure 11. Construction of rat EHM. A Rat EHMs were maintained in casting molds for consolidation for 7 days. **B** Rat EHMs were exposed to mechanical loading on phasic stretchers at 1 Hz for 24 hours and 2 Hz for the following 4 days until force measurement (Zimmermann et al. 2002). **C** Measurement of force of contraction (FOC) under isometric conditions in a thermostatted organ bath (37 °C) filled with Tyrode's solution (Appendix A1).

2.3.2 Mouse EHM

mESC-derived cardiomyocytes (mCMs) were mixed with GFP^+ mCPCs or mEFs in a 70/30% ratio to generate mouse EHM (mEHM). Co-cultured cells were subsequently mixed with a master mix containing collagen type I isolated from rat tail (**Table 3**). Briefly, the mEHM cell mixture was cast in circular molds with an inner/outer diameter

of 2/4 mm (Tiburcy et al. 2014) as shown in **Figure 13** and supplemented with mEHM medium (Appendix A1) following incubation for 1 hour at 37 °C. On culture day 3, mEHMs were transferred onto static stretchers where they were exposed to mechanical loading for an additional 11 days.

Number of mEHMs	4x mEHMs
	Volume (µl)
Rat collagen (4.2 mg/ml)	399
2x mEHM DMEM (Appendix A1)	399
0.1 N NaOH	78.5
Cell suspension (1.5 x 10^6/EHM)	1223.5
Total volume	2100
	450 µl/EHM

Table 3. mEHM master mix.

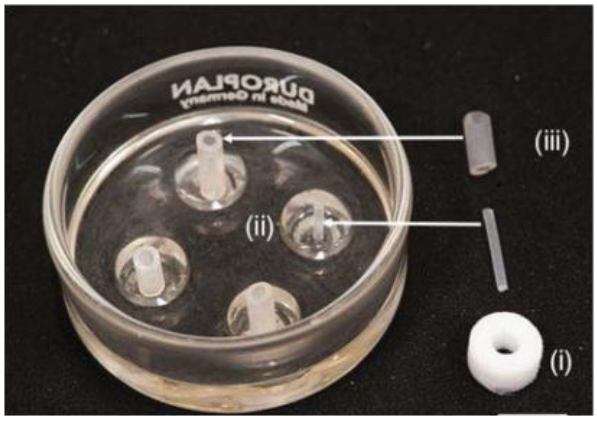

Figure 12. Casting mold for mouse and human EHM. Teflon disc (i) with 11 mm diameter, 5 mm height) was used as a spacer upon addition of silicone. Removal of the Teflon discs after hardening of the silicone established circular recesses (Tohyama et al. 2013). Silicone tubing (iii) with inner/outer diameter of 2/4 mm (Tiburcy et al. 2014) was placed on a central silicone core (Tohyama et al. 2013) in the center of recesses, providing the circular space for the casting of the EHM mixture (Soong et al. 2012).

2.3.3 Human EHM

Human engineered heart muscle (hEHM) was generated by mixing RFP^+ hCMs with GFP^+ hCPCs or GFP^+ hFFs in 70/30% ratio in a master mix containing bovine collagen type I (**Table 4**).

Number of hEHMs	4x hEHMs
	Volume (µl)
Bovine collagen (6.9 mg/ml)	271
2x hEHM RPMI (Appendix A1)	271
0.1 N NaOH	53
Cell suspension (1.45 x 10^6/EHM)	1511
Total volume	2106
	450 µl/EHM

Table 4. hEHM master mix.

hEHM mixture was cast into circular molds (**Figure 12**) with an inner/outer diameter of 2/4 mm and supplemented with serum-free hEHM medium (Appendix A1) following an incubation for 1 hour at 37 °C. On culture day 3, hEHMs were transferred onto static or dynamic stretchers to be exposed to mechanical loading. After culture day 14 or 28, hEHMs were subjected to isometric force measurements.

2.4 Isometric force measurement

EHM functionality was assessed by isometric force measurement in thermostatted organ baths (37 °C; **Figure 11C**) perfused with carbogen (95% O2, 5% CO2) to stabilize the pH at 7.4 as described previously (Zimmermann et al. 2000). EHMs were exposed to electrical stimulation (mEHM and rEHM: 2 Hz, hEHM: 1.5 Hz, 200 mA) to contract in Tyrode's solution (Appendix A1). EHMs were firstly preloaded to the maximum length where they generated the maximum force (Lmax according to the Frank-Starling mechanism). EHMs kept at Lmax were exposed to cumulatively increasing calcium concentrations (0.2 mM to 4 mM) to document maximal inotropic capacity and calcium sensitivity. Subsequently, EHMs were exposed to 1 µmol/L isoprenaline and 10 µmol/L carbachol (both from Sigma-Aldrich) at EC_{50} calcium concentrations. Force of contraction (FOC) data was acquired by BMON 32 and analyzed by AMON 32 software (Föhr Medical Instruments).

2.5 Immunostaining and microscopy

EHMs were fixed with 4% formaldehyde (FA) overnight at 4 °C followed by washes in PBS. From this step on, EHM pieces were either directly proceeded to whole mount staining or the complete EHM rings were embedded in 4% agarose for subsequent vibratome sectioning (Leica vibratome). EHM pieces or sections with 100 µm of thickness were blocked in permeabilizing blocking buffer (Appendix A1) overnight at 4 °C. Next, EHMs were treated with primary antibodies (see Appendix A3 for antibody dilutions) in the blocking buffer overnight at 4 °C. Primary antibodies were extensively washed; two times with PBS and one time with blocking buffer. Thereafter, EHMs were incubated in blocking buffer with suitable secondary antibodies (see Appendix A3 for antibody dilutions) and Hoechst (10 µg/ml, BD Biosciences, see Appendix A3 for the dilution) for DNA staining overnight at 4 °C. Following the washing steps; two times with PBS, one time with permeabilizing blocking buffer and one time with PBS, EHMs were mounted on microscope slides and proceeded to confocal microscopy imaging (Zeiss LSM 710).

2.6 Flow cytometry

For single cell analyses by flow cytometry EHM had to be dispersed enzymatically and exposed to specific antibody and DNA labeling.

2.6.1 Dissociation of EHM

EHMs were incubated in 1 ml of collagenase solution (Appendix A1) for 1 hour at 37 C. The supernatant was collected and the remaining EHM fragments were again exposed to 1 ml of fresh hCM digestion solution (Appendix A1) for 30 minutes at 37 C to achieve a complete dissociation. Supernatant volume was recorded and subjected to automated cell counting by an electric current exclusion assay (CASY model TTC; Roche) to measure cell number and viability. Thereafter, cells were passed through a 70 µm cell strainer to remove clumps and either directly proceeded to flow cytometry for live analysis or fixed with ice-cold 70% ethanol or 4% FA at RoT for immunofluorescence staining.

2.6.2 Immunostaining for intracellular antigens

Cells digested from EHM were labeled with primary antibodies directed against sarcomeric α-actinin (see Appendix A3 for the antibody dilution) to determine the myocyte amount out of total cell population within the EHM. Firstly, ethanol was removed by a centrifugation step (300 x g, 5 minutes) and subsequently cells were permeabilized in permabilizing blocking buffer (Appendix A1) for 10 minutes on ice. Next, cells were incubated with the primary antibody for 45 minutes on ice. Subsequent to washing steps; one time with PBS and one time with the blocking buffer, cells were incubated with a suitable secondary antibody (see Appendix A3) together with Hoechst DNA-binding dye (10 µg/ml, BD Biosciences, see Appendix A3 for the dilution) for 30 minutes in the dark at RoT. Following the washing steps; one time with PBS and one time with the blocking buffer, cells were suspended in 500 µl of PBS and subjected to flow cytometry analysis.

2.6.3 Immunostaining for cell surface proteins

CPCs and fibroblasts were stained with the corresponding antibodies against cell surface antigens; progenitor/stem cell markers (c-Kit, Sca-1), endothelial cell marker (PECAM1 [CD31]), mesenchymal cell markers (CD90, CD105, PDGFRA), and the common leukocyte marker (CD45). CPCs and fibroblasts were used directly from frozen aliquots. Cells were thawed in culture medium and subsequently washed with PBS. Next, CPCs and fibroblasts were exposed to the indicated antibodies (see Appendix A3 for the antibody dilution) in PBS with 5% FBS for 15 minutes at 4 °C in the dark. After an additional washing step with 3 ml of PBS, cells were subjected to flow cytometry (BD LSR II; BD Biosciences).

2.6.4 Sorting of EHM-derived cells

Cell mixtures composed of RFP^+ cardiomyocytes and GFP^+ non-myocytes (hFFs and hCPCs) obtained from EHM digestion were proceeded to fluorescence-activated cell sorting (FACS) based on their fluorescence labeling. EHM cells were stained with Sytox red dead cell stain (# S34859, Molecular Probes) and Hoechst DNA-binding dye (10 µg/ml, BD Biosciences, see Appendix A3 for the dilution) to exclude dead cells and cell clusters, respectively, during flow cytometry analysis. RFP^+ myocytes

and GFP^+ non-myocytes were recorded within the population gated for live (Sytox negative) and single cells were subsequently sorted (FACSAria II; BD Biosciences) into separate 15 ml polypropylene tubes containing Trizol (Invitrogen) for RNA isolation.

2.7 Gene expression analysis

Gene expression analysis was done by semi-quantitative PCR (PCR), quantitative PCR (qPCR) and RNA-sequencing (RNAseq).

2.7.1 RNA isolation

Total RNA was isolated using Trizol reagent according to manufacturer's instructions. The amount and purity of RNA (to assess DNA and phenol contaminations respectively; OD_{260}/OD_{280}: ~2.0, OD_{260}/OD_{230}: 2.0-2.2) were identified by the Nanodrop spectrophotometer (Thermo Scientific).

Gene expression analysis in rEHMs was performed by Alberto Izarra (Spanish National Center for Cardiovascular Research - CNIC). rEHM samples were shipped to CNIC on dry ice for RNA isolation followed by PCR for *insulin-like growth factor 1* (*IGF-1*), *fibroblast growth factor 2* (*bFGF*), *vascular endothelial growth factor A* (*VEGF-A*) and *hepatocyte growth factor* (*HGF*) with mouse specific primers to only amplify transcripts encoding the respective growth factors in the mouse Sca-1-CPC population in rEHMs (Izarra et al. 2014).

2.7.2 Reverse transcription

RNA samples were treated with DNase I (#04716728001, Roche) according to the protocol described below (**Table 5**) to remove possible contaminating genomic DNA.

	Volume
RNA (1 µg)	8 µl
DNase incubation buffer	1 µl
DNase (10 U/µl)	0.2 µl

Table 5. Composition of DNase treatment.

Dnase treatment reaction was performed at 37 °C for 20 minutes. Subsequently, 1 µl of EDTA solution (1:5 diluted from RNase free EDTA stock solution, 0.2 mol/L, pH 8.0) was pipetted into the reaction mix to inhibit DNase activity and incubated at 75 C for 10 minutes.

cDNA synthesis was performed by using High Capacity cDNA Reverse Transcription kit according to the manufacturer's instructions (Applied Biosystems). Briefly, 10 µl of Master mix for cDNA synthesis (**Table 6**) was mixed with 10 µl of RNA sample as described above and cDNA reverse transription reaction was run following the program summarized in **Table 7**.

	Volume
10x RT buffer	2 µl
25x dNTPs (100 mM)	0.8 µl
10x RT Random Oligo dT primers	2 µl
RNase inhibitor	1 µl
Diethylpyrocarbonate (DEPC) water	3.2 µl
Multiscribe Reverse Transcriptase (50 U/µl)	1 µl

Table 6. Composition of cDNA synthesis reaction.

Temperature	25 °C	37 °C	85 °C	4 °C
Time	10 min	120 min	5 min	–

Table 7. cDNA synthesis protocol.

2.7.3 Polymerase chain reaction

Subsequent to cDNA synthesis, semi-quantitative PCR was performed with primers targeting transcripts from specific genes of interest (Appendix A2) using TaKaRa Ex Taq kit. Briefly, 50 ng of cDNA was mixed with a master mix containing 5' and 3' primers with either 100 nmol/L or 200 nmol/L final concentration as indicated in the tables below (**Table 8 and 9**) for each gene (*IGF-1*, *FGF-2*, *VEGF-A*, *HGF*, *platelet derived growth factor* [*PDGF*], *v-kit hardy-zuckerman 4 feline sarcoma viral oncogene homolog* [*c-Kit*], *Nk2 homeobox 5* [*NKX2-5*], *Gata binding protein 4* [*GATA4*], *Actin, alpha, cardiac muscle 1* [*ACTC1*], *Cardiac troponin I, type 3* [*CTnI*], *PECAM1* [*CD31*] and *Glyceraldehyde-3-Phosphate Dehydrogenase* [*GAPDH*]). The PCR reactions were run on a Veriti® 96-Well Thermal Cycler (Applied Biosystems) as indicated below (**Table 10-14**).

	Master Mix
Number of samples	4x
10x ExTaq Buffer	5 µl
dNTP mix	4 µl
ExTaq	0.25 µl
5' primer (10 µmol/L)	1 µl (final con. 200 nmol/L)
3' primer (10 µmol/L)	1 µl (final con. 200 nmol/L)
ddH_2O	36.75 µl
	12 µl/sample
cDNA sample	1 µl
Total volume/sample	13 µl

Table 8. Composition of the PCR reaction for all targets without CD31.

	Master Mix
Number of samples	4x
10x ExTaq Buffer	5 µl
dNTP mix	4 µl
ExTaq	0.25 µl
5' primer (10 µM)	0.5 µl (final con. 100 nM)
3' primer (10 µM)	0.5 µl (final con. 100 nM)
ddH_2O	37.75 µl
	12 µl/sample
cDNA sample	1 µl
Total volume/sample	13 µl

Table 9. Composition of the PCR reaction for CD31.

Cycle step	Temperature	Time	Cycles
Initial denaturation	95 °C	60 sec.	1x
Denaturation	95 °C	15 sec.	35x
Annealing	60 °C	15 sec.	
Extension	72 °C	30 sec.	
Final extension	72 °C	300 sec.	1x

Table 10. PCR program for FGF-2/VEGF-A/PDGF/GAPDH.

Cycle step	Temperature	Time	Cycles
Initial denaturation	95 °C	60 sec.	1x
Denaturation	95 °C	15 sec.	35x
Annealing	60 °C	30 sec.	
Extension	72 °C	60 sec.	
Final extension	72 °C	300 sec.	1x

Table 11. PCR program for IGF-1/GATA4/ACTC1/CTnI.

Cycle step	Temperature	Time	Cycles
Initial denaturation	95 °C	60 sec.	1x
Denaturation	95 °C	30 sec.	35x
Annealing	56 °C	30 sec.	
Extension	72 °C	60 sec.	
Final extension	72 °C	300 sec.	1x

Table 12. PCR program for NKX2-5.

Cycle step	Temperature	Time	Cycles
Initial denaturation	95 °C	60 sec.	1x
Denaturation	95 °C	30 sec.	30x
Annealing	60 °C	30 sec.	
Extension	72 °C	60 sec.	
Final extension	72 °C	300 sec.	1x

Table 13. PCR program for CD31/c-Kit.

Cycle step	Temperature	Time	Cycles
Initial denaturation	95 °C	60 sec.	1x
Denaturation	95 °C	30 sec.	35x
Annealing	55 °C	30 sec.	
Extension	72 °C	60 sec.	
Final extension	72 °C	300 sec.	1x

Table 14. PCR program for HGF.

2.7.4 Agarose gel electrophoresis

Amplified DNA fragments by PCR were visualized by agarose gel electrophoresis for gene expression analysis. 2% agarose gels (ultra-pure agarose; AppliChem) were prepared in TAE buffer (Appendix A1). The agarose gel mixture was heated in a microwave until agarose particles were completely dissolved. Prior to gel polymerization ethidium bromide was added (final concentration 0.2 µg/ml) for visualization of the DNA under UV light. Agarose gels were poured into standard casting trays. Upon polymerization, agarose gels were loaded with the cDNA

samples mixed with DNA gel loading dye (#R0611, ThermoFisher Scientific) and a DNA ladder (Gene ruler^{TM} 100 bp Plus DNA ladder, #SM0321, ThermoFisher Scientific). Elecrophoretic separation was at 90 V for 1-2 hours at RoT.

2.7.5 Quantitative PCR

To analyze the expression of cardiac genes in flow cytometry sorted cells (2550±634 RFP^+ cells, 1349±348 GFP^+ cells per reaction, from three experiments) quantitative PCR (qPCR) was performed using Fast SYBR Green Master Mix kit (Applied Biosystems) according to manufacturer's instructions. Briefly, 5-10 ng cDNA was mixed with a master mix containing 5' and 3' primers (50 nmol/L each; **Table 15**). qPCR was performed in ABI PRISM 7900HT Fast Real-Time PCR system (Applied Biosystems) on 384-well plate format according to the PCR program shown in **Table 16**. qPCR analysis was performed using ΔΔCt method and *GAPDH* was used as the reference gene for normalization (Livak and Schmittgen 2001).

	Master Mix
Number of samples	30x
ddH_2O	108 µl
5' primer (10 µmol/L)	1.25 µl
3' primer (10 µmol/L)	1.25 µl
Sybr Master Mix	150 µl
	9 µl/sample
cDNA sample	1 µl
Total volume/sample	10 µl

Table 15. Composition of qPCR reaction.

Initial denaturation	95 °C	1x
Denaturation	95 °C	40x
Annealing	60 °C	
Extension	60 °C	
Final extension	60 °C	1x
Inactivation	95 °C	1x

Table 16. qPCR protocol.

2.7.6 RNA sequencing

RNA was isolated as described in section 2.7.1 and the quality was assessed with the Agilent Bioanalyzer 2100. Total RNA was subjected to library preparation (TruSeq Stranded Total RNA Sample Prep Kit from Illumina) and RNA-sequencing on an Illumina HighSeq-2000 platform (SR 50 bp; >25 Mio reads /sample). Sequence images were transformed with the Illumina software BaseCaller to bcl files, which were demultiplexed to fastq files with CASAVA (v1.8.2). Fastq files were mapped to GRCh38/hg38 using STAR 2.4 or TopHat2 (Kim et al. 2013) and Reads Per Kilobase of transcript per Million (RPKM) were calculated based on the Ensembl transcript length as extracted by biomaRt (v2.24) or Fragments Per Kilobase of transcript per Million (FPKM) calculated by Cufflinks (Trapnell et al. 2012). We only considered "protein_coding" transcripts for further analysis. Gene ontology (GO) analysis was performed through DAVID (Huang da et al. 2009). To determine cardiomyocyte, fibroblast and CPC specific genes the following algorithm was applied: (1) normalized counts of purified hES2.R26-derived cardiomyocytes (n=3) and fibroblasts from two different sources (foreskin and heart; n=3 from each source) and human GFP+ CPCs (n=3) were pooled and the differentially expressed genes (DEG, $p<0.05$) between cardiomyocyte, fibroblast and CPC pools determined; (2) log2 changes of DEG were calculated and genes omitted with a log2 difference lower than mean log2 of all cardiomyocyte genes; (3) resulting cardiomyocyte-, fibroblast-, and CPC-enriched genes were screened for RPKM values in adult healthy heart. Transcribed genes with RPKM <1 in adult heart were omitted.

2.8 Cell based models of cardiomyocyte hypoxia

To investigate possible cardioprotective activity of CPCs, we developed a new EHM injury model based on hypoxia/reoxygenation (H/R) or chronic hypoxia. Embryonic stem cells from ODD-Luc mice (refer to 2.1.2) or a newly generated human ODD-Luc reporter embryonic stem cell line (refer to 2.11) were used as cardiomyocyte sources for EHM construction according to the protocols outlined above.

2.8.1 Imaging hypoxia in mouse ODD-Luc cardiomyocytes

ODD-Luc fusion protein has been shown to be responsive to hypoxia and can be used as a noninvasive bioluminescence imaging technique to monitor the temporal kinetic of endogenous HIF-1α regulation in different cell types (Moroz et al. 2009, Viola et al. 2008). Being the main regulatory protein for adaptation of cellular response to hypoxia, identification of HIF-1α regulation may provide mechanistic insight into diseases like ischemia/reperfusion injury. To visualize and analyze the response to hypoxia in cardiomyocytes, we utilized the ODD-Luc x α-MHC-NeoR mESC line to give rise to ODD-Luc cardiomyocytes which ubiquitously express HIF-1α-ODD-Luc fusion protein. ODD-Luc cardiomyocytes were incubated in hypoxia chamber (Invivo 400 workstation, Ruskinn, UK) under 1% O_2 for 8-72 hours. After hypoxia treatment, ODD-Luc CMs were lysed with a lysis buffer (Dual-Luciferase® Reporter Assay Systems, Promega) diluted 1:5 with ddH_2O water and supplemented with protease and phosphatase inhibitors (both diluted in 1:1000 dilution, see Appendix A1 for stock solutions) inside the hypoxia chamber. Thereafter, the enzymatic reaction depicted in **Figure 13** was performed according to manufacturer's protocol using Centro LB 960 Microplate Luminometer (BERTHOLD Technologies) and Microwin 2000 software (Informer Technologies).

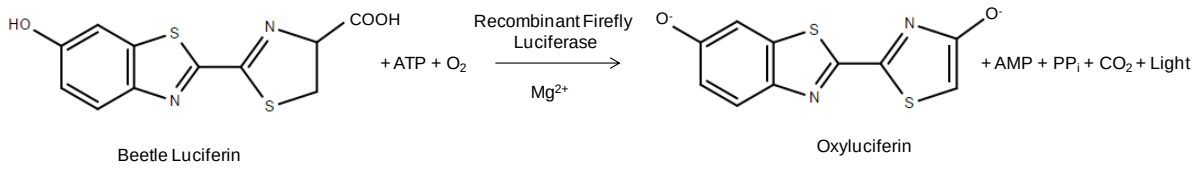

Figure 13. Bioluminescent reaction catalyzed by firefly luciferase. Luciferase activity assay involves oxidation of luciferin substrate in the presence of O_2, ATP and Mg^{2+}. Schematic adapted from the Promega user manual.

2.8.2 Imaging hypoxia in mouse ODD-Luc EHM

In the next step, ODD-Luc hypoxia reporter CMs (70%) and mEFs (30%) were utilized to construct ODD-Luc mouse EHM to monitor hypoxia at a tissue level. ODD-Luc EHMs were incubated in 1% O_2 for 1-72 hrs. Thereafter, ODD-Luc EHMs were transferred into PBS containing 1 mg/ml of luciferin (Caliper life sciences) and immediately visualized for bioluminescence development using LAS-3000

luminesence image analyzer (Fuji). Analysis of luminescence intensity was done by Image J software.

2.8.3 Generation of ODD-Luc human embryonic stem cell line

The plasmid ODD-Luciferase-pcDNA3 was a kind gift from the Kaelin lab (Dana-Farber/Harvard Cancer Center). ODD-Luc transgene was cloned from the original plasmid into a pAAVS1 vector under the control of CAG promoter resulting in pAAVS1-CAG-ODD-Luc-EF1α-GFP donor vector. ODD-Luc hES2 cells were generated via transfection with the ODD-Luc expressing pAAVS1 donor vector in conjuction with pAAVS1 Trancription activator-like effector-nuclease (TALEN) pair plasmids following the principle as described in **Figure 14**. Briefly, TALE nucleases encoded by TALEN pair plasmids recognize and cut specific DNA sequences in the AAVS1 safe harbor genomic locus, facilitating homologous recombination of the transgene flanked by TALE recognizing sequences. The donor vector was constructed by Dr. Claudia Noack (Institute of Pharmacology and Toxicology, University Medical Center Göttingen) and transfection of hESCs was kindly performed by Krasimira Sharkova (Institute of Pharmacology and Toxicology, University Medical Center Göttingen). Next, puromycin selected ODD-Luc expressing hES cells (ODD-Luc hESCs) were differentiated into human cardiomyocytes (hCMs) giving rise to the formation of ODD-Luc hCMs.

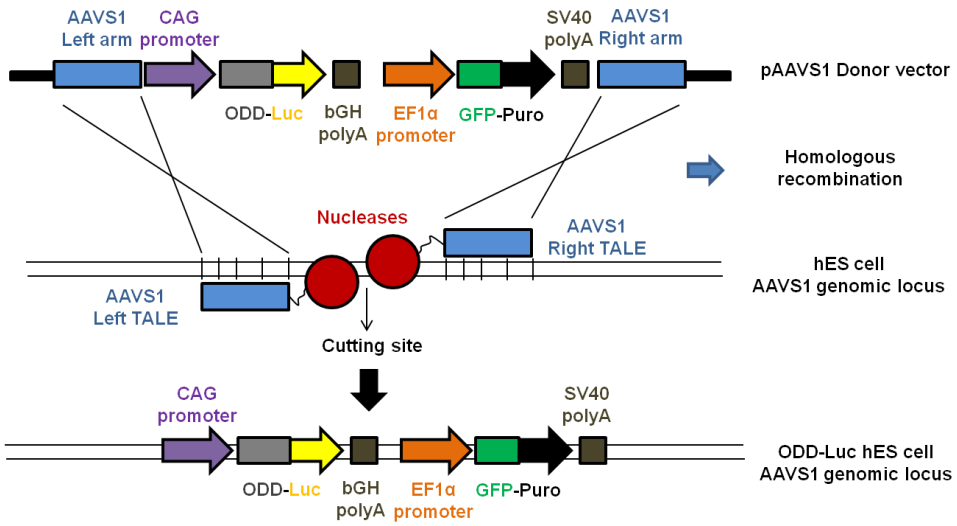

Figure 14. ODD-Luc hES cells generated using TALEN technology. pAAVS1 donor vector encoding for ODD-Luc under CAG promoter control and the GFP-puromycin (puro) fusion protein under EF-1α promoter control flanked by AAVS1 specific DNA sequences. TALE nucleases recognize and cut specific DNA sequences in AAVS1 genomic locus in hES cells, leading typically to homologous recombination of gene of interest in the targeted site.

2.8.4 Hypoxia imaging in ODD-Luc human cardiomyocytes

Human cardiomyocytes differentiated from ODD-Luc hESCs were dissociated as described above (section 2.1.3) and seeded on Matrigel™ (Corning, 1:30 diluted in PBS)-coated 6-well plates with a seeding density of 0.5 x 10^6 cells/well in hCM medium (Appendix A1). After 5-7 days of metabolic selection in hCM selection medium (Appendix A1) to reduce non-myocyte content, cardiomyocytes were cultured in 21% or 1% O_2 for 4 hours and subjected to Luc-signal measurements as described above (section 2.8.1).

2.8.5 Hypoxia/Reoxygenation injury in human EHM

hEHMs generated from hCMs (70%) and hFFs (30%), so called hFF-EHMs were exposed to 1% O_2 for 8-120 hours in DMEM SF-B27 medium (Appendix A1). After hypoxia exposure, hEHMs were incubated in 21% O_2 in freshly prepared DMEM SF-CMR medium (Appendix A1) to induce reoxygenation. In order to analyze cardioprotective paracrine effects of hCPCs and hFFs, hEHMs were treated with hCPC- or hFF-Conditioned medium (ConM; Appendix A1) during reoxygenation.

After H/R injury, cardiomyocyte content, structure and function were assessed. In addition, lactate dehydrogenase (LDH) release was assessed according to the manufacturer's protocol (Lactate dehydrogenase activity assay kit, #MAK066, Sigma-Aldrich) to estimate the amount of cell death.

2.8.6 Chronic hypoxia injury in human EHM

Next, we investigated the possible cardioprotective effect of hCPCs under chronic hypoxia stimulation for 120 hours in 1% O_2. We developed another hEHM model mainly composed of hCMs and hFFs partially included with hCPCs, so called hFF+hCPC-EHM (input cell numbers [x10^6] per hEHM; hCM/hFF/hCPC: 0.84/0.36/0.09). hFF- and hFF+hCPC-EHMs were incubated in DMEM SF-B27 medium (Appendix A1) at 21% or 1% O_2 without any medium change for 120 hours. Afterwards, hEHMs were subjected to isometric force measurements. In addition, myocyte content, structure and function were analyzed in hEHM co-cultures.

2.9 Western blot analyses

Response of human embryonic stem cell-derived cardiomyocytes (hCMs) to hypoxia was assessed by detection of HIF-1α stabilization using western blot technique.

2.9.1 Protein isolation

hCMs were seeded in Matrigel™ (Corning, 1:30 diluted in 1 X PBS)-coated 6-well plates within the density of 0.3 x 10^6 cells/well in hCM medium (Appendix A1) and subjected to 1% O_2 for 0-72 hours. Cells were lysed with 500 µl lysis buffer (Dual-Luciferase® Reporter Assay Systems, Promega)/well as described above (see section 2.8.1), followed by a short centrifugation step (16,000 x g, 10 seconds, at 4 C) to pellet cell debris. The supernatant was used for the Western blotting.

2.9.2 Bradford assay

Protein concentration was measured using the Bradford assay. Serial dilutions (in µg/ml: 0, 0.312, 0.625, 1.25, 2.5, 5) of bovine serum albumin (BSA; stock concentration of 1 mg/ml) in distilled water were used as reference. Absorbance of samples (5 µl) supplemented with Bradford dye (95 µl of 1:10 in sterile water diluted

dye) was measured in a 96-well plate at 595 nm (FlexStation 3 Multi-Mode Microplate Reader, Molecular Devices). The accuracy of the measurement was defined based on R^2 of the standard curve. The experimental R^2 value for this test was 0.96 (n=1 experiment). Protein concentration was calculated based on the slope intercept formula.

2.9.3 SDS-gel electrophoresis

Proteins were seperated using 12% seperating gel (Appendix A1). The separating gel was poured in between two glass plates. The upper part of the gel was covered with isopropanol during polymerization. Upon polymerization of the gel, isopropanol was removed and washed with distilled water. Next, a stacking gel (Appendix A1) was poured on top of the separating gel with a comb placed inside. The comb was carefully removed upon polymerization.

20 µg of protein was mixed with 6x Laemmli loading buffer (Appendix A1) and kept at 95 °C for 3 minutes prior to loading. Samples (30-40 µl) and a standard protein ladder sample (The Precision Plus™ Protein Kaleidoscope™ protein, BIO-RAD) were loaded and run in Running buffer (Appendix A1) for ~2 hours at 100 V and RoT. Next, proteins were transferred from the SDS-gel to a polyvinylidene fluoride (PVDF) by electroblotting in Transfer Buffer for 1.5 hours at 100 V and 4 °C.

2.9.4 Immunoblotting

PVDF membranes, after proteins transfer, were incubated with blocking buffer (Appendix A1) for 1 hour at RoT. After a short washing step in PBS-T (PBS with 0.1% Tween-20), PVDF membranes were incubated with primary antibodies (HIF-1α from BD Transduction and β-actin from Sigma-Aldrich; see Appendix A3 for antibody dilutions) in blocking buffer overnight at 4 °C. After three additional washing steps in PBS-T, membranes were incubated with appropriate secondary antibodies (IgG-HRP-conjugated, Dako, see Appendix A3 for antibody dilution) in blocking buffer overnight at 4 °C. After three washes in PBS-T for 15 minutes each, membranes were incubated with the substrate (SuperSignal® West Femto Trial Kit, Themofischer scientific) which catalyzes the activity of horseradish peroxidase to generate a chemiluminesence signal. The chemiluminesence signal was detected by a

VersaDoc™ XR Imaging System and the images were analzyed using Image Lab software from BioRad.

2.10 Quantification of lactate release

hCMs were seeded into 24-well plates (62.500 cells/well) in hCM medium (Appendix A1). Culture medium was changed with DMEM SF-B27 medium (Appendix A1) before incubation at 1% O_2 for 0-72 hours. Prior to analysis, medium was collected in 1.5 ml polypropylene tubes, centrifuged for 20-25 minutes at 16,000 x g to remove any cell debris. Supernatant was transferred into a new polyprolylene tube. 100 µl of medium was added into the master mix prepared according to manufacturer's instructions (L-lactic acid UV-method, Boehringer/R-Biopharm). The complete mixture was transferred into plastic cuvettes to initiate the enzymatic reactions (**Figure 15**) and subjected to spectrophotometric measurement of NADH at 340 nm (Centro LB 960 Microplate Luminometer, BERTHOLD Technologies). Lactic acid concentration was calculated based on the equation described in the related protocol.

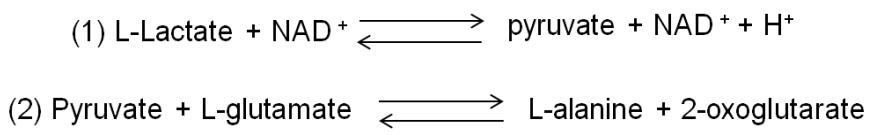

Figure 15. Lactic acid catalyzing reaction. 1 L-Lactate is oxidized to pyruvate in the presence of NAD^+ and L-Lactate dehydrogenase (L-LDH). **2** Pyruvate from reaction 1 is trapped in the presence of L-glutamate and Glutamate-Pyruvate transaminase, leading the eqilibrium in reaction 1 to be displaced in favor of pyruvate and $NADH^+$.

2.11 Quantification of intracellular ATP

hCMs were seeded in matrigel (Corning, 1:30 diluted in 1x PBS)-coated 96-well luminometer plate within the density of 2.5 x 10^4 cells/well in hCM medium. Cells were put into 1% O_2 for 0-72 hours following medium change with DMEM SF-B27 medium (Appendix A1). Prior to analysis, ATP standards were prepared in each 96-well plate with the concentrations ranging from 1 µM to 10 nM by serial ten fold dilutions. 100 µl of Cell titer Glo Reagent (mixture of Luciferin substrate and Luciferase) were added on top of the medium. The luminescence signal generated

was directly proportional to the amount of ATP present. ATP amount was calculated based on the ATP standard curve. All steps were performed according to manufacturer's instructions (CellTiter-Glo® Luminescent Cell Viability Assay, Promega).

2.12 Statistics

Data are presented as arithmetic mean with standard error of the mean (SEM). Statistical analyses were done using two-tailed unpaired Student's *t*-test, one-way ANOVA, and two-way ANOVA with indicated *post hoc* tests using GraphPad Prism5 program. P value smaller than 0.05 (*$p<0.05$) was considered significant.

3 Results

3.1 Characterization of CPCs in monolayer culture

Cardiac progenitor cells (CPCs) derived from adult mouse (mCPCs) or adult human heart (hCPCs) were characterized for their expression of specific cell-type markers using PCR and flow cytometry. Additionally, transcriptome profiling of hCPCs was performed by RNA-sequencing (RNAseq) to gain broader insight into their origin and biological activity.

3.1.1 Mouse CPCs show a mesenchymal phenotype

Two previously reported types of CPCs from adult mouse heart, selected by surface markers - (1) v-kit hardy-zuckerman 4 feline sarcoma viral oncogene homolog (c-Kit; c-Kit-mCPCs; kindly provided by Mark Sussmann; San Diego State University; (Fischer et al. 2009)) and (2) lymphocyte antigen 6a (LY6A; Sca-1-mCPCs; kindly provided by Antonio Bernad; CNIC-Madrid; (Izarra, 2014 #95)) - were characterized. c-Kit expression could not be confirmed by PCR (**Figure 16B**) or flow cytometry (**Figure 16C**) in either of the tested mCPCs in monolayer culture. Flow cytometry showed that most of the c-Kit-selected mCPCs were positive for Sca-1 and the mesenchymal cell markers platelet derived growth factor receptor, alpha polypeptide (PDGFRA) and endoglin (CD105; **Figure 16C**). Additional PCR analyses showed that both mCPC types (c-Kit- and Sca-1-CPCs) also express *discoidin domain receptor tyrosine kinase 2* (*Ddr2*), indicating their mesenchymal origin (**Figure 16B**). The absence of the cardiomyocyte development implicated transcription factor, *Nkx2-5* suggested that both of these cell types were not committed towards a cardiomyocyte fate (**Figure 16B**).

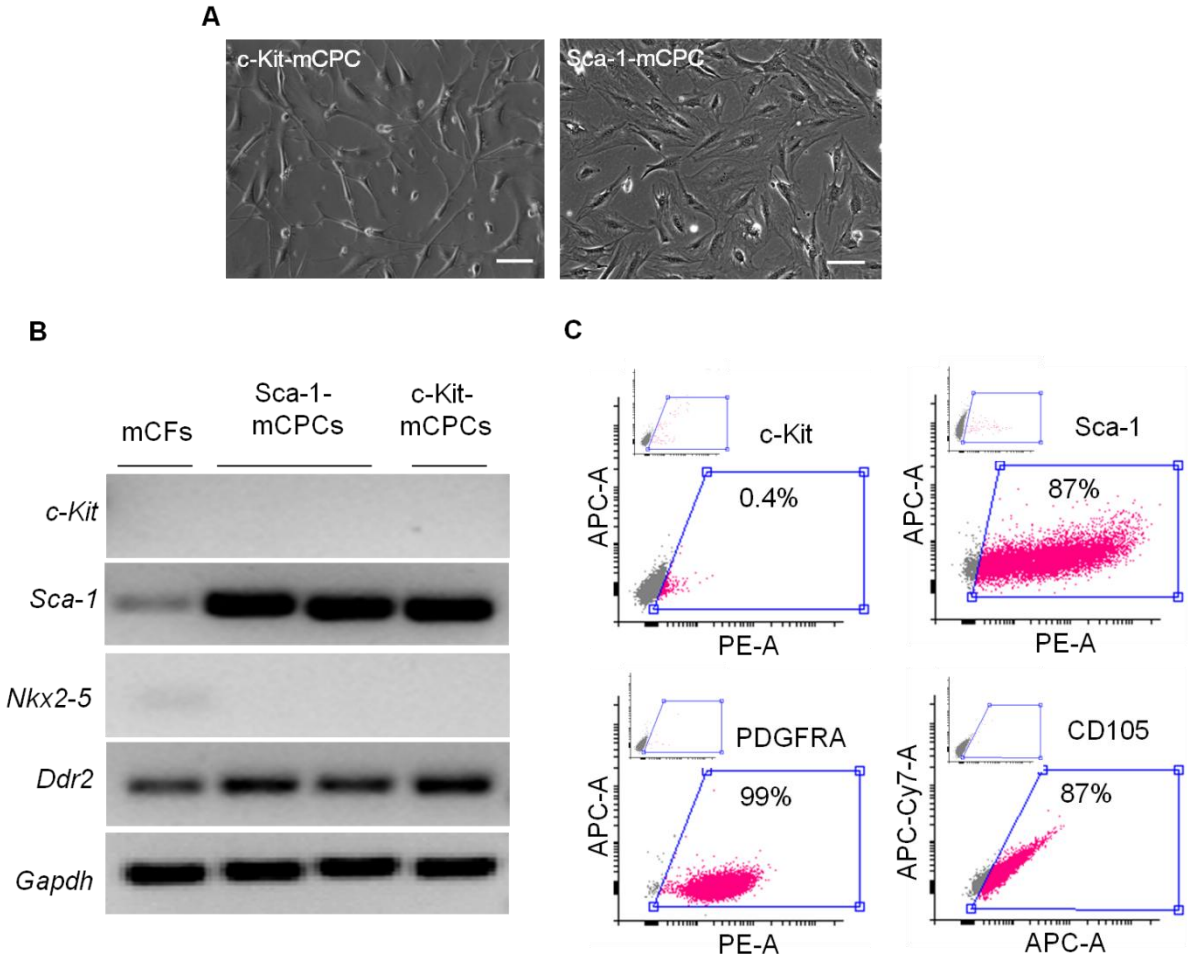

Figure 16. Characterization of mCPCs. A Morphology of c-Kit- and Sca-1-mCPCs in monolayer culture. **B** RNA expression of stem cell markers *c-Kit* and *Sca-1*, early cardiac marker *Nkx2-5* and fibroblast marker *Ddr2* in mouse cardiac fibroblasts (mCFs), Sca-1-mCPC and c-Kit-mCPC by PCR. *Glyceraldehyde-3-phosphate dehydrogenase* (*Gapdh*) was used as housekeeping gene for loading control. **C** Flow cytometry characterization of c-Kit-mCPCs for the expression of the "stem cell markers" c-Kit and Sca-1 (LY6A) as well as mesenchymal cell markers PDGFRA and CD105.

3.1.2 Human CPCs are morphologically distinct from fibroblasts

Human CPCs (hCPCs) isolated based on the c-Kit surface marker were delivered in frozen aliquots from Coretherapix (Spain) as part of a collaboration within the EU FP7 CARE-MI Consortium. hCPCs were used immediately after thawing for characterization without additional culture in our laboratory to avoid technical artifacts that could modify the expression profile and original phenotype of the cells. hCPCs were characterized in direct comparison with human fibroblasts (hFFs: human foreskin fibroblasts) and human embryonic stem cell-derived cardiomyocytes (hCMs).

hCPCs and hFFs showed distinct cell morphologies *in vitro*. hCPCs seemed to display a more spreaded phenotype with frequent protrusions, while hFFs were more elongated (**Figure 17**). hCPCs and hFFs with stable expression of GFP were used.

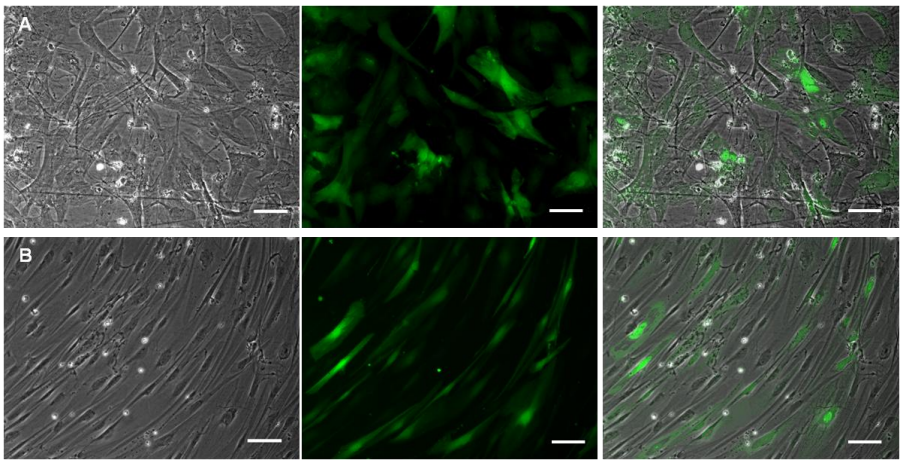

Figure 17. Morphologically distinct phenotypes in hCPC and hFF monolayer cultures. A hCPCs (plated after thawing upon receipt from Coretherapix) and **B** hFFs in brightfield (left), GFP fluorescence (middle) and merged (right) images. Scale bars: 100 µm.

3.1.3 Human CPC pools contain mesenchymal/endothelial cells

Similar as for the mCPCs, there was no c-Kit expression detected in hCPC on mRNA level, although they were originally isolated based on the c-Kit receptor. Interestingly, hFFs were positive for c-Kit on the mRNA level, but also not by flow cytometry. hCPCs showed no expression of the definitive cardiac markers *cardiac troponin I* (*TNNI3*) and *cardiac actin* (*ACTC1*). *NKX2-5* was also not detected in contrast to *GATA4* and the endothelial cell marker *PECAM1* (**Figure 18**).

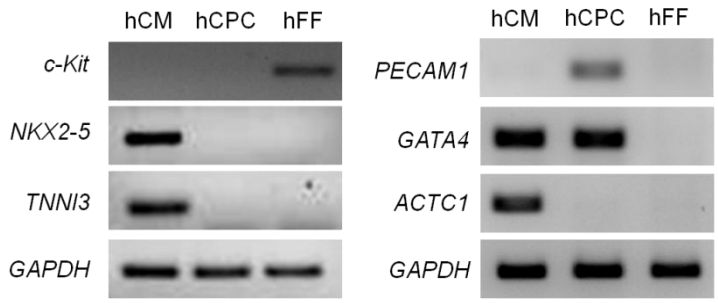

Figure 18. Expression of cardiac cell markers in hCPCs. RNA expression of the "stem cell" marker *c-Kit*, cardiac transcription factors *NKX2-5* and *GATA4*, cardiac markers *TNNI3* and *ACTC1*, endothelial cell marker *PECAM1* in hCMs, hCPCs and hFFs by PCR. *GAPDH* was used as housekeeping gene for loading control.

Next, flow cytometry analysis of cell surface receptor expression confirmed that hCPCs lack c-Kit receptor expression (**Figure 19**). In line with the PCR data (**Figure 19**), a small fraction of hCPCs expressed PECAM1 (7.3±3.7%, n=3/group). In addition, a larger fraction of the hCPCs were decorated by CD90 (35.6±9.9%, n=3/group) and CD105 (60%, n=1/group), indicating a mesenchymal phenotype (**Figure 19**). Given the fact that CD105 plays an important role in angiogenesis (Duff et al. 2003), partial expression of CD105 together with vessel associated marker such as PECAM1 in hCPCs might give a hint for angioblast-like characteristics of hCPCs in the heart. The absence of CD45 positive cells suggested there is no detectable leukocyte contamination (**Figure 19**).

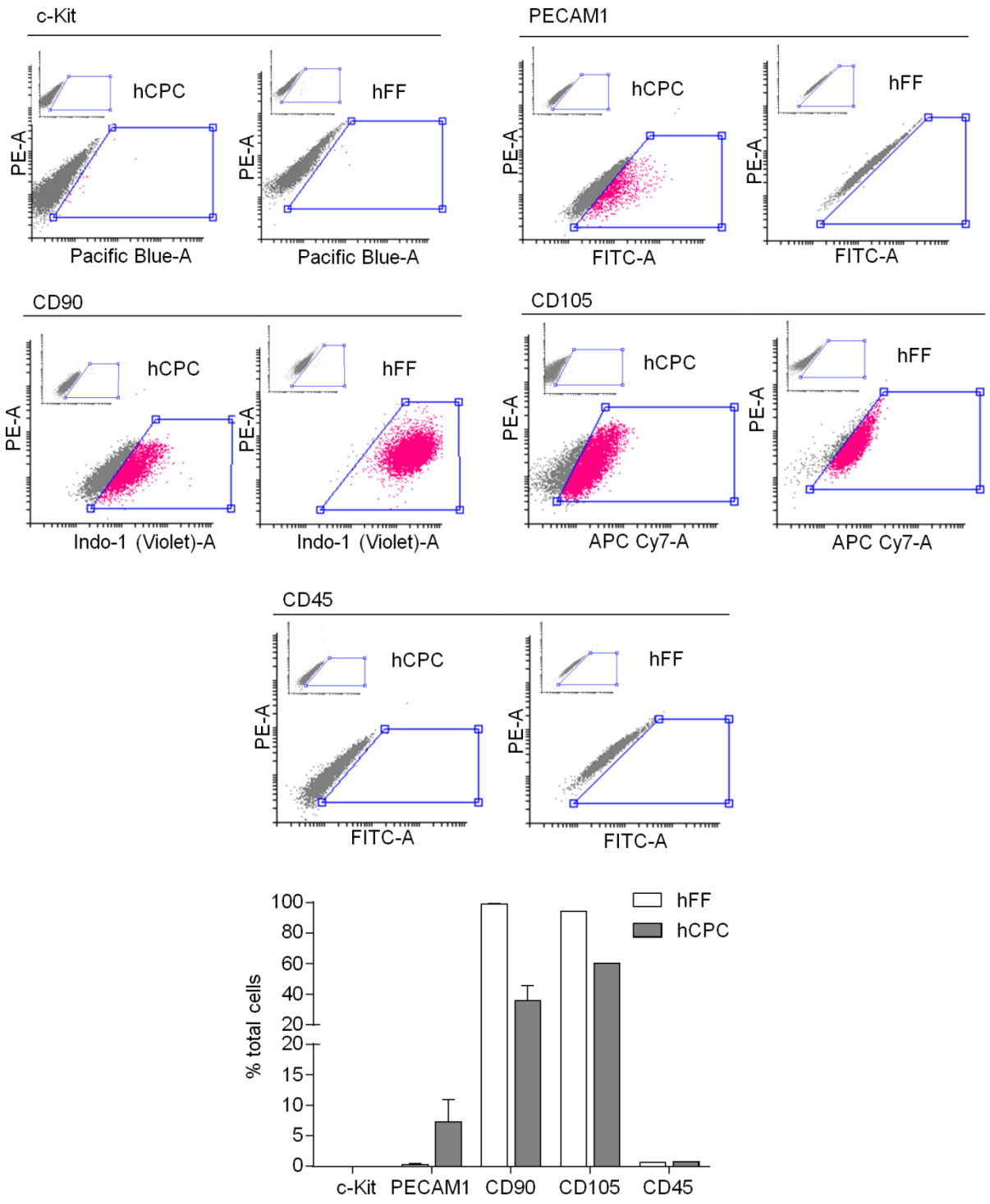

Figure 19. Flow cytometry characterization of hCPCs. Immunophenotype analysis for the expression of stem cell marker c-Kit (n=2/group), endothelial cell marker PECAM1 (n=3/group), pan-leukocyte cell marker CD45 (n=2/group), mesenchymal cell markers CD90 (n=3/group) and CD105 (n=1/group) in hFFs and hCPCs. The bar graph below shows quantification of percentage of positively stained cells for the markers mentioned above. Insets show the respective flow cytometry analyses after exposure to suitable isotype control antibodies.

Collectively, the PCR and flow cytometry data suggest that hCPCs comprise a heterogeneous population, composed of mesenchymal and endothelial cells. GATA4 expression might indicate some cardiomyogenic potential within the hCPC population (**Figure 18**).

3.1.4 Human CPCs exhibit a unique transcriptome profile

The initial PCR and flow cytometry analyses indicated that hCPCs differ from human foreskin fibroblasts (hFFs) and comprise a heterogeneous population of mesenchymal/endothelial cells. RNAseq was performed to further corroborate and extend these findings. Transcriptomes from hCPCs, human cardiac fibroblasts (hCFs), human embryonic stem cell-derived cardiomyocytes (hCMs) and hFFs were compared (**Figure 20**). Principal component analysis (PCA) showed that hCPCs differ from fibroblasts (hFFs and hCFs) and cardiomyocytes, confirming their unique identity (**Figure 20A**). Comparative transcriptome analysis between hCPCs and fibroblasts revealed a set of differentially expressed genes (DEGs) specific for each cell type (hCPC: 1,528, hFF: 1,612, hCF: 1,270 genes; **Figure 20B**). Genes specifically expressed in hCPCs differently than hCFs and hFFs (1,528 genes highlighted with orange color in the Venn diagram) were clustered into certain functional groups by gene ontology analysis suggesting that hCPCs actively transcribe unique plasma membrane, cell adhesion, cytoskeleton, and extracellular proteins (**Figure 20C**). All hCPC specific DEGs with their classifications are summarized in Appendix A5.

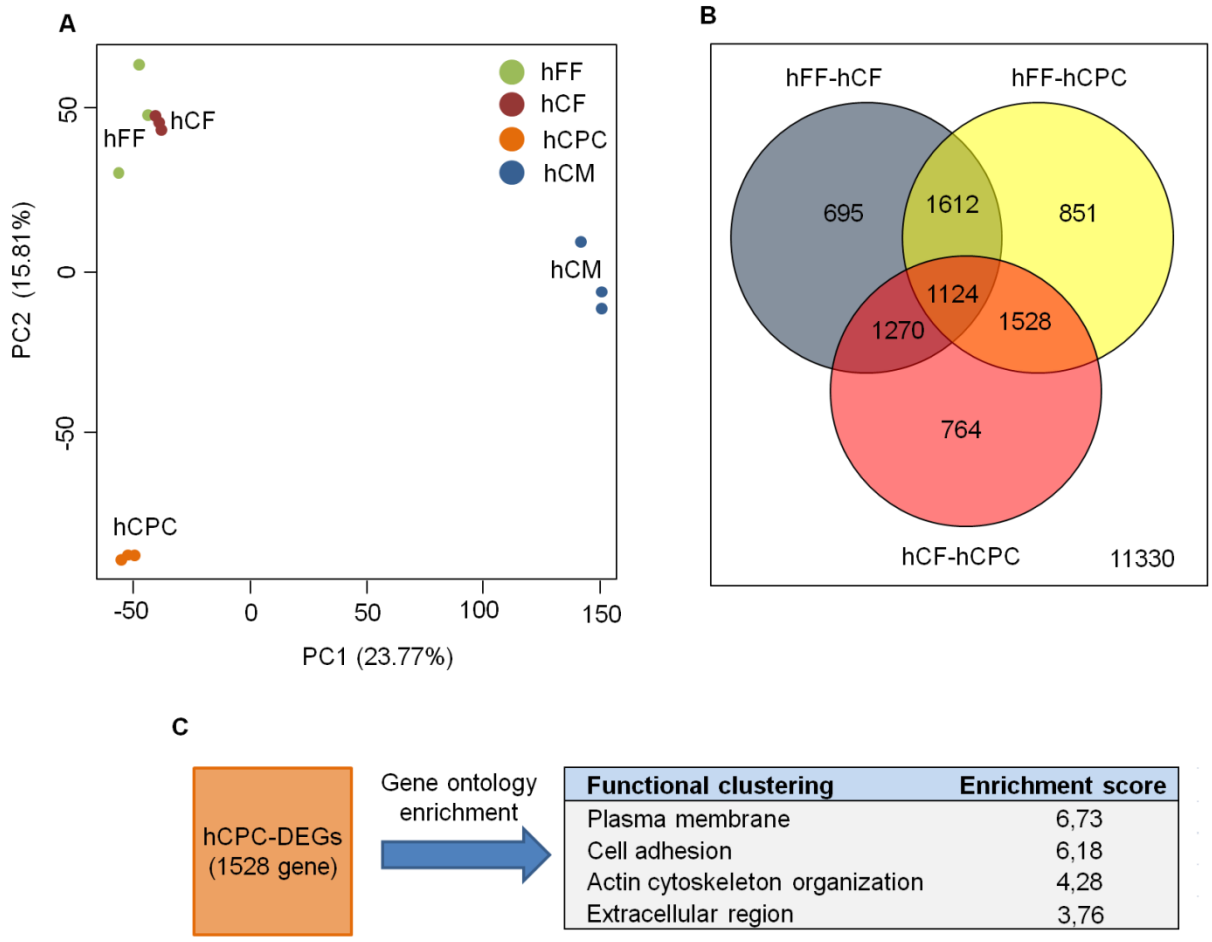

Functional clustering	Enrichment score
Plasma membrane	6,73
Cell adhesion	6,18
Actin cytoskeleton organization	4,28
Extracellular region	3,76

Figure 20. Comparative transcriptome analysis. A Principal component analysis of gene expression in hFFs, hCFs, hCPCs and hCMs (n=3/group). **B** Venn diagram representing the number of differentially expressed genes (DEGs) (Gray: DEGs in hFFs and hCFs, Yellow: DEGs in hFFs and hCPCs, Red: DEGs in hCFs and hCPCs. Intersection of yellow and red circles (in orange) represent DEGs (1,528) specific to hCPCs. **C** Gene ontology enrichment analysis of hCPC-specific DEGs (1,528 genes; represented in orange in the Venn diagram above).

The RNAseq data were further utilized to better define the identity of hCPCs, by analyzing the expression level of genes typically expressed in specific cell populations in the heart: (1) cardiomyocytes, (2) fibroblasts, (3) smooth muscle cells, (4) endothelial cells, (5) pericytes and (6) perivascular MSC-like cells.

hCPCs did not express the mature cardiac marker, *TNNI3* and early cardiac marker *NKX2-5*, but *GATA4* in comparison to hCMs, confirming the earlier PCR data (**Figure 21A**). GATA4 was also detected in hCFs in line with published evidence (Furtado et al. 2014) (**Figure 21A**). hCPCs showed low levels of endothelial cell marker expression comparable to hCFs such as *vascular endothelium calcium dependent*

adhesion molecule (*CDH5*), *CD31* (*PECAM1*) and *kinase insert domain receptor* (*KDR*; **Figure 21B**). Expression analysis of smooth muscle cell markers further indicated that they express *smooth muscle actin* (*ACTA2*), but not mature smooth muscle cell markers like *desmin* (*DES*) and *myosin heavy chain 11* (*MYH11;* **Figure 21C**). They expressed the fibroblast markers *transcription factor 21* (*TCF21*) and *periostin* (*POSTN*) at lower levels, but higher level of *DDR2* compared to hCFs (**Figure 21D**). Interestingly, they seemed to be positive for all the markers expressed in pericytes; especially *MCAM* and *chondroitin sulfate proteoglycan* (*CSPG4*) when compared to all other cell types as well as the *PDGFR beta subunit* (*PDGRB*; **Figure 21E**). Lastly, hCPCs also showed markedly higher expression of perivascular mesenchymal stem cell (MSC)-like cells associated marker (Kramann et al. 2015) *glioma associated oncogene homolog 1* (*GLI1*; **Figure 21F**).

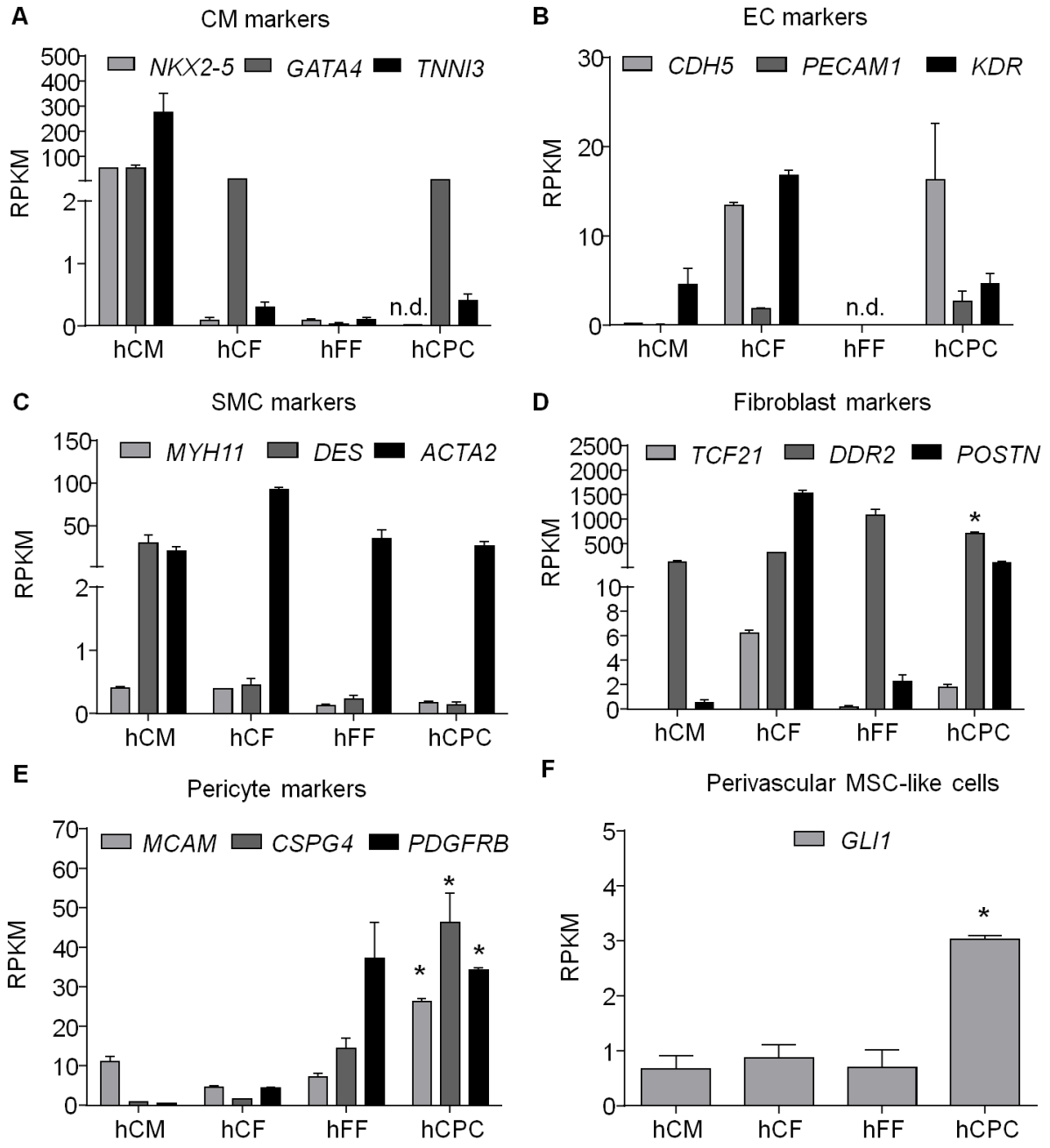

Figure 21. Expression profile of cardiac cell-specific markers. Data is from RNAseq datasets and displayed as RPKM (reads per kilobase of transcript per million mapped reads) values from the individual cell populations (hCMs, hCFs, hFFs and hCPCs; n=3/group). **A** Cardiomyocyte (CM) markers *NKX2-5*, *GATA4*, and *TNNI3*; **B** endothelial cell (EC) markers *CDH5*, *PECAM1* and *KDR*; **C** smooth muscle cell (SMC) markers *MYH11*, *DES* and *ACTA2;* **D** fibroblast markers *TCF21*, *DDR2* and *POSTN*; **E** pericyte markers *MCAM*, *CSPG4* and *PDGFRB;* **F** perivascular MSC-like cell marker *GLI1*. *p<0.05, hCF vs. hCPC by one-way ANOVA with Dunnett's *post-hoc* test.

Taken together, transcriptome profile analyses suggested a pericyte and MSC-like origin of hCPCs with little evidence for cardiomyocyte, smooth muscle, fibroblast or endothelial fate.

3.2 Cardio-supportive effects of mouse CPCs in EHM

Stromal cells play an important role in supplying key factors (e.g. extracellular matrix, growth factors, cytokines) for the formation of a cardiogenic niche (Christalla et al. 2012, Tiburcy et al. 2011). Engineered heart muscle (EHM), as a model of heart muscle development *in vitro*, may be utilized as an experimental platform to gain insight into specific cardio-instructive properties of stromal cells, including CPCs.

3.2.1 CPCs support functional maturation of EHM

To investigate if mouse CPCs support cardiac muscle formation, EHMs were made from purified mouse ESC-derived cardiomyocytes (mCMs; 82±4% α-actinin positive, n=5; **Figure 22A,B**) and mouse adult heart derived c-Kit-mCPCs. In a first set of experiments the optimal myocyte/non-myocyte ratio was determined. mCMs and mCPCs were mixed in different ratios (CM/CPC) ranging from 100/0% to 50/50% respectively, keeping the total cell number the same. After 3 days of hydrogel consolidation inside custom-made molds, tissues were transferred onto static stretchers to be mechanically stimulated for functional maturation for the following 11 days (**Figure 22C**).

Macroscopic analysis of muscle morphology showed that EHMs composed of only cardiomyocytes were distinctly larger and softer than the EHMs supplemented with mCPCs or mouse cardiac fibroblasts (mCFs), supporting the previously identified role of stromal cells (CFs) for tissue compaction. mCPCs supported EHM formation similarly as mCFs (**Figure 22D**).

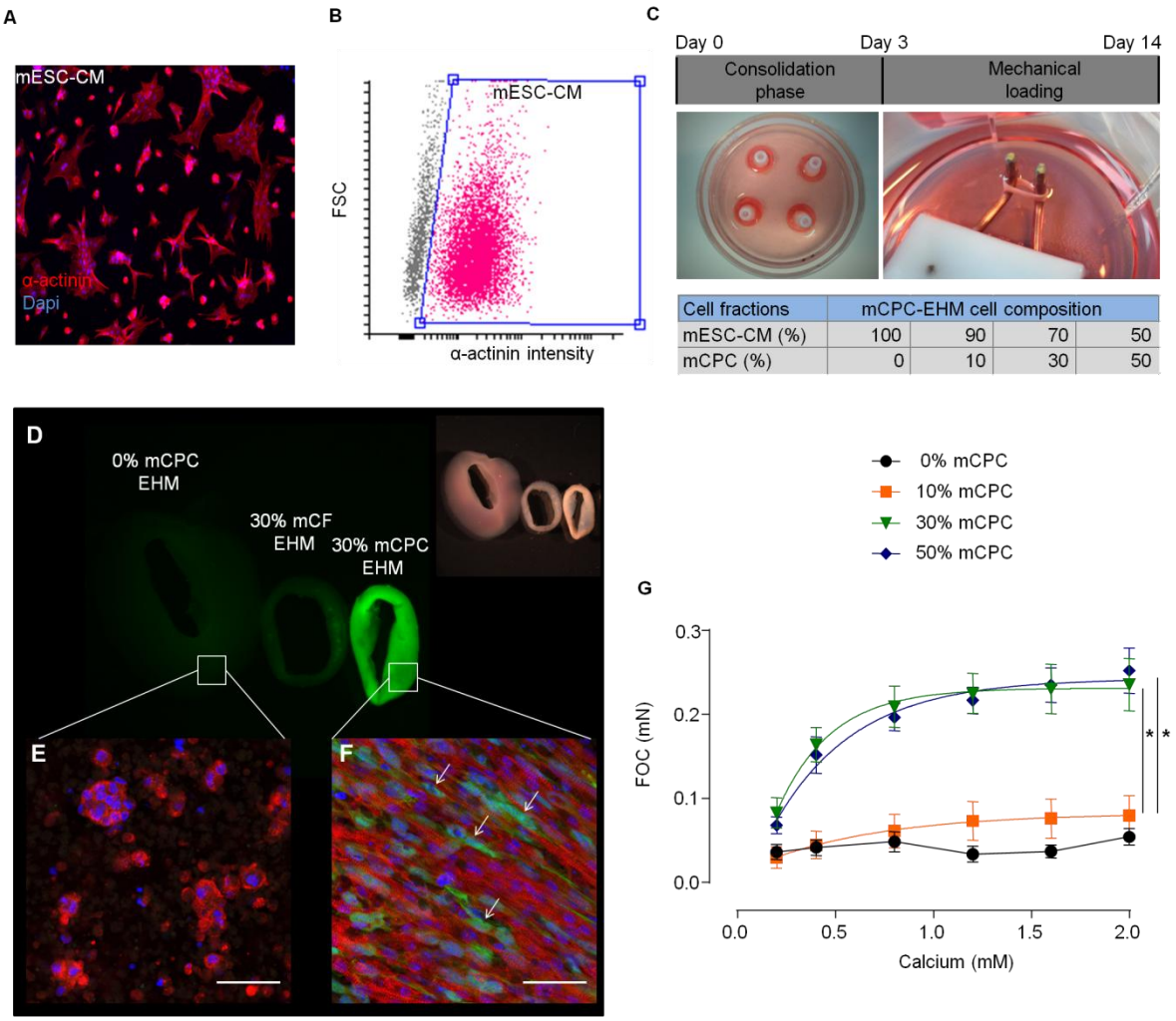

Figure 22. EHM structure and function enhanced by mCPCs. **A** Cardiomyocytes dissociated from antibiotic-selected mouse cardiac bodies after spontaneous cardiac differentiation (red: α-actinin, blue: Hoechst nuclear staining) and **B** flow cytometry analysis after staining for sarcomeric α-actinin to determine cardiomyocyte purity (n=5). **C** EHM cell composition: cardiomyocytes (mESC-CMs) and mCPCs ratio were as indicated in the box; the culture as indicated for 3 days in custom-made molds for tissue consolidation, followed by 11 days of mechanical stimulation for functional maturation. **D** GFP fluorescence (mCPCs were GFP^+) and brightfield images (top right) of EHM without CPCs (0%), 30% mCFs and 30% GFP^+ mCPCs. **E** Cardiomyocyte structure and alignment in mEHM with 0% GFP^+ mCPCs and **F** 30% GFP^+ mCPCs (indicated by arrows). **G** Force of contraction (FOC) generated in mEHM in response to increasing extracellular calcium concentration (n=7/group from two experiments, two-way ANOVA, *p<0.05).

Immunostaining of EHMs without CPCs (CM/CPC; 100/0%) revealed that cardiomyocytes (red, α-actinin positive) remained round shaped in small clusters and distributed randomly without proper alignment and coupling throughout the matrix

(**Figure 22E**). Consistent with the underdeveloped structure of the cardiomyocytes, EHMs without mCPCs failed to develop any measurable force (**Figure 22G**). In contrast, EHM composed of cardiomyocytes supplemented with mCPCs showed enhanced alignment and sarcomere development. Accordingly, force of contraction (FOC) was markedly enhanced in EHM supplemented with >10% mCPC (**Figure 22F,G**).

We next wanted to scrutinize potential differential effects of mCPCs and fibroblasts on functional maturation of EHM. For this, a supplementation of mCMs with 30% mCPCs or mouse embryonic fibroblasts (mEFs) was performed. Indeed, EHMs generated with mCPCs produced FOC similar to the EHMs supplemented with mEFs, suggesting that mCPCs have comparable cardio-instructive properties as fibroblasts (mEF-EHM: 0.36±0.05 mN, mCPC-EHM: 0.29±0.04 at 3.2 mM calcium, n=16/group; **Figure 23A**). Interestingly, mCPC-EHM displayed markedly higher sensitivity to calcium, suggesting for a more immature calcium handling machinery when compared to mEF-EHM (mEF-EHM: 0.74±0.05 mM EC_{50} calcium, mCPC-EHM: 0.53±0.22 mM EC_{50} calcium; $p<0.05$, n=16/group **Figure 23B**).

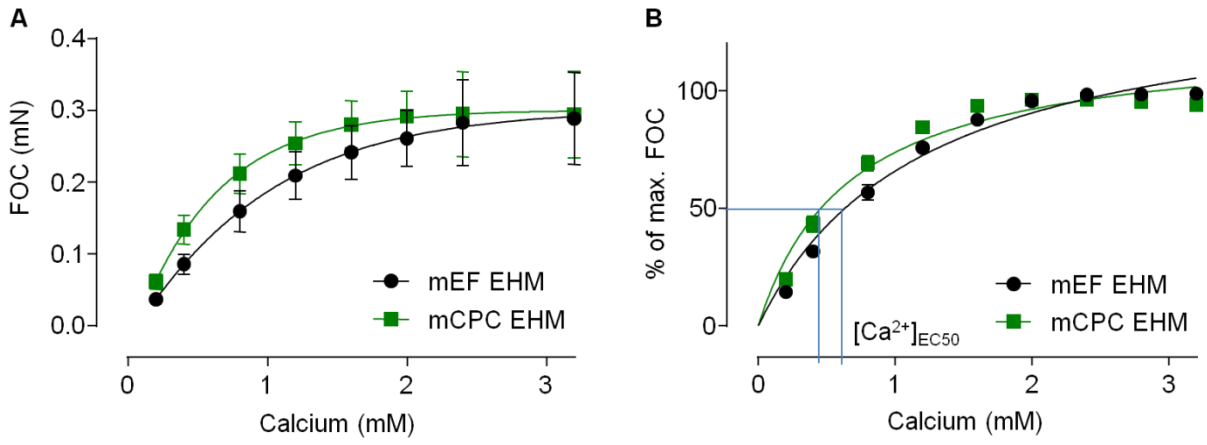

Figure 23. Functional comparison of mCPC- and mEF-EHMs. A Force of contraction (FOC) generated in mCPC- and mEF-EHM under increasing extracellular calcium concentration in thermostatted (37 °C) Tyrode's solution and electrical field stimulation (2 Hz; n=16/group). **B** Display of FOC as percent of maximal FOC to determine the EC_{50} for calcium in mEF-EHM and mCPC-EHM; the EC_{50} for the respective groups is marked by blue lines (n=16/group, unpaired *t*-test, *****$p<0.05$).

3.3 Enhanced paracrine support by genetic manipulation of mouse CPCs

Paracrine factors are one of the key components contributing to the cardiogenic niche (Christalla et al. 2012). The paracrine activity of mCPCs may support cardiac function and could be augmented by overexpression of microRNA-133a. MicroRNA (miR)-133a is one of the muscle specific microRNAs that play an important role in the regulation of embryonic heart development and cell death (Meder et al. 2008).

Further, it was observed that mCPCs overexpressing miR-133a enhance cardiac functions upon injection into the heart after myocardial infarction in a rat model (Izarra et al. 2014). Reduced cardiomyocyte death and hypertrophy as well as increase in the number of DNA-replicating cardiomyocytes were suggested as the possible mechanisms underlying the beneficial effect *in vivo*, which could have been mediated by enhanced paracrine activity in CPCs overexpressing miR-133a. To further scrutinize this hypothesis, we developed an EHM model with defined neonatal rat cardiomyocytes and mCPC composition (3:1 ratio). mCPCs were genetically modified to express miR-control or miR-133a. Purity of neonatal rat cardiomyocytes was enhanced by preplating (84±3% α-actinin positive, n=8), the remaining ~15% percent are mainly comprised of rat firbroblasts (**Figure 24**). mCPC supplemented EHM could be easily distinguished by the expression of GFP (**Figure 25A**).

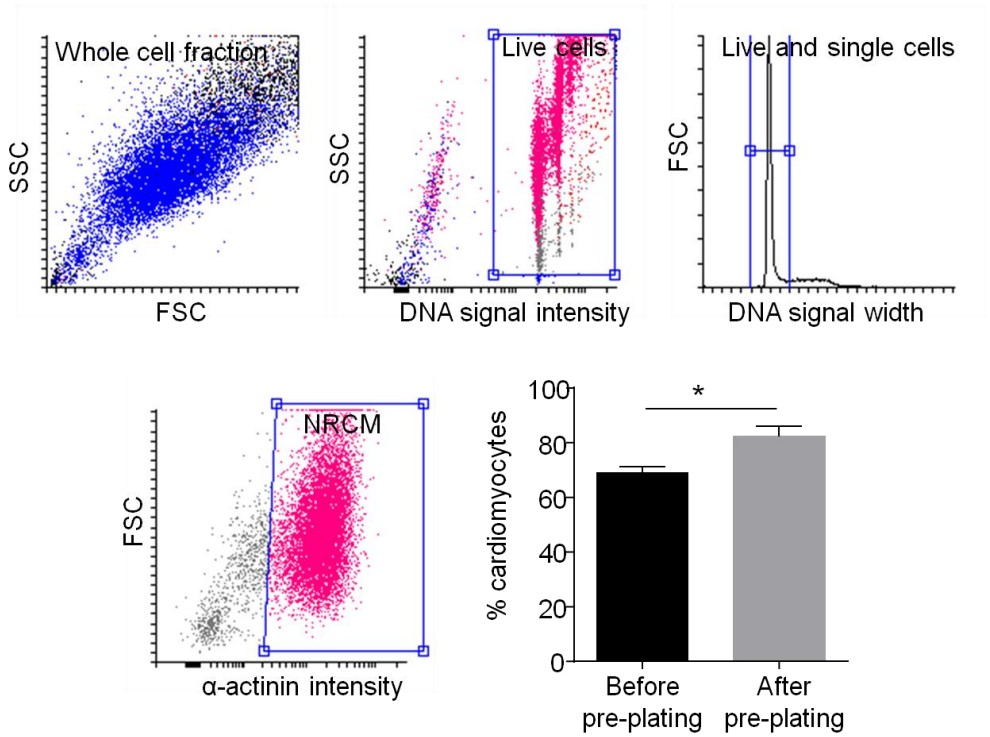

Figure 24. Purification of neonatal rat cardiomyocytes. Gating strategy of the flow cytometry analysis of cardiomyocyte purity is displayed. Forward (FSC) and sideward scatter (SSC) analyses were followed by gating living cells based on DNA signal intensity and signal width (Hoechst-nuclear staining). Cardiomyocytes were identified by specific labelling for α-actinin positive before and after myocyte enrichment by pre-plating (n=8/group from 8 experiments, unpaired *t*-test, *p<0.05).

EHMs with miR-133a-CPCs developed significantly higher FOC (**Figure 25B**). The number of apoptotic cardiomyocytes (caspase-3 positive) was reduced at day 3, which resulted in a higher percentage of cardiomyocytes remaining in miR-133a-EHM at day 12 when compared to miR-control-EHM (**Figure 25C,D**). Real-time PCR analysis of growth factor expression in mCPCs revealed that expression level of *Igf-1, Vegf, Hgf and bFgf*, which are involved in cardiomyocyte survival, growth and proliferation, were all increased in miR-133a-EHM, suggesting an involvement of miR-133a in the paracrine activity of mCPCs (**Figure 25E**). Collectivley, this data supported the *in vivo* studies in providing addition evidence for genetically enhanced paracrine activity of mCPCs by miR-133a.

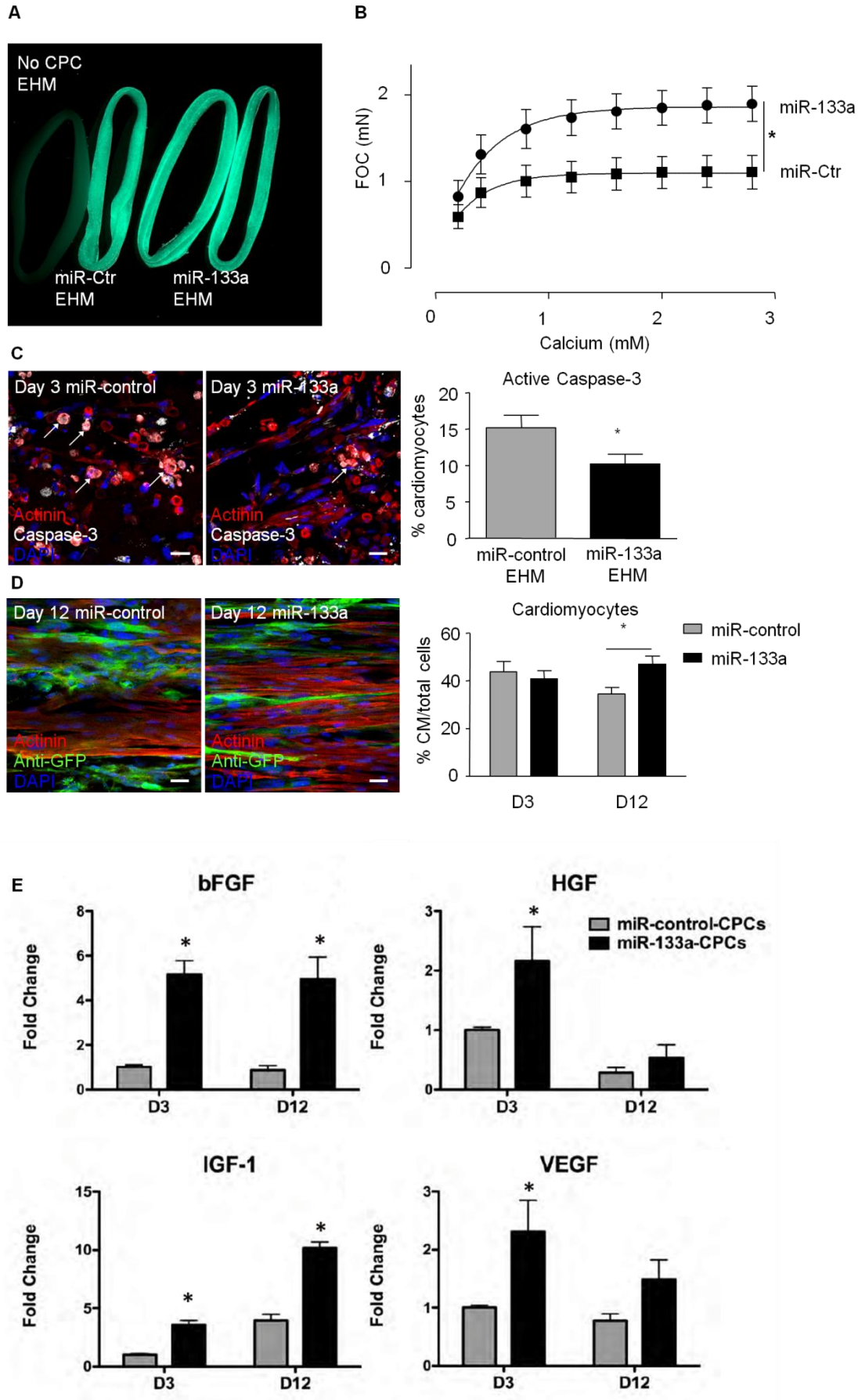
A
No CPC
EHM
miR-Ctr
EHM
miR-133a
EHM
B
FOC (mN)
Calcium (mM)
miR-133a
miR-Ctr
*
C
Day 3 miR-control
Day 3 miR-133a
Actinin
Caspase-3
DAPI
Active Caspase-3
% cardiomyocytes
miR-control
EHM
miR-133a
EHM
D
Day 12 miR-control
Day 12 miR-133a
Actinin
Anti-GFP
DAPI
Cardiomyocytes
% CM/total cells
miR-control
miR-133a
D3
D12
E
bFGF
HGF
IGF-1
VEGF
Fold Change
miR-control-CPCs
miR-133a-CPCs
D3
D12

Figure 25. miR-133a enhanced paracrine activity of mCPCs. **A** EHM containing mCPC could be identified by GFP^+ fluorescence; images were taken on culture day 12. **B** Force of contraction (FOC) generated in miR-control (n=6) and miR-133a-CPC-EHMs (n=6) in response to calcium. **C** Representative images of whole-mount caspase-3 staining in miR-control- and miR-133a-CPC-EHMs (left; α-actinin, red; activated caspase-3, white; DAPI-stained nuclei, blue; scale bars: 20 µm); bar graph (right): quantification of the percentage of caspase-3 positive cardiomyocytes in EHM at culture day 3; n>1,000 cells from three experiments. **D** Representative images of cardiomyocytes with miR-control- and miR-133a-CPCs (left; α-actinin, red; antibody detected GFP, green; DAPI-stained nuclei, blue; scale bar: 20 µm); bar graph (right): quantification of the percentage of cardiomyocytes in EHM at culture days 3 and 12; n>1,000/group from two and three experiments. **E** Expression level of *bFgf*, *Hgf*, *Igf-1* and *Vegf* in miR-control- and miR-133a-CPC-EHMs at culture day 3 and 12; PCR was performed by Alberto Izarra (n=3/group from three experiments). *p<0.05 by two-way ANOVA with Bonferroni *post-hoc* test (**B**) and unpaired, two-tailed Student's *t*-test (**C-E**). Data was published in (Izarra et al. 2014).

3.4 Human EHM model

To investigate possible cardiogenic function of human CPCs (hCPCs), hEHMs using the same principles as in the mouse model were generated. Human cardiomyocytes were derived from human embryonic stem cells (HES2-RFP) after directed differentiation and metabolic selection (average cardiomyocyte purity: 89±3% α-actinin$^+$ cells; n=3, **Figure 26A**). In parallel, hEHMs were made with fibroblasts derived from human foreskin (hFFs) to serve as a reference (**Figure 26B**).

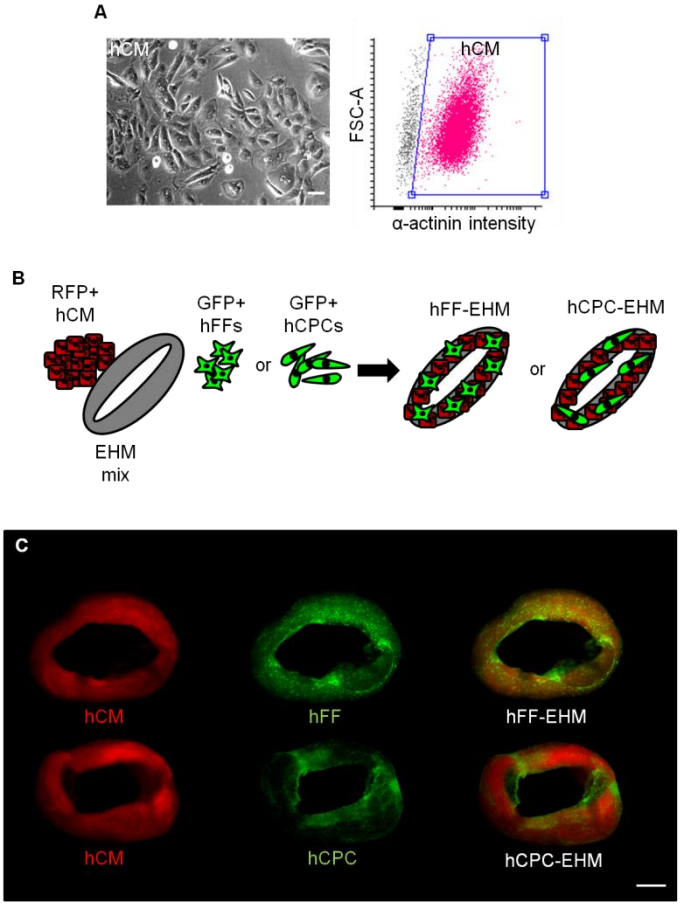

Figure 26. Defined hEHM model composed of RFP$^+$-hCMs and GFP$^+$-non-myocytes. **A** Brightfield image of hCMs with a representative flow cytometry plot (right) with the identification of cardiomyocytes (sarcomeric α-actinin$^+$). **B** Schematic representation of hEHM construction strategy with cell-type color-coding: hCMs RFP$^+$ / hFFs GFP$^+$ / hCPCs GFP$^+$. **C** hFF-EHM (RFP$^+$ hCMs, GFP$^+$ hFFs) and hCPC-EHM (RFP$^+$ hCMs, GFP$^+$ hCPCs) under GFP and RFP fluorescence, with merged images (rightmost). Scale bar: 1 mm.

Based on the fluorescence imaging of RFP and GFP positive cells in EHM sections, cardiomyocytes and fibroblasts were observed more randomly distributed within the hFF-EHM matrix, whereas hCPCs tended to cluster towards the surface of the hCPC-EHM (**Figure 27A**). This finding suggests that hCPCs have the property to migrate in EHM. Cardiomyocytes showed similar elongation and cross-striations in both hFF- and hCPC-EHMs (**Figure 27B**).

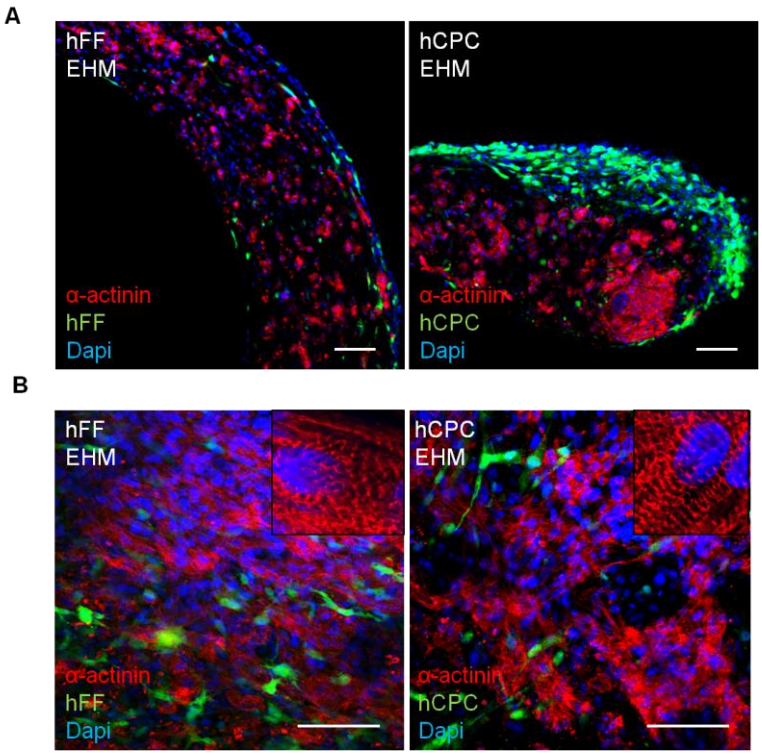

Figure 27. Cell distribution and cardiomyocyte morphology in hEHM. **A** Low magnification overview of RFP^+ hCMs and GFP^+ non-myocytes in hFF-EHM (left) and hCPC-EHM (right). **B** Orientation and structure of cardiomyocytes in hFF-EHM (left) and hCPC-EHM (right). (Cardiomyocytes: red, α-actinin$^+$; hFFs and hCPCs: GFP^+; nuclei stained with the DNA-binding dye Hoechst in blue). Scale bars: 100 µm.

3.4.1 Contractile performance in human EHM

hFF-EHM developed significantly higher FOC than hCPC-EHM (hFF-EHM: 0.67±0.08 mN, hCPC-EHM: 0.43±0.03 mN at 4 mM calcium, n=29/group *p<0.05; **Figure 28A**). On the other hand, they showed similar sensitivity to calcium (hFF-EHM: 0.88±0.26 mM EC_{50} calcium, hCPC-EHM: 0.97±0.37 mM EC_{50} calcium, n=29/group; **Figure 28B**) suggesting similar maturation of calcium handling machinery. β-adrenergic stimulation with isoprenaline (1 µmol/L) significantly enhanced FOC development in both hEHMs at EC_{50} calcium concentration (increase in FOC from baseline: 91±14% in hFF-EHM, 61±9% in hCPC-EHM; n=29/group), with however no obvious difference between the investigated groups (**Figure 28C**). Both hEHM co-cultures responded to cholinergic stimulation (carbachol) with the anticipated decrease in FOC, with however a significantly smaller reduction in FOC in hCPC-EHMs as compared to

hFF-EHM (decrease in FOC: hFF-EHM: 17±2%, hCPC-EHM: 12±2%, n=29/group, *p<0.05; **Figure 28C**).

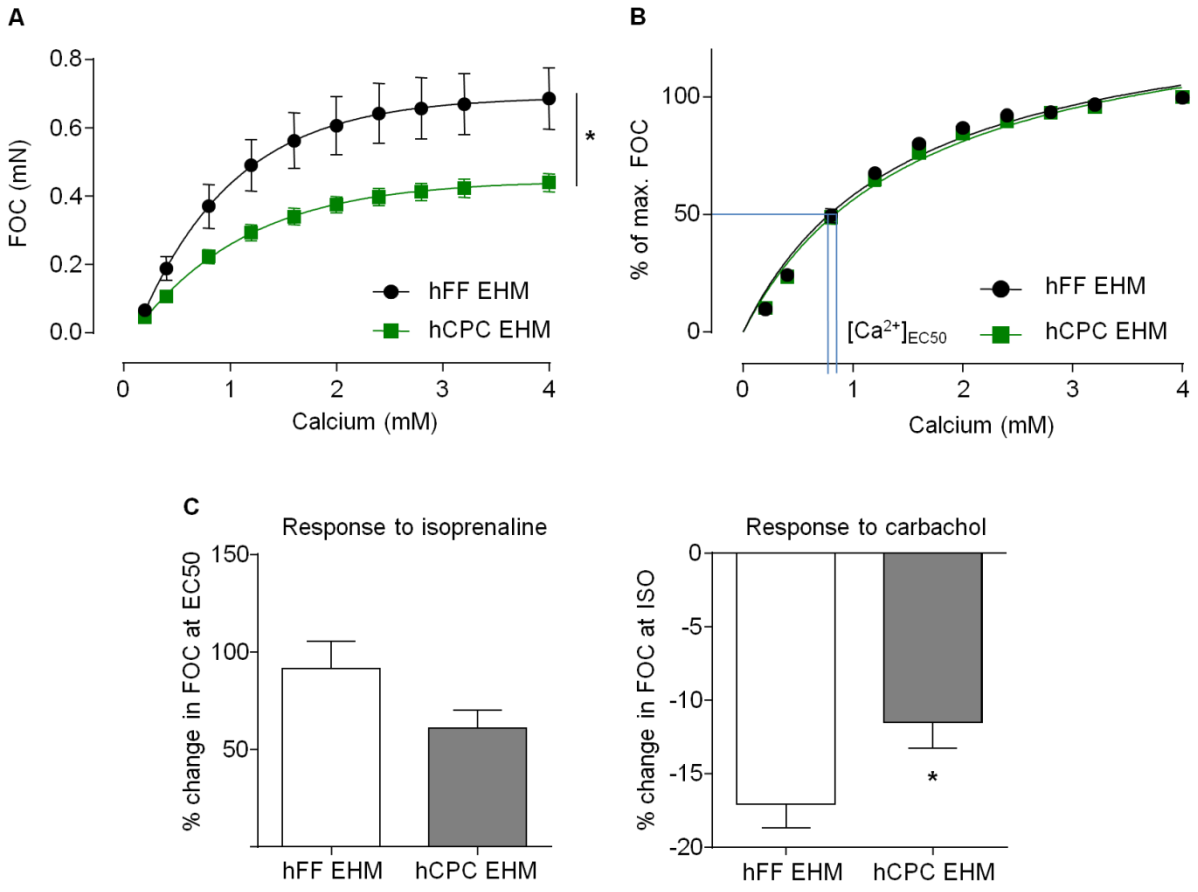

Figure 28. hCPCs and hFFs supported EHM. A Force of contraction (FOC) generated in hFF- and hCPC-EHM in response to gradually increasing extracellular calcium concentrations. **B** FOC as percent of maximal FOC to determine the apparent EC_{50} for calcium in hFF- and hCPC-EHM; the EC_{50} for the respective groups is marked by blue lines (n=29/group). **C** Response to isoprenaline (1 µmol/L) as percentage change in FOC at EC_{50} calcium and response to carbachol (10 µmol/L) as percentage change in FOC after treatment with isoprenaline (n=29/group, unpaired *t*-test, *p<0.05).

3.4.2 Passive biomechanical properties in human EHM

Besides the role of providing structural support and organization to the tissue, the biophysical properties of EHM may be affected by stromal cells. Stromal cells are key contributors to EHM stiffness (Naito et al. 2006). To identify whether hFFs and hCPCs influence tissue stiffness differentially, resting tension (ReT – diastolic force) was determined and found to be similar in hFF-EHM and hCPC-EHM (**Figure 29A**).

Accordingly, FOC/ReT ratio was higher in hFF-EHM as compared to hCPC-EHM (2.5±0.3 vs. 1.5±0.2, n=28/group, unpaired t-test, *p<0.05; **Figure 29B**).

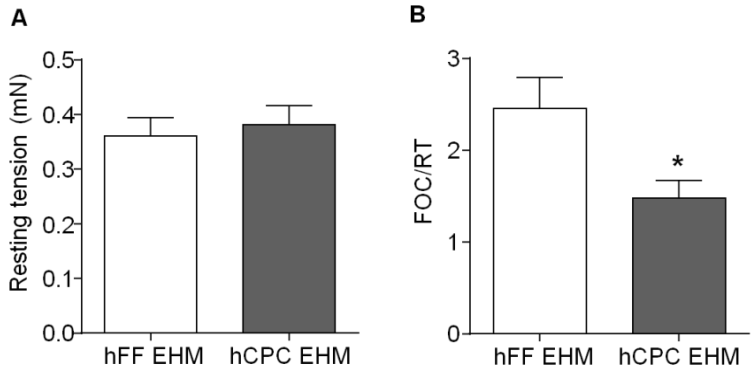

Figure 29. Passive mechanical properties of hEHM. **A** Resting tension (ReT) at Lmax and **B** ratio of force of contraction (FOC) to ReT in hFF- and hCPC-EHMs (n=28 /group, unpaired *t*-test, * p<0.05). Lmax: length at maximum FOC.

Taken together, histological and functional analysis of hEHMs suggested that hCPCs were able to support heart muscle formation in EHM, albeit less efficiently as compared to hFFs. Differences in hFF versus hCPC localization, i.e., homogeneous versus surface localization will require further investigations.

3.4.3 Cardiomyocyte structure and function in human EHM

To further investigate the underlying mechanisms leading to less functional development in hCPC-EHM, cardiomyocyte content, maturation and structural development were assessed in comparison to hFF-EHM.

Cardiomyocyte amount in EHM was assessed through quantification of sarcomeric α-actinin positive cells by flow cytometry. The number of cardiomyocytes recovered from EHM after 14 days of culture was similar between the groups (hFF- vs. hCPC-EHM: 3±0.3 x 10^5 vs. 3.2±0.2 x 10^5, n=10/group from three experiments; **Figure 30A**) suggesting that the actual reason of lower FOC development in hCPC-EHM was not due to the muscle cell amount, but less FOC generation per cardiomyocyte (hFF- vs. hCPC-EHM: 3±0.4 vs. 1.6±0.1 nN, n=3/group, from three experiments, *p < 0.05; **Figure 30B**). To investigate the possible reason behind this impaired functional

maturation of cardiomyocytes in hCPC-EHM, the percentage of cardiomyocytes expressing Ki67 as a marker for maintained cell cycle activity in cardiomyocytes was analyzed. However, no significant difference was detected between the EHM co-culture groups (hFF- vs. hCPC-EHM: 19±5 vs. 17±4%, n>1,000 cells/group from three experiments; **Figure 30C**). Next, cardiomyocyte size and actinin intensity were compared to assess their structural maturation in the EHMs by flow cytometry analysis. Cardiomyocytes were not different in size (n=10/group from three experiments; **Figure 30D**), but demonstrated almost 10% less sarcomeric α-actinin in hCPC-EHM compared to the cardiomyocytes in hFF-EHM (actinin signal intensity/cardiomyocyte relative to hFF-EHM group: 1±0.03 vs.0.91±0.04 in hCPC-EHM, n=10/group from three experiments, *p<0.05 (**Figure 30E**).

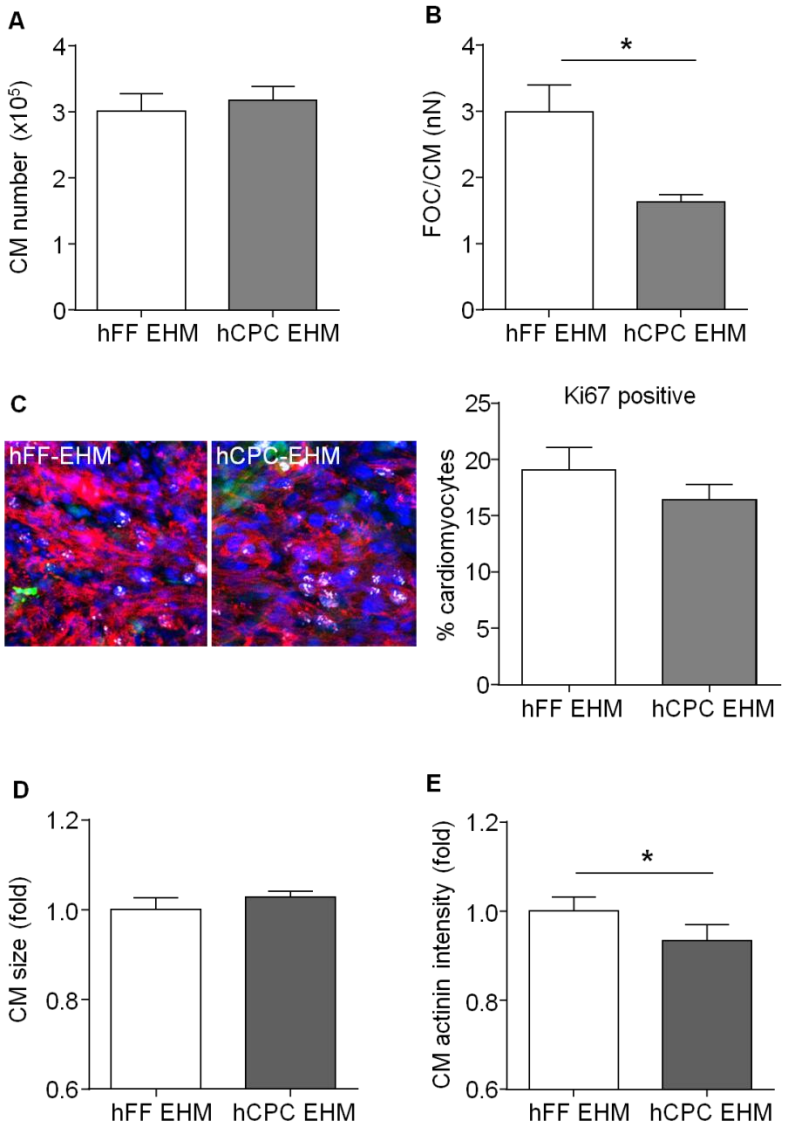

Figure 30. Cardiomyocyte amount and phenotype in hEHM. A Number of cardiomyocytes (α-actinin positive cells detected by flow cytometry) in hFF- and hCPC-EHM (n=10/group). **B** Force of contraction (FOC) per EHM-cardiomyocyte (maximum FOC at 4 mM of calcium concentration divided by total cardiomyocyte number in EHM; n=3/group, unpaired *t*-test, *p<0.05). **C** Representative images of whole-mount Ki67 stainings in hFF- and hCPC-EHM (left; red: α-actinin, white: Ki67 and blue: Hoechst stained nuclei); bar graph (right) with quantification of percentage of Ki67 positive cardiomyocytes at day 14, n>1,000 cells from three experiments. **D** Relative size of cardiomyocytes (FSC-A median of α-actinin positive cells by flow cytometry; n=10/group from three experiments; reference group: hFF-EHM). **E** Relative α-actinin intensity (median fluorescence intensity of α-actinin positive cells by flow cytometry, n=10/group from three experiments; reference group: hFF-EHM; unpaired *t*-test, *p<0.05).

Taken together, these findings suggest that the potential mechanism behind reduced contractile function in hCPC-EHM when compared to hFF-EHM could be suboptimal structural and functional maturation of cardiomyocytes.

3.4.4 Human CPC retention in EHM

Cell retention is generally low after intramyocardial injection (Tossios et al. 2008). Retention of hCPCs in EHM was determined by flow cytometry. Upon dissociation of the EHM into single cell suspension living cells were identified by flow cytometry based on the Sytox DNA binding dye exclusion; single cells were identified by Hoechst staining (**Figure 31A**). Next, color-coded cell fractions were separated based on their respective fluorescence signals (cardiomyocytes: RFP^+, stromal cells: GFP^+); potential cell fusion events should be revealed as double positive cells for RFP and GFP (**Figure 31B**). A marked reduction on GFP^+ (hCPC or hFF) cell number was observed by hEHM culture day 14 (day 0: 3.6×10^5 GFP^+ cells, hFF-and hCPC-EHM on culture day 14: $0.48 \pm 0.04 \times 10^5$ and $0.36 \pm 0.06 \times 10^5$ GFP^+ cells, respectively; n=14/group from three experiments). Double positive cells were rarely detected with 0.7±0.2 and 0.3±0.05% in hFF- and hCPC-EHM; **Figure 31B**).

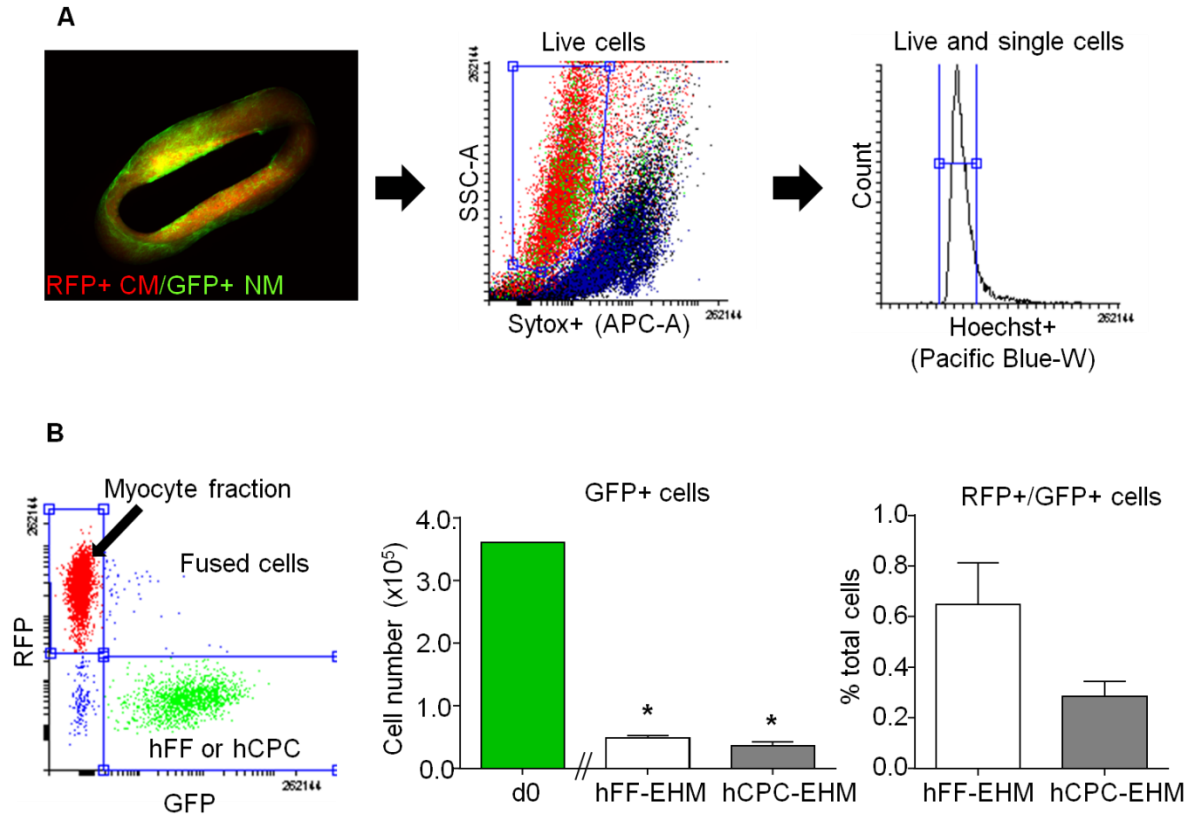

Figure 31. Retention of non-myocytes in hEHM. A Flow cytometry gating strategy to determine living (Sytox negative), single cells (Hoechst positive, with uniform signal width) in color-coded hEHM (cardiomyocytes: RFP^+; non-myocytes: GFP^+; representative image on the left). **B** Left plot: flow cytometry gating protocol to separate RFP^+ cardiomyocytes and or GFP^+ non-myocytes (NMs: hFFs or hCPCs); middle panel: quantification of the number of GFP^+ hFFs or GFP^+ hCPCs at day 0 (input number) in comparison to the respectively isolated hFFs and hCPCs from EHM on culture day 14 (n=14/group); right panel: quantification of the percentage of double positive cells for RFP and GFP (RFP^+/GFP^+ cells; n=14/group); *P<0.05 vs. d0 by Student's *t*-test.

3.4.5 No evidence of cardiomyocyte transdifferentiation in human EHM

To investigate whether hCPCs are able to differentiate into cardiomyocytes, EHM were digested into single cells and subjected to the following analyses: (1) flow cytometry analysis of α-actinin expressing GFP^+ cells (**Figure 32A**), (2) fluorescence-activated cell sorting (FACS) followed by qPCR for *cardiac musle α-actin* (*ACTC1*) transcipts in the RFP^+ cardiomyocyte and GFP^+ stroma cell pools (**Figure 32B**).

The cardiomyocyte ($actinin^+$) and non-myocyte populations could be clearly separated by flow cytometry analysis with a small amount of double positive cells,

suggesting cell fusion or transdifferentiation in EHM culture; interestingly, there was no difference in the amount of actinin$^+$/GFP$^+$ cells in the hFF- and hCPC-EHM (hFF- vs. hCPC-EHM: 4.0±0.7% vs. 7.4±1.8%, n=6/group from four experiments; **Figure 32A**). Given no evidence for transdifferentiation of hFFs, we concluded that the similarity of the amount of double positive cell populations in hFF- and hCPC-EHM was most likely due to false-positive antibody labelling in the non-myocyte pool. To further scrutinize this, RFP$^+$ cardiomyocytes and GFP$^+$ non-myocytes from culture day 14 hEHM were separated by FACS and independently subjected to RNA isolation followed by qPCR to analyze transcription of the cardiomyocyte specific *ACTC1* gene. The data from this experiment indicated a 100-fold higher *ACTC1* abundance in the hCM pool in comparison to the respective hFF and hCPC pools (**Figure 32B**). Interestingly, *ACTC1* transcript abundance was also 100-fold higher in the GFP$^+$ cells isolated from EHM as compared to the input GFP$^+$ populations. A separate qPCR amplification of RFP (unique cardiomyocyte label) suggested carry-over during the separation of the GFP$^+$ cell pools by FACS (**Figure 32C**). This notion was further supported by fluorescence microscopy of the separated cell pools with little, but detectable contaminating RFP$^+$ cells in the GFP$^+$-sorted cell population (**Figure 32D**). Taken together and despite some hints for non-myocyte differentiation or fusion we conclude that the most likely explanation for RFP$^+$/actinin$^+$ cells in the GFP$^+$ hFF and hCPC pools would be cardiomyocyte carry-over. Single cell PCR and RNA-sequencing technologies may help to further identify whether transdifferentiation of hFFs or hCPCs had occurred in EHM. Nonetheless, it appears unlikely that these rare events contributed to the cardio-supportive effects of the non-myocyte pools in EHM.

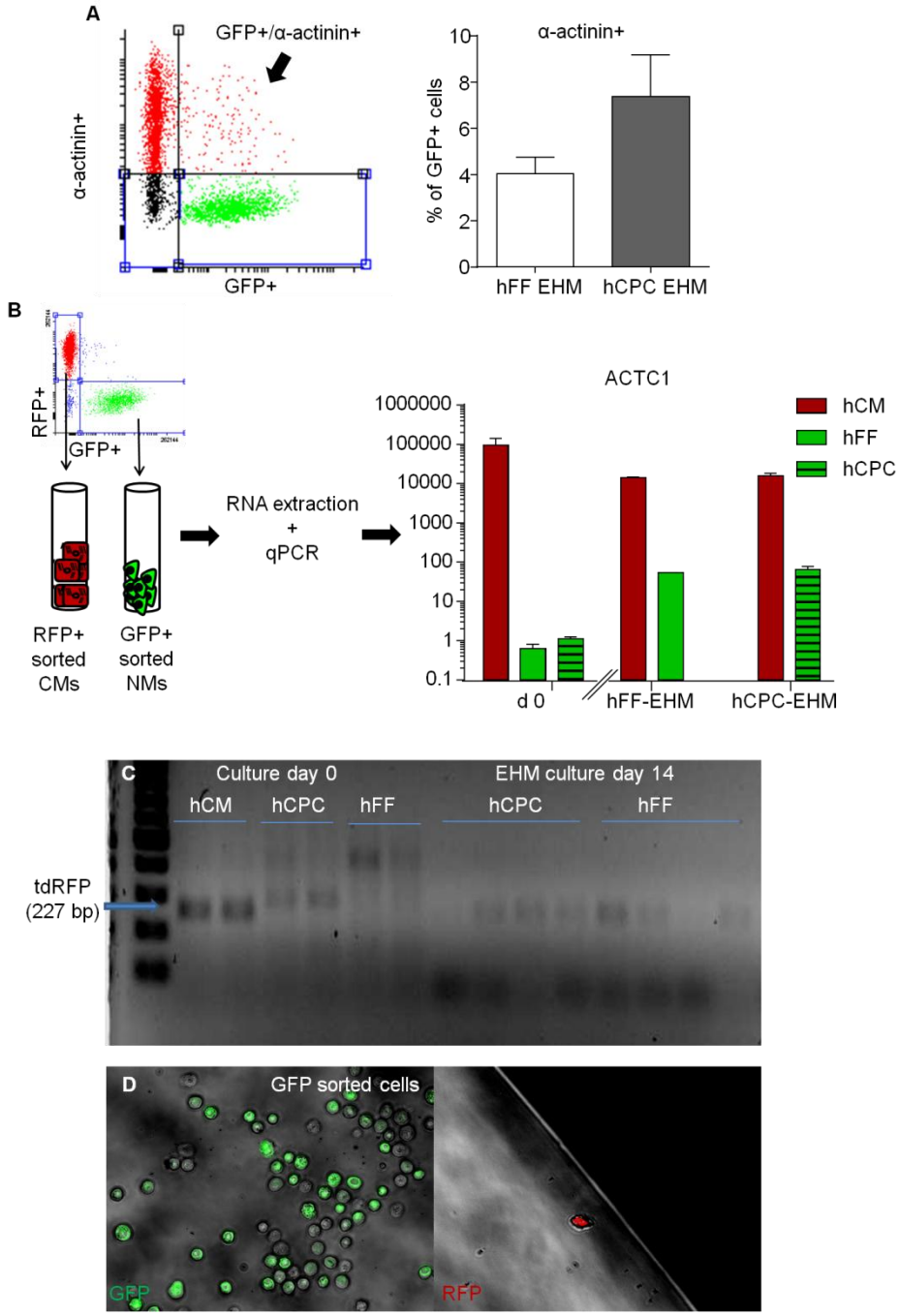

Figure 32. Strategies to investigate cardiac differentiation of hCPCs in EHM. A Flow cytometry analysis of GFP$^+$/α-actinin$^+$ cells digested from either hFF- or hCPC-EHM (n=6/group from four experiments). **B** FACS of RFP$^+$ CMs (cardiomyocytes) and GFP$^+$ NMs (non-myocytes) after digestion from EHM co-cultures and qPCR analysis of cardiac actin gene expression in the separately sorted pools (normalized to hFFs at culture day 0; n=2/group). **C** Electrophoretic separation of RFP transcripts (specific band at 227 bp) after qPCR amplification in hCM, hCPC and hFFs at culture day 0 and in GFP-sorted hCPCs and hFFs at EHM culture day 14. **D** GFP and RFP fluorescence signals on GFP-sorted cells after flow cytometry sorting.

3.5 Modeling hypoxic injury in EHM

Experimental hypoxia/reoxygenation (H/R) models are useful tools to investigate cardio-protective strategies against myocardial infarction (Portal et al. 2013). To investigate cardio-protective effect of hCPCs, the aim was to first develop EHM models of acute and chronic hypoxia-dependent injury.

3.5.1 Hypoxia response in human cardiomyocytes

To characterize the effect of hypoxia on the physiological state of cardiomyocytes, HIF-1α protein stability and metabolic modifications were analyzed under hypoxia (1% O_2) exposure for 8-72 hrs. Cardiomyocytes responded to hypoxia with HIF-1α stabilization after 8 hrs of hypoxia exposure (**Figure 33A**). Metabolic activity changed accordingly as exemplified by a drop in intracellular ATP amount (**Figure 33B**). In agreement with these findings, a gradual increase in lactate was detected starting after 8 hrs of hypoxia (**Figure 33C**). Accumulation of lactate suggests that human cardiomyocytes shift their energy metabolism from aerobic respiration to anaerobic gycolysis. Constant ATP levels at 8 and 24 hrs of hypoxia suggested that the cardiomyocytes seem to adapt their metabolism to hypoxia within this time frame. Extended hypoxia (72 hrs) appeared to cause hypoxic damage, leading to a drop in ATP synthesis with strong lactate accumulation (**Figure 33B,C**).

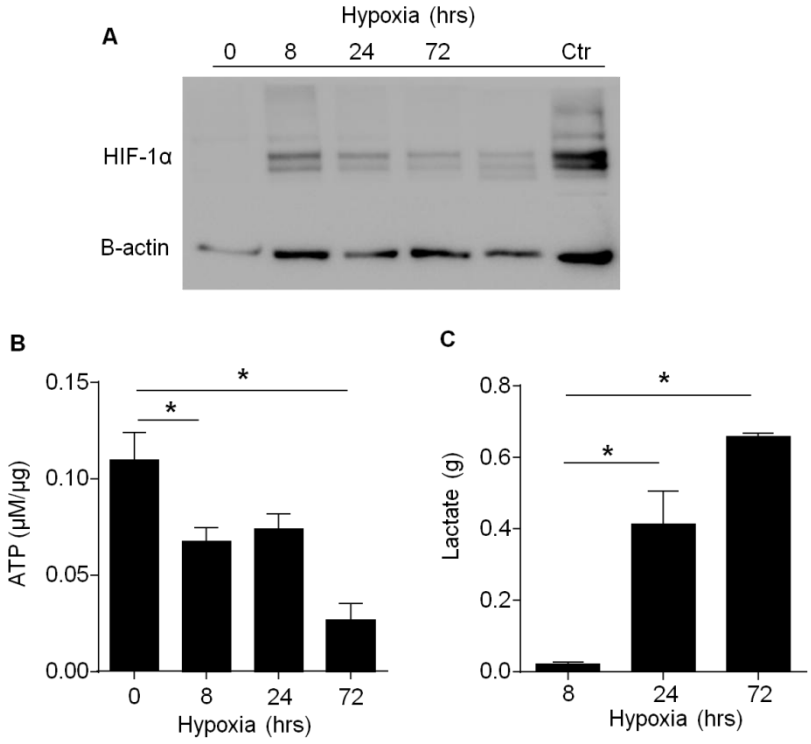

Figure 33. Metabolic adaptation of human cardiomyocytes under hypoxia. **A** HIF-1α protein abundance by Western blot detection. **B** Intracellular ATP amount and **C** released lactate into the culture medium (n=4-5/time-point; $^{*}p<0.05$ as indicated by one-way ANOVA, Dunnett's multiple comparison test).

3.5.2 Hypoxia response in human EHM

hFF-EHMs were exposed to 1% O_2 for 8-120 hrs. Lactate release was increased after 8 hrs of hypoxia, reaching maximal levels at 72 hrs (**Figure 34**). This was in line with the lactate release profile observed in human cardiomyocytes under hypoxia. Note that lactate release was also observed in EHM developed under 21% O_2 ("normoxia") without medium exchange reaching similar levels as observed in the hypoxic EHM after 120 hrs in culture. Thus, the hypoxia related cell damage occured within the first 96 hrs of hEHM culture at 1% O_2. Beyond that time window, nutrient depletion may have contributed to general cell damage.

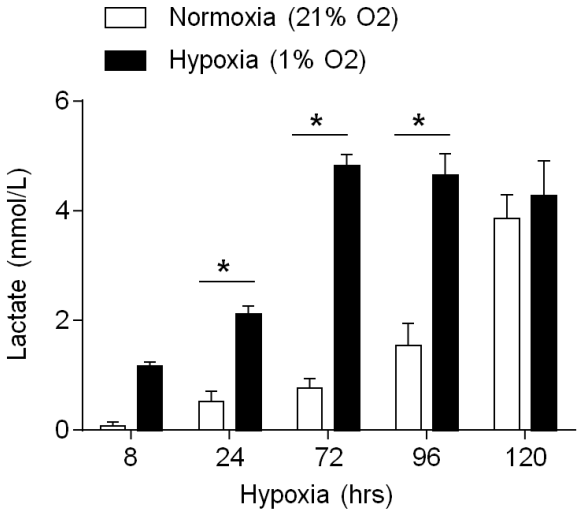

Figure 34. Lactate production by hEHM cultured under normoxia and hypoxia. Lactate accumulation in hEHM culture medium under normoxia (21% O_2) and hypoxia (1% O_2) for 8-120 hrs with no medium change (n=4/group, *p<0.05 by two-way ANOVA with Sidak's multiple comparison test).

3.5.3 Hypoxia/Reoxygenation damage in human EHM

hEHMs were exposed to different durations of hypoxia (H; 1% O_2; 8-120 hours) followed by 24 hrs of reoxygenation (R; 21% O_2) to identify whether hypoxia/reoxygenation (H/R) damage could be simulated (**Figure 35A**). We did not observe any reduction in FOC of hEHMs under hypoxia for 8-72 hrs (8 and 24 hrs time points not shown). However, reoxygenation after 72 hrs hypoxia resulted in a marked reduction in EHM contractility (**Figure 35B**). Conversely, 120 hrs of hypoxia caused EHM damage, which could not be further aggravated by reoxygenation (**Figure 35C**).

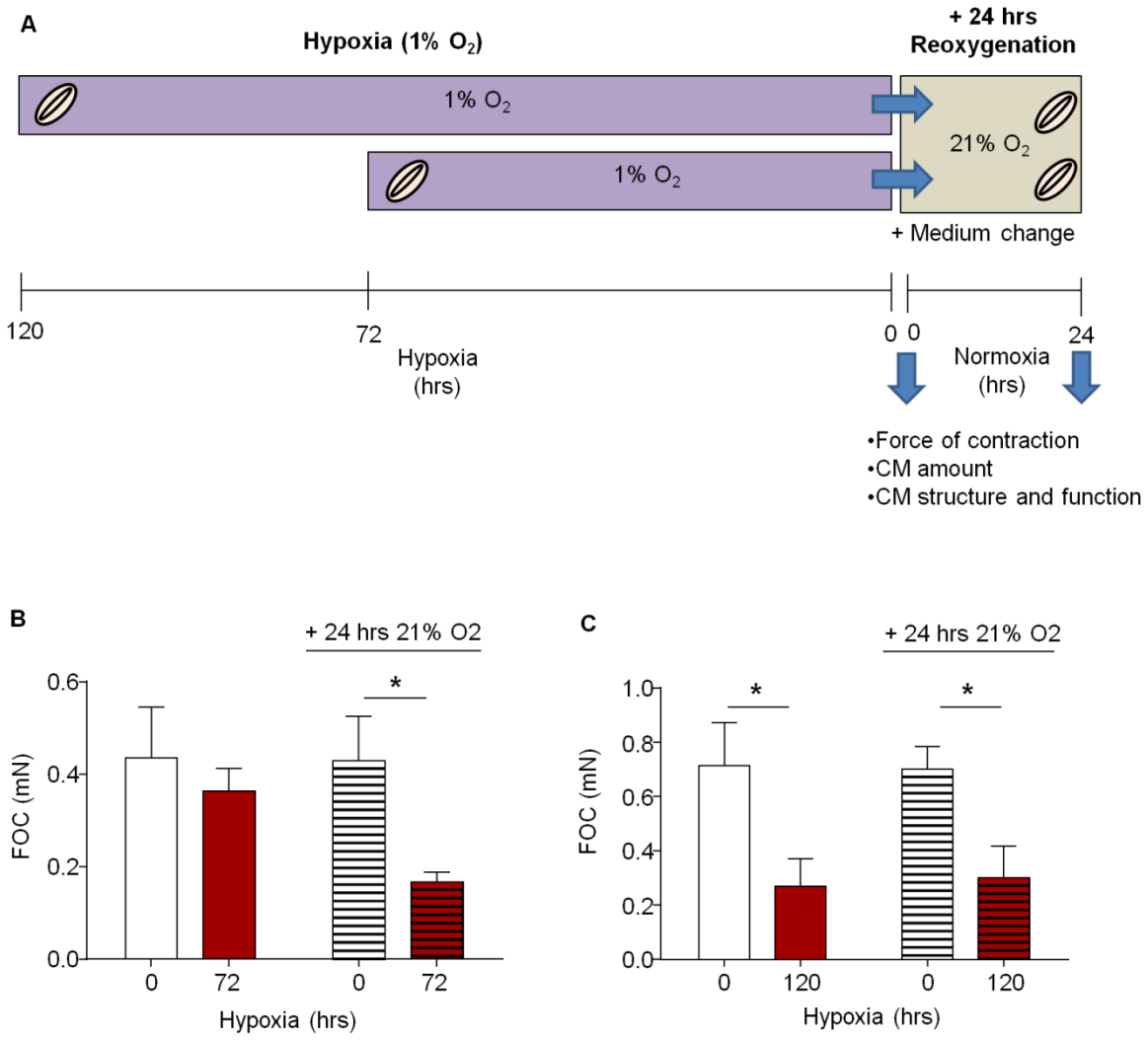

Figure 35. Development of a hypoxia/reoxygenation injury hEHM model. A Schematic overview of the experimental setting of H/R injury in hEHMs. hEHMs incubated in 1% O_2 for 72 or 120 hrs and reoxygenated in 21% O_2 in an oxygenated fresh medium for 24 hrs and subsequently analyzed at functional and structural level. **B** Force of contraction (FOC) in hEHM after only 72 hrs of hypoxia or 72 hrs hypoxia followed by 24 hrs of reoxygenation (n=5-6/group from two experiments, unpaired *t*-test, *p<0.05). **C** FOC in hEHM after only 120 hrs of hypoxia or 120 hrs of hypoxia, followed by 24 hrs of reoxygenation (n=8/group from two experiments, unpaired *t*-test, *p<0.05). hEHMs at 0 hr of hypoxia served as normoxia control for the corresponding experimental conditions.

Interestingly, cardiomyocyte quantity per EHM was significantly reduced after 72 hrs (**Figure 36A**), without an obvious impact on EHM contractility (**Figure 35B**). Reoxygenation aggravated the cardiomyocyte loss after 72 hrs of hypoxia (**Figure 36A**), which was in-line with the observed functional decay (**Figure 35B**). As expected, chronic hypoxia stimulation (120 hrs) resulted in a pronounced decrease in cardiomyocyte numbers, (**Figure 36A**) with at best a tendency to enhanced

cardiomyocyte survival after enzymatic digestion from EHM subjected to 24 hrs of reoxygenation. Note that the discrepancy between contractile performance and cardiomyocytes count after 72 hrs hypoxia could result from a higher susceptibility of hypoxic cardiomyocytes to enzymatic EHM digestion. We further employed a LDH activity assay to evaluate cell damage upon reoxygenation and found that extended reoxygenation (24 hrs) caused substantial damage (**Figure 36B**).

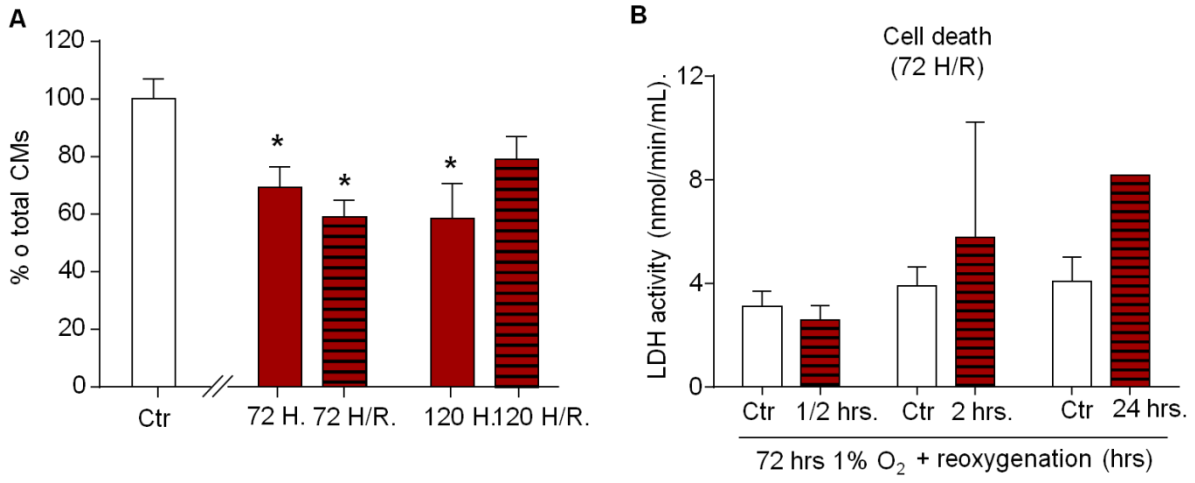

Figure 36. Validation of the hypoxia/reoxygenation injury hEHM model. A Percentage of total cardiomyocytes after 72 hrs (72 H; n=3-4/group, unpaired *t*-test, *p<0.05) and after 120 hrs of hypoxia (120 H; n=6-8/group, unpaired *t*-test, *p<0.05 vs. Ctr), with the following 24 hrs of reoxygenation induction (72H/R or 120 H/R). **B** LDH activity as an indicator of cell damage/death during 24 hrs of reoxygenation following 72 hrs of hypoxia (n=2-3/group). Ctr: Control EHM incubated under normoxia for the corresponding experimental condition.

Collectively, these data define the time windows for the simulation of hypoxic (120 hrs 1% O2) and hypoxia/reoxygenation (72 hrs 1% O2 followed 24 hrs 21% O2) damage in human EHM.

3.6 Assessment of the protective effects of human CPCs in EHM

hCPCs are tested clinically for myocardial protection after myocardial infarction (Makkar et al. 2012). Here, we aimed at investigating potential cardio-protective effects of hCPCs in the EHM hypoxia/reoxygenation and chronic hypoxia injury models.

3.6.1 No evidence for paracrine protection by CPCs

hEHMs were exposed to H/R injury as established before (see 3.5.3) and exposed to either hCPC- or hFF-conditioned medium (ConM) during reoxygenation after 4 weeks of regular EHM culture (**Figure 37A**). As expected, H/R significantly reduced hEHM function markedly compared to normoxia control EHM (EHM-Ctr: continuously incubated at 21% O_2). hEHM treated with hCPC-ConM did not show any rescue from H/R injury. Interestingly, hFF-ConM treatment during reoxygenation partially preserved contractile function of hEHM, reducing the injury effect by ~50% (**Figure 37B**). H/R injured hEHMs (EHM H/R: treated with fresh medium) showed increased calcium sensitivity (EC_{50}: Ctr. 0.7±0.1, n=9/group vs. H/R 0.3±0.1 mmol/L, n=4/group, $p<0.05$ by Student's *t*-test; **Figure 37C**). hFF-ConM and hCPC-ConM shifted the calcium sensitivity in H/R towards Ctr levels with a slightly more enhanced effect in hFF-ConM (fold difference in EC_{50} in mmol/L: hFF-ConM 0.6±0.1, n=9/group vs. hCPC-ConM 0.5±0.1 mmol/L, n=5/group; **Figure 37C**). The latter finding needs further investigations on the molecular level to determine whether calcium-homeostasis is indeed altered and involved in the functional deterioration as well as protection in H/R EHM.

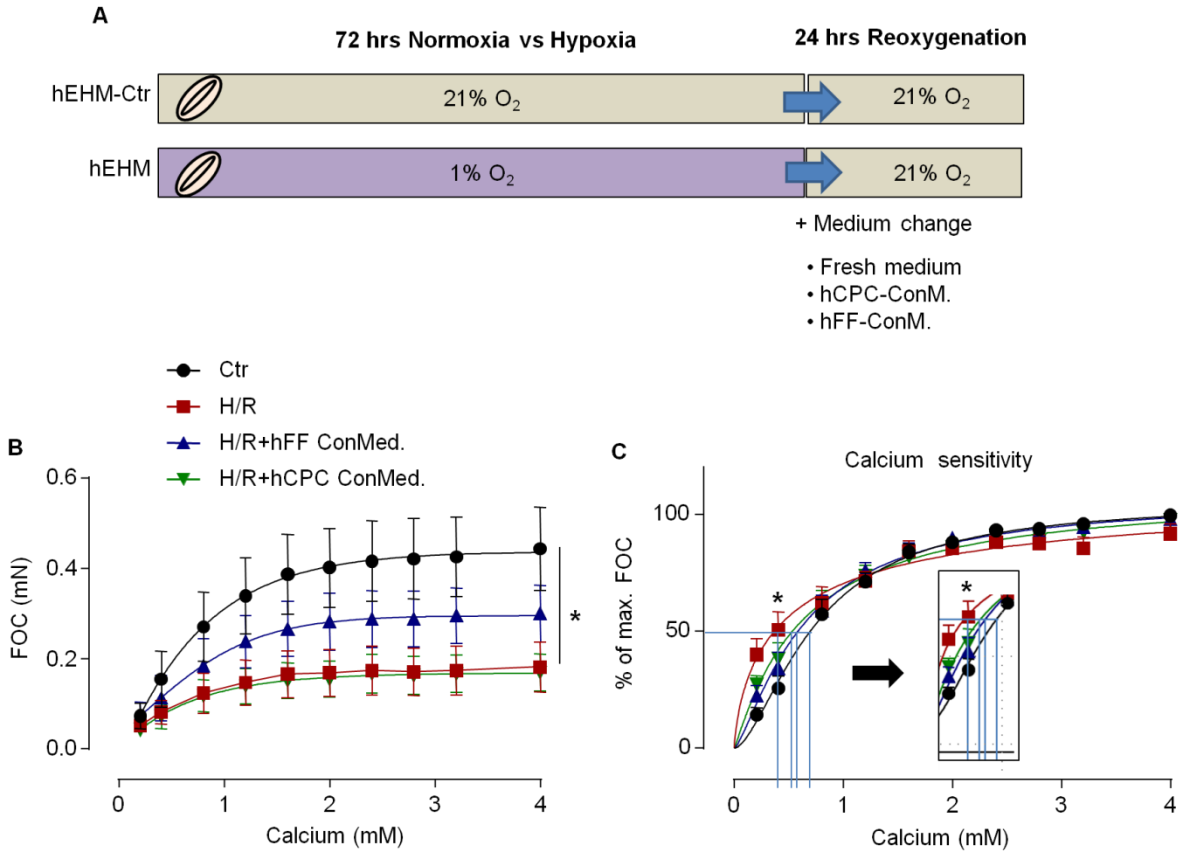

Figure 37. Effects of conditioned medium on EHM function upon H/R injury. A Schematic overview of the experimental design to test potential protective mechanisms of hCPC-conditioned culture medium. Following 72 hrs of hypoxia, hEHMs were exposed to 24 hrs of reoxygenation in the presence of hCPC- or hFF-Conditioned medium (ConM); regular medium exchange in the H/R model served as "injury" control; standard hEHM cultures served as "healthy" controls. **B** Force of contraction (FOC) and **C** calcium sensitivity in Ctr (normoxia), H/R (H/R injury), H/R+hCPC-ConM and hEHM-H/R+hFF-ConM (n=9-10/EHM from three experiments, *p<0.05 vs. Ctr. by two-way ANOVA, Dunnett's multiple comparison test **B** and Student's *t*-test **C**.

Consistent with the data on EHM function (**Figure 37B**), H/R caused a significant reduction in cardiomyocte content and reduced contractile function. Similarly as reported for EHM function, there was no protection from cardiomyocyte death upon H/R injury by hCPC-ConM. Conversely, cardiomyocyte amount and contractility as a fuction of cardiomyocyte number was markedly enhanced in hFF-ConM treated hEHMs (**Figure 38A,B**), suggesting that hFFs rather than hCPCs were able to protect cardiomyocytes from H/R by paracrine mechanisms.

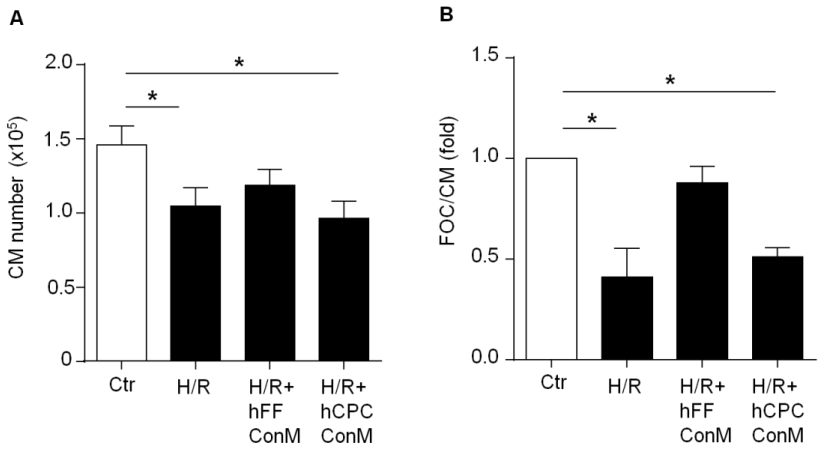

Figure 38. Effects of conditioned medium on EHM cardiomyocyte content upon H/R injury. A Cardiomyocyte number (n=8-10/group) and **B** force of contraction (FOC) as a function of cardiomyocyte content in Ctr, H/R, H/R+hFF-ConM and H/R+hCPC-ConM EHM. n=3/group; *p<0.05 vs. Ctr by one-way ANOVA with Dunnett's *post-hoc* test.

To investigate whether H/R impaired the responsiveness to β-adrenergic stimulation the response to maximally effective isoprenaline (1 µmol/L) was tested. These analyses showed a markedly depressed isoprenaline response in H/R treated EHM irrespective of the attempted conditioned medium rescue (**Figure 39**).

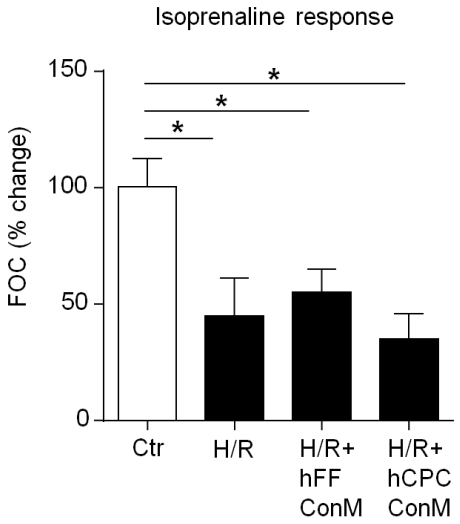

Figure 39. Impaired β-adrenergic signaling in hEHM after H/R injury. Force of contraction (FOC) in percent of the inotropic effect induced by isoprenaline in control EHM at EC_{50} calcium concentrations; n=9-10/group; *p<0.05 vs. Ctr by one-way ANOVA with Dunnett's *post-hoc* test.

3.6.2 Discrimination of paracrine effects by transcriptome profiling

CPCs have been reported to possess paracrine potency to reduce cell death and support cardiomyocyte proliferation as well as play angiogenic (Chimenti et al. 2010, Li et al. 2012, Malliaras et al. 2013) and anti-inflammatory roles (Liu et al. 2014). To gain preliminary insight into the specific paracrine activity of hCPCs and hFFs and to explain the differential effect of conditioned medium, a number of growth factors and cytokines that are involved in cell survival, proliferation, angiogenesis and inflammation (see Appendix A6 for the full list of growth factors and cytokines) were selected and screened in the pool of differentially expressed genes from RNAseq data in hCPCs vs hFFs. Several clusters of genes were detected that were differentially expressed between hCPCs and hFFs (**Figure 40A**)**.** Ontology enrichment identified that hCPC genes involved in angiogenesis and immune response were strongly regulated. Paracrine factors up-regulated in hFFs were more involved in the regulation of cell proliferation and survival (**Figure 40A**). We also confirmed the expression of the specific growth factors *FGF-2*, *VEGF*, *IGF-1*, *HGF* and *PDGF* – all with a known effect on cell proliferation, survival and migration – by PCR (**Figure 40B**). The enrichment of transcripts encoding for cell survival enhancing factors in hFFs was in line with their effects on cardiomyocyte survival in EHM upon H/R injury (**Figure 38A**). Given the major effect of hFF-ConM on the protection of cardiomyocyte function after H/R injury, it might be worth to investigate the mechanism behind the impairment in cardiac function, first and further screen for related cardio-supporting factors secreted from these fibroblasts. On the other hand, possible pro-angiogenic and inflammation modulatory role of hCPCs according to the RNAseq data might provide a possible mechanism for their ameliorating effect on tissue injury *in vivo* (Liu et al. 2014). No effect in EHM may be attributed to the lack of vascular cells and leukocytes in EHM.

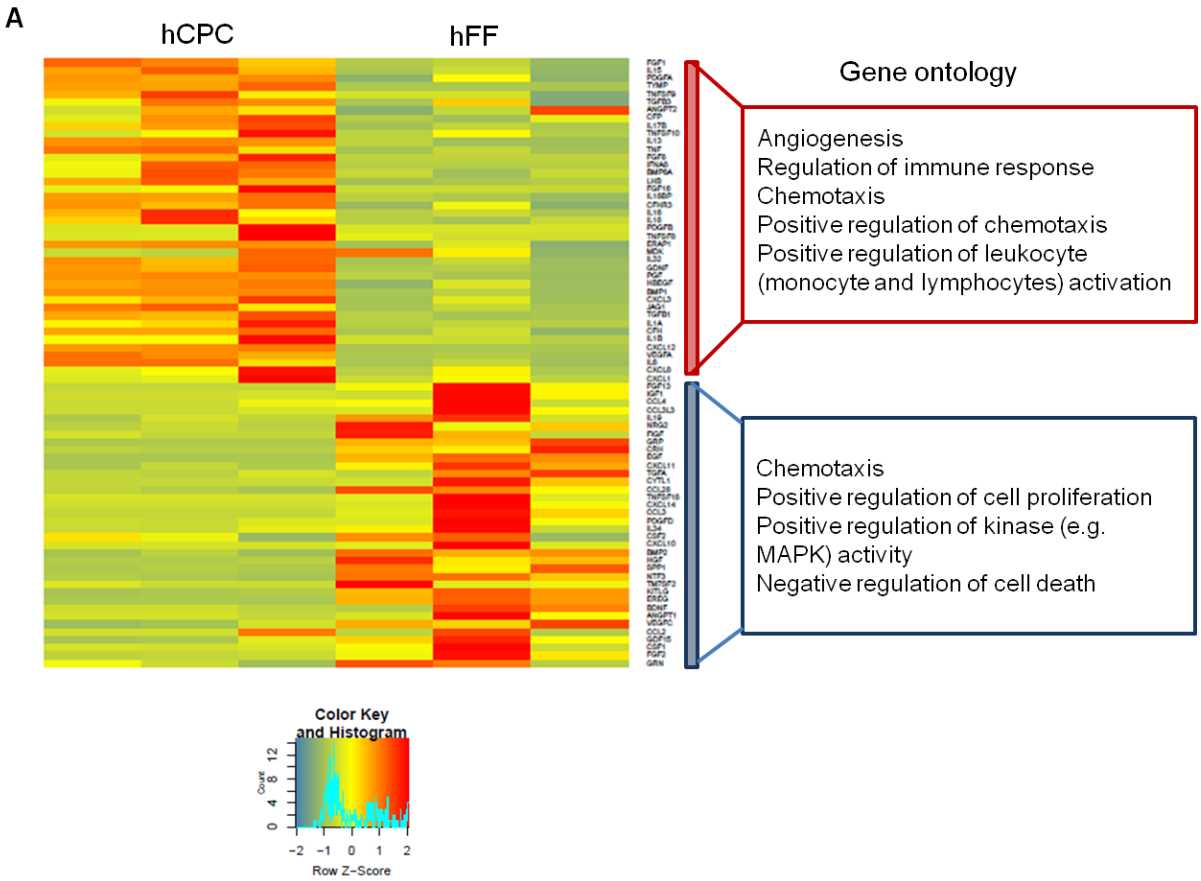

Figure 40. Paracrine activity in hCPCs and hFFs. Heatmap analysis of genes encoding for paracrine factors involved in cell survival, proliferation, angiogenesis and inflammation in hCPCs and hFFs; on the right functional annotation of differentially expressed genes in gene clusters; Red and blue reflect high and low expression levels, respectively as scaled in color key bar (n=3/group). **B** PCR analysis of a selected number of transcripts encoding for growth factors with implications in cardiac homeostasis: *FGF2, VEGF, IGF1, HGF* and *PDGF; GAPDH* served as housekeeping reference gene.

3.6.3 Cardio-protective effects of CPCs in EHM exposed to chronic hypoxia

To investigate whether or not hCPCs elicit a cardio-protective role under chronic hypoxia and following the hypothesis that hCPCs may elicit their effects only under more physiological conditions, EHMs were constructed from CMs (65%) and hFFs (28%) with the addition of hCPCs (7%) and exposed to 1% oxygen for 120 hrs after 4 weeks of regular EHM culture (**Figure 41A**). Chronic hypoxia decreased FOC by almost 68±6% in hFF-EHM in agreement with the findings reported before (refer to **Figure 35C**). Interestingly, hFF+hCPC-EHM already under normoxic control conditions presented with slightly enhanced forces and an only mildly reduced FOC under chronic hypoxia (**Figure 41B**). Calcium sensitivity (average EC_{50}: 0.34±0.03 mmol/L) was similar in all groups suggesting differential effects of H/R and chronic hypoxia on calcium homeostasis (**Figure 41C**).

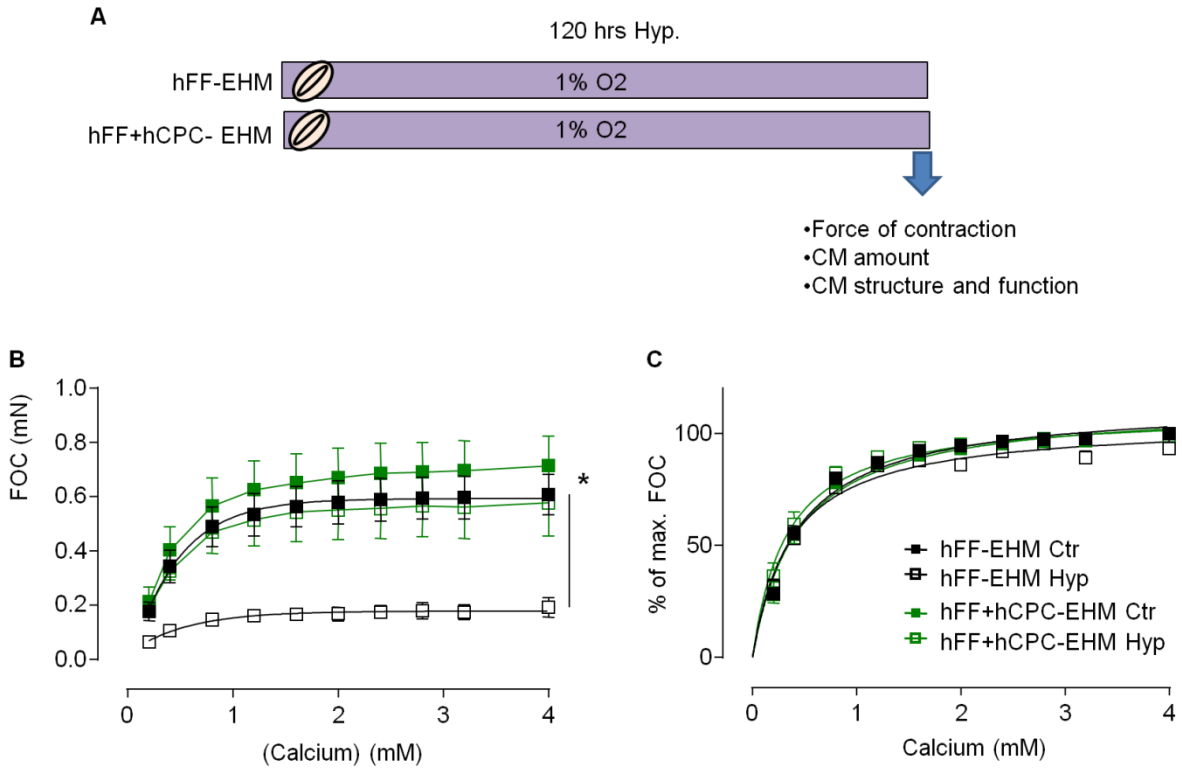

Figure 41. Effects of CPC in EHM tri-cultures upon chronic hypoxia. A Schematic overview of the experimental design to test potential protective mechanisms of hCPCs on EHM composed of hFFs and CMs with or without hCPC supplementation. Following 4 weeks of regular culture, EHMs were exposed to 1% O_2 for 120 hrs (hypoxia: Hyp) or maintained under 21% ambient O_2 (Ctr) without culture medium exchange; hFF-EHM: 70% CMs and 30% hFFs; hFF+CPC-EHM: 65% CMs, 28% hFFs, 7%CPCs. **B** Force of contraction (FOC) and **C** calcium sensitivity in Ctr in the indicated groups; n=4/group, *p<0.05 by two-way ANOVA with Tukey's multiple comparison *post hoc* test.

No obvious difference was detected in cardiomyocyte amount between hFF- and hFF+hCPC-EHM under normal conditions. After chronic hypoxia, cardiomyocyte content was significantly decreased in hEHM with or without hCPC supplementation (**Figure 42A**); however, a trend to a better cardiomyocyte preservation was apparent in the hCPC supplemented EHMs. α-Actinin content and function per cardiomyocyte were preserved only in hFF+hCPC-EHM, suggesting a beneficial effect of hCPCs on cardiomyocytes in EHM tri-cultures (**Figure 42B,C**). Further investigations are needed to identify the apparently cell context dependent effects of CPCs.

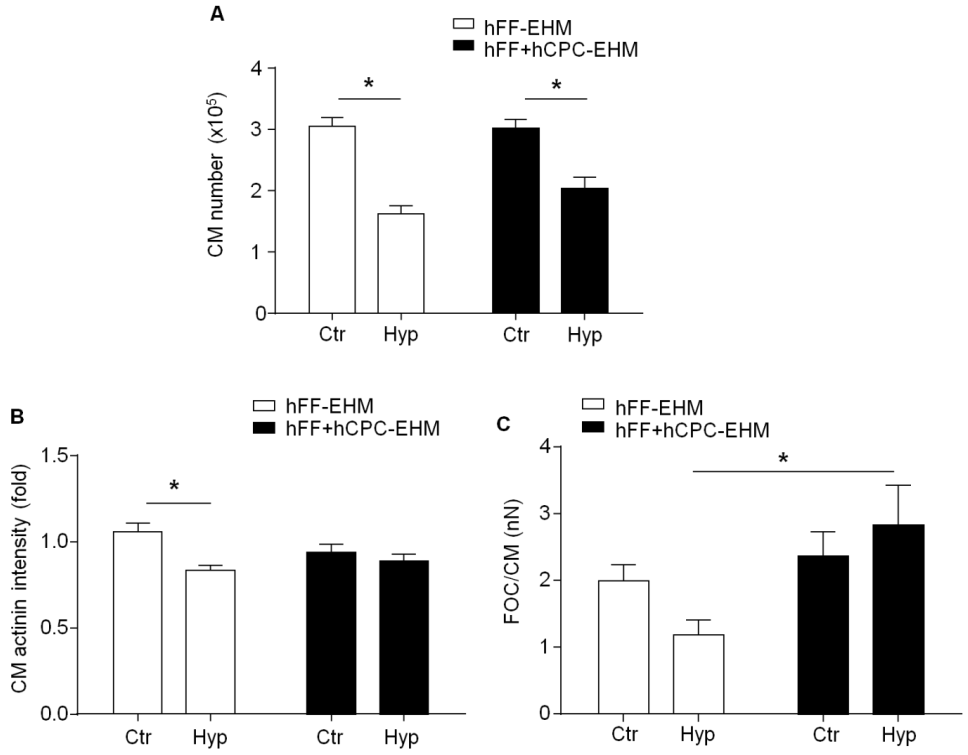

Figure 42. Enhanced cardiomyocyte survival and function in EHM tri-cultures. Experimental conditions were as outlined in Figure 41A with EHM exposed to chronic hypoxia. **A** Cardiomyocyte number/EHM, **B** cardiomyocyte α-actinin content by mean fluorescence intensity measurements and **C** FOC as a function of EHM cardiomyocyte content (n=4/group same EHM as in Figure 46); *p<0.05 as indicated by two-tailed, unpaired Student's *t*-test.

3.7 Development of a genetic hypoxia indicator model

Cell and tissue hypoxia models would benefit greatly from tools for life-cell imaging of cell oxygenation states. First steps towards the ultimate goal to develop a hEHM model comprising cardiomyocyte-specific hypoxia sensors are described below.

3.7.1 Hypoxia sensing in ODD-Luc mouse cardiomyocytes

In order to identify the biological response of cardiomyocytes to hypoxia, a genetically modified mouse ODD-Luc ESC line (see Appendix A4) was utilized to generate ODD-Luc mouse cardiomyocytes. The ubiquitously expressed reporter in this ODD-Luc ESC line comprised a HIF-1α oxygen-dependent degradation domain (ODD) fused to a firefly luciferase (Luc). Stability of the ODD-Luc fusion protein depends on the oxygenation level. Under normoxia, prolyl residues in the ODD domain are hydroxylated by prolyl-4-hydroxylase-domain (PHD) enzymes, which subsequently

results in ubiquitination and rapid degradation of the protein. Under hypoxia, reduced PHD enzyme activity leads to stabilization of HIF-1α (Schofield and Ratcliffe 2004). According to this system, any decrease in oxygen amount should lead to stabilization of the ODD-Luc protein and thus an increase in Luc signal intensity (**Figure 43A**).

To validate whether the response to hypoxia can indeed be measured in this cell-based reporter model, ODD-Luc cardiomyocytes were exposed to 1% O_2 for 1-72 hrs and Luc signal was analyzed at multiple time-points. ODD-Luc cardiomyocytes showed a significant increase in Luc signal with peak intensity at 24 hrs (**Figure 43B**). Luc signal intensity showed a good correlation with the abundance of ODD-Luc protein and endogenous HIF-1α protein (**Figure 43C**). Elevation of PHD2 protein at 24 hrs, as a negative feedback mechanism may be an additional explanation for the decrease in endogenous HIF-1α and ODD-Luc protein in extended culture (**Figure 43C**). Collectively, these findings support the use of the ODD-Luc model in sensing hypoxia in cardiomyocytes.

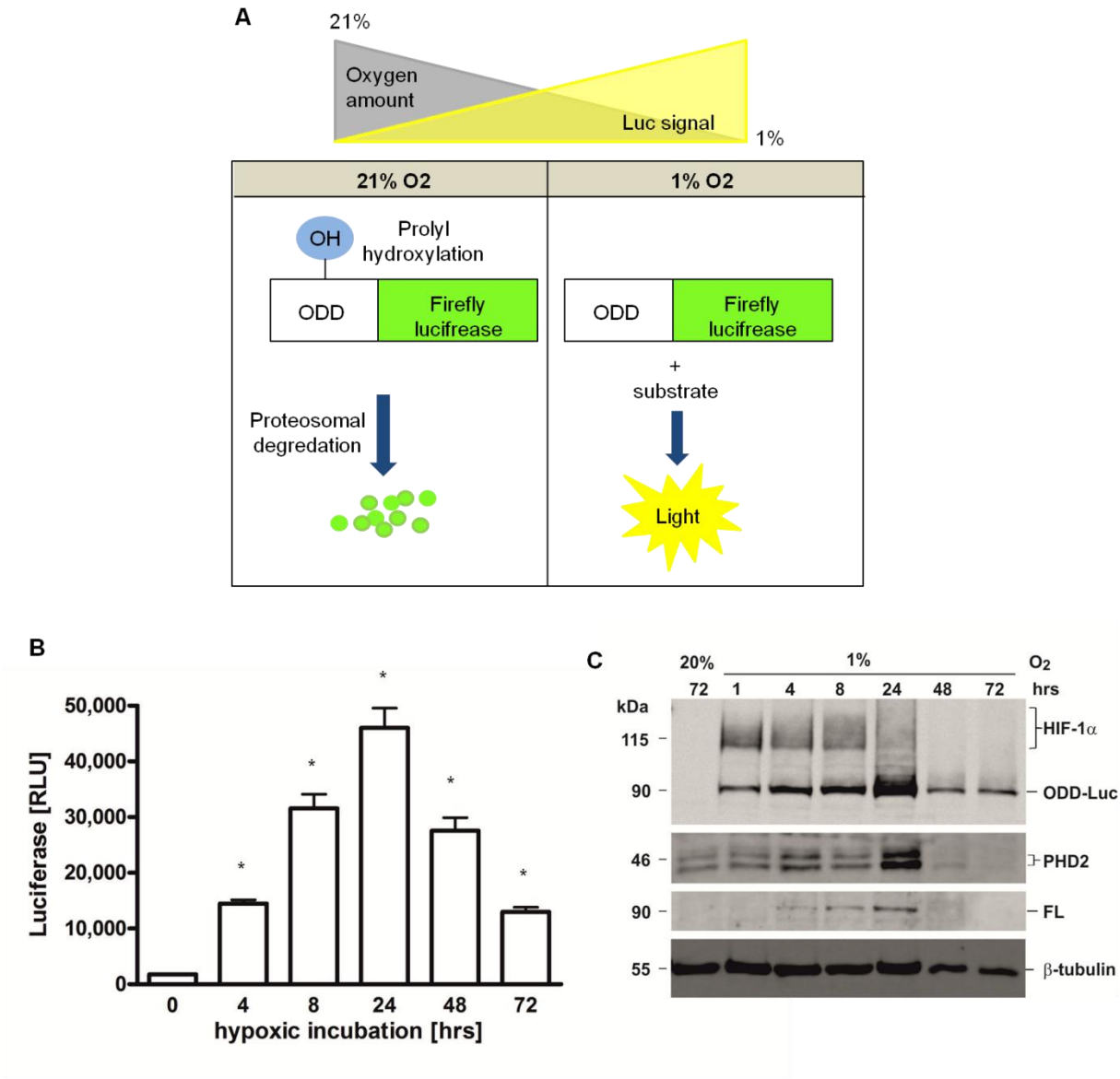

Figure 43. Validation of ODD-Luc hypoxia reporter in cardiomyocyte culture. A Schematic representation of the mechanisms regulating the stability of ODD-Luc fusion protein based on ambient oxygen levels (21% O_2: hydroxylation of prolyl residues in HIF-1α-ODD results in proteosomal degradation of the ODD-Luc fusion protein, 1% O_2: no post-translational modification in HIF-1α-ODD and stabilization of ODD-Luc fusion protein). **B** Time-dependent Luc signal development in antibiotically selected ODD-Luc cardiomyocytes (mouse model) upon exposure to 1% O_2 for 1-72 hrs (n=6/group). **C** Protein expression of endogenous HIF-1α, ODD-Luc fusion protein, PHD2 protein, firefly luciferase (FL) and β-tubulin using western blot (provided by Anke Zeiseniss; Institute of Cardiovascular Physiology, UMG). Data was published in (Hesse et al. 2014).

3.7.2 Hypoxia sensing in ODD-Luc mouse EHM

ODD-Luc cardiomyocytes were utilized to generate EHMs with genetically naïve fibroblasts, based on the mouse EHM protocol as described previously (section 2.3.2). ODD-Luc EHMs showed the highest signal at 24-48 hrs after the induction of hypoxia with a subsequent signal decrease (**Figure 44A**). Reoxygenation of ODD-Luc EHMs at 21% O_2 after 4 hrs of hypoxia rapidly diminished the Luc signal intensity with an apparent half-life of 15±3 min (n=3) for the ODD-Luc protein complex (**Figure 44B**)

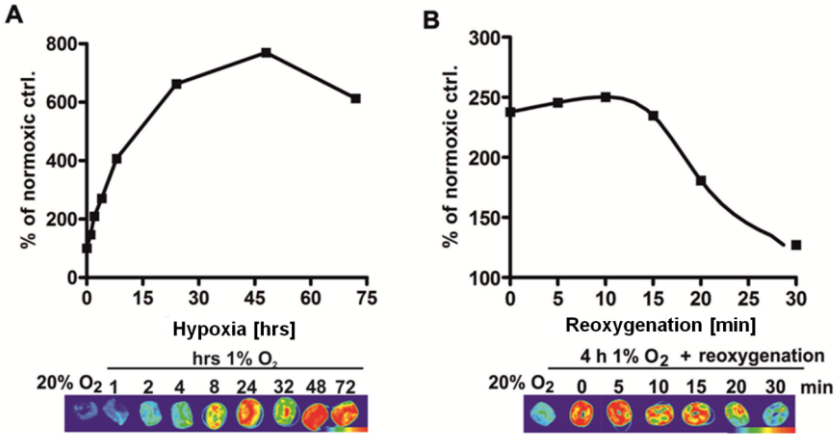

Figure 44. Hypoxia and repoxygenation responses in ODD-Luc EHM. A Time-dependent Luc signal development in ODD-Luc EHM during hypoxia (1% O_2) for 1-72 hrs (n=3/time point). **B** Time-dependent reduction of Luc signal in ODD-Luc EHM after reoxygenation following 4 hrs of hypoxia (n=3/time-point). Panels below display signals recorded from representative ODD-Luc EHM (blue indicates low and red indicates high Luc signal). Data was published in (Hesse et al. 2014).

3.7.3 Hypoxia sensing in human cardiomyocytes

After obtaining proof-of-concept in the mouse model that the ODD-Luc reporter system can be used as a tool to monitor tissue oxygenation and hypoxia response, we attempted to establish the same system in a human model. For this purpose, ODD-Luc hESCs were generated using TALEN technology. Briefly, wild-type hESCs were targeted with pAAVS1-CAG-ODD-Luc-EF1α-GFP donor vector (section 2.8), which was generated by Dr. Claudia Noack and pAAVS1 TALEN Left and Right vectors. Resulting ODD-Luc expressing hES cells were differentiated into ODD-Luc

expressing human cardiomyocytes (ODD-Luc hCMs). ODD-Luc hCMs were validated for their hypoxic response with significantly higher expression of Luc signal after 4 hrs of hypoxia (1% O_2) exposure (**Figure 45**). In future experiments, we intend to use these ODD-Luc hCMs to generate ODD-Luc hEHMs as a human heart muscle model to gain a better understanding on their response to hypoxia and reoxygenation.

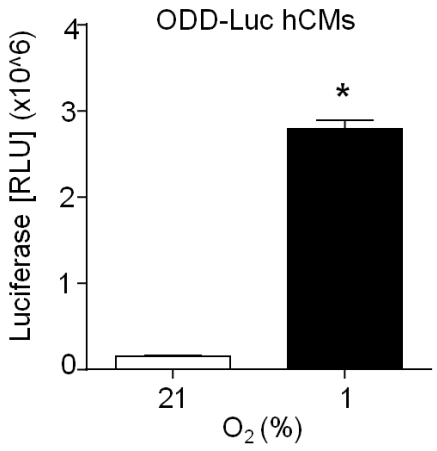

Figure 45. Hypoxia response in ODD-Luc human cardiomyocytes. Luc-signal development in ODD-Luc hCMs cultured in 21% and 1% O_2 for 4 hours (n=3/group, unpaired t-test, *p<0.05).

4 Discussion

Cardiac progenitor cells (CPCs) were identified in the heart based on Sca-1 and c-Kit surface markers (Beltrami et al. 2003, Oh et al. 2003). Despite some evidence for Sca-1-like cells in the human heart (Smits et al. 2009), c-Kit has been used as a common marker for CPCs in the human heart. The biological relevance of CPCs is under debate since their introduction more than 10 years ago (Beltrami et al. 2003) with several clinical trials being underway to identify the therapeutic utility of CPCs in the human heart (Bolli et al. 2011, Makkar et al. 2012). The interpretation of the biological relevance of CPCs in the heart is diverse, ranging from being transiently extravagated leukocytes or mast cells (Kubo et al. 2009) to being resident progenitors with strong cardiomyogenic activity (Ellison et al. 2013). Despite the ongoing clinical trials, phenotypic characterization and the perceived mode of action of CPCs are still under debate (Chong et al. 2014). The aim of this thesis was to make use of the EHM platform to scrutinize the biological activity of CPCs. The following specific hypotheses were tested:

1) CPCs support functional heart muscle formation *in vitro*.

2) CPCs elicit cardioprotective effects upon hypoxic injury.

The key results are summarized below:

1) CPCs are phenotypically distinct from fibroblasts.

2) Human CPCs contain a pericyte transcriptome signature.

3) CPCs and fibroblasts show a similar function as to the support of EHM formation.

4) Paracrine activity of CPCs can be enhanced by enforced miR-133a expression.

5) No evidence for CPC transdifferentiation into cardiomyocytes could be obtained.

6) Different EHM models of hypoxic damage could be established.

7) Fibroblats, but not CPCs protected from hypoxia/reoxygenation injury.

8) CPCs protected EHM under chronic hypoxia.

9) Novel tools for imaging of cardiomyocyte oxygenation could be established.

4.1 Characterization of CPCs

Phenotypic characterization of c-Kit-CPCs isolated from adult mouse and human heart revealed that they do not express c-Kit, although they were isolated based on c-Kit expression. It is likely that the CPCs lost their c-Kit expression in culture over time, as observed in muscle-derived stem cells, which change their phenotype immediately after being isolated (Jankowski et al. 2001). Different types of CPCs have been characterized by expression of different cell surface markers, so far. Whether these CPCs represent unique cell types or are related to each other is still under debate (Torella et al. 2008). PDGFRα$^+$/Sca-1$^+$ mesenchymal stem cell (MSC)-like cells have been reported to exist in the adult mouse myocardium, with the potential to differentiate into three cardiac lineages. These cells were suggested to originate from epicardium and express c-Kit in a small subset (Chong et al. 2011). In our study, ~90% of mouse c-Kit-CPCs were found to be PDGFRα$^+$/Sca-1$^+$ as well as CD105$^+$, indicating a mesenchymal/endothelial origin. Furthermore, lack of *Nkx2-5* expression, as an early cardiac marker suggested that these CPCs were not committed to the cardiomyocyte lineage. Conversely, PDGFRα$^+$/Sca-1$^+$ cells have been related to epicardial progenitors, which are mainly involved in the constitution of the vascular compartments of the developing heart, including smooth muscle cells and pericytes (Kennedy-Lydon and Rosenthal 2015).

Pericytes are multipotential MSC-like cells that are positive for several distinct markers (MCAM, CSPG4, PDGFRβ, α-SMA) as well as more broadly expressed mesenchymal cell markers including CD90, CD73, CD105, CD44 and can apparently be induced to differentiate into cardiomyocytes and smooth muscle cells (Chen et al. 2013, Crisan et al. 2008). Interestingly, human CPCs (hCPCs) showed a marked gene expression of *MCAM*, *CSPG4* and *PDGFRβ*, suggesting a pericyte-like

phenotype. However, detection of *PECAM1* expression in hCPCs, although at a low abundance, would not be fully compatible with this hypothesis (Chen et al. 2013).

Adventitial cells are another type of MSC-like progenitors expressing the endothelial/hematopoietic progenitor marker CD34 and mesenchymal cell markers (e.g. CD90, CD73, CD105 and CD44) with a potential to differentiate into endothelial-like and smooth muscle cells (Crisan et al. 2012). hCPCs did not express CD34. However, when compared to other cell types, hCPCs demonstrated an elevated expression of *GLI1*, which has recently been shown as a new marker to identify perivascular progenitors in the pericyte niche (Kramann et al. 2015). Although these cells are supposed to be negative for pericyte markers, they can indeed gain expression of pericyte-specific and smooth muscle cell-specific phenotypes (e.g. α-SMA$^+$) depending on *in vitro* and *in vivo* conditions (Kramann et al. 2015). In this respect, if hCPCs are true GLI1$^+$ perivascular progenitors, this may explain the reason why they seem to show a high heterogeneous expression profile *in vitro*.

Mesoangioblasts resemble another blood vessel associated stem cell type, with apparent multipotential characteristics (Crisan et al. 2008). These cells can show heterogeneous characteristics with partial expression of endothelial cell, pericyte, perivascular progenitor markers, as well as c-Kit. Consistent with the heterogeneous gene expression profile in hCPCs, cardiac mesoangioblasts might be another candidate in describing the lineage identity of hCPCs.

Taken together, although each progenitor is defined by a combination of certain markers, these markers seem to be shared between different cell types (pericytes, adventitial cells and mesoangioblasts) suggesting that they may actually represent different intermediate forms of the same stem cell population in the heart. In this perspective, it is difficult to put CPCs under a specific class of stem cell population defined, so far. However, our phenotypic analysis suggests that they match closely with progenitor cells identified to be localized in perivascular niches.

4.2 Human CPCs might have an epicardial origin

c-Kit$^+$ cells were identified to be located predominantly in the subepicardium of the right atria and adjacent to myocardial intersititium in the heart (Chong et al. 2013, Keith and Bolli 2015, Limana et al. 2007, Limana et al. 2010). These subepicardially located c-Kit$^+$ cells are believed to be epicardial progenitors expressing epicardial developmental genes (e.g. Wt1 and Tbx18) during embryonic heart development and myocardial infarction (Limana et al. 2010). Given the fact that hCPCs in our study were originally isolated from the right atrial appendage, it is likely that they might be representing a subgroup of *in vivo* c-Kit$^+$ progenitors subepicardially located in the right atria of the adult human heart.

In addition, epicardial progenitors are normally derived by a process called ‘’epithelial to mesenchymal transformation’’ (EMT), whereby they develop a mesenchymal phenotype (Keith and Bolli 2015). In our study, we showed that not all, but a certain fraction of hCPCs present expression of mesenchymal markers; 36% CD90$^+$ and 60% CD105$^+$, suggesting conversion to a mesenchymal transition state. Considering that the c-Kit receptor plays an important role in cell survival, migration and proliferation (Lennartsson and Ronnstrand 2012), c-Kit expression might have enabled progenitor cells to actively migrate towards the myocardium and gain an intermediate phenotype during the EMT process. Epicardial progenitors that undergo EMT highly contribute to vascular and interstitium compartments with little evidence of cardiomyocyte differentiation (Keith and Bolli 2015). In line with this, hCPCs did not show any late (*cardiac actin* and *cardiac troponin I*) or early cardiac marker (*Nkx2-5*) expression, but only enhanced *GATA4*. Furthermore, a small fraction (10%) of hCPCs were PECAM1$^+$ as an indication for their vasculogenic potential. Moreover, relatively higher expression of EMT associated proteins; *periostin* and *TCF21* in hCPCs can be considered supporting evidence for a epicardial origin. Considering the role of epicardium in the development of vascular compartment in the heart, it is likely that hCPCs may represent a subgroup of vascular associated progenitors migrated from the epicardium and localized in tunica adventitia.

On the other hand, as demonstrated by gene ontology analysis of differentially expressed genes, hCPCs were found to express a number of genes related to cell

adhesion, actin cytoskeleton organization, thereby cell migration (Appendix A5; e.g. Ras homology [Rho] GTPase family members RhoGTPase activating and RhoGTPase target genes as well as talin 1 [*TLN1*]). Considering the fact that c-Kit$^+$ epicardial progenitors are highly invasive migrating from the epicardium to mesoethelial layer during EMT process (Keith and Bolli 2015), it can be speculated that these hCPCs might have been derived from these epicardial progenitors preserving their intrinsic behavior and migration capacity. However, it should be also noted that hCPCs might be representing only a group of perivascular cells, which tend to cluster in oxygen-rich surface regions in EHM resembling their *in vivo* stem cell niche environment.

4.3 CPCs and fibroblasts support EHM formation

We demonstrated that mouse and human CPCs are capable of supporting functional heart muscle formation *in vitro* similar to fibroblasts, although they seemed to not support functional development optimally as indicated by lower contractile performance in CPC-EHM vs. fibroblast-EHM. Biochemical (e.g. hormones and growth factors) and biophysical cues (e.g. mechanical loading, substrate stiffness and isotropy) play an important role in mediating cardiac function (Liaw and Zimmermann 2016). Biochemical factors including triiodothyronine (T3), insulin, growth hormone and IGF-1 as an activator of PI3K/Akt signaling pathway are among the particular factors involved in physiological hypertrophy and calcium homeostasis (Louch et al. 2015). As demonstrated from RNAseq data, hCPCs seem to have a different secretome profile than fibroblasts. One interesting observation, which could be related to the lower contractile performance in CPC-EHM, was lower *IGF-1* expression by hCPCs. In previous studies, we observed that insulin and IGF-1 can enhance contractile performance of EHM (Zimmermann et al. 2002); with both effects likely mediated via the IGF-1 receptor. Also the data on CPC optimization by enforced miR133-a expression, in the mouse model, suggested a important involvement of IGF-1 in EHM functionality and cardimoyctye survival (Izarra et al. 2014). Thus one may conclude that CPCs have a limited paracrine activity under basal conditions, which can be enhanced by genetic manipulation to achieve optimal heart muscle support. Whether similar genetic modifications would also enhance the biololgical activity of other cell types, such as fibroblasts, remains to be investigated.

4.4 CPCs do not contribute to cardiac homeostasis under normal conditions

Isolated CPCs require special microenvironmental conditions for the induction of cardiomyocyte differentiation *in vitro*, such as stimulation with chemicals including dexamethasone (Beltrami et al. 2003) and 5-azacytidine (Oh et al. 2003), growth factors (Goumans et al. 2007) as well as co-culturing with cardiomyocytes (Bearzi et al. 2007). However, hCPCs were not detected to differentiate into cardiomyocytes in the EHM co-culture model, as demonstrated by lack of sarcomeric α-actinin expression in GFP-labelled CPCs. This finding was in contrary to other studies describing myogenic specification of CPCs co-cultured with adult cardiomyocytes (Pfister et al. 2005). Obvious reasons for the failure to detect cardiomyocyte transdifferentiation could be: (1) hESC-derived cardiomyocytes and hFFs may not support CPC transdifferentiation; (2) hCPCs do not possess a cardiogenic potential.

Cardiosphere-derived progenitors have been reported to enhance cell cycle activity of endogenous cardiomyocytes when injected into the myocardium after myocardial infarction (Malliaras et al. 2013). In addition, delivery of c-Kit$^+$ CPCs into the infarcted myocardium promoted the formation of proliferative new cardiomyocytes in long-term (Tang et al. 2016). According to these published evidences, one of the mechanisms underlying cardio-regenerative effect of CPCs seems to work through induction of proliferation of endogenous cardiomyocytes. In contrast to this proposed mechanism, we did not detect any additional proliferating response in cardiomyocytes co-cultured with hCPCs.

4.5 CPCs can be modified to enhance their tissue-supporting activity

Low cell retention and engraftment are limiting factors that weaken the success of a cell-based therapy. Genetic modification is one of the key approaches to enhance delivery efficacy of transplanted cells (Terrovitis et al. 2010). Survival of CPCs after injection into the infarcted myocardium was studied by our collaborators (CARE-MI FP7 Consortium; Antonio Bernad; (Izarra, 2014 #95). Overexpression of miR133a in CPC enhanced their therapeutic efficacy *in vivo*. These observations were in line with reports on the ciritical role of mir-133a in stimulating cardiomyocyte proliferation during heart development (Meder et al. 2008). Unexpectedly, enforced mir-133a

expression did not increase CPC engraftment *in vivo*. In agreement with the enhanced therapeutic efficacy *in vivo* we observed an increased paracrine activity of mir-133a-CPCs in rat EHM. The observed reduced cardiomyocyte apoptosis in CPC-miR133a supplemented EHM could have accounted for the improved functional outcome in EHM, but also in the *in vivo* experiments. These experiments demonstrate the utility of the EHM culture format in defining the mode of action in potential cell therapeutics. Whether the specific modification tested would only be effective in CPCs remain to be studied.

4.6 Development of EHM models of hypoxic damage

Heart muscle can undergo a temporal dysfunction, so called myocardial stunning or be permanently damaged leading to lethal ischemia/reperfusion injury. In addition, response to ischemia/reperfusion injury can also depend on the cell type and organ (Kalogeris et al. 2012). Although the exact mechanism that shifts from reversible ischemia to irreversible ischemia/reperfusion injury is not well-known, it most likely requires a number biochemical and metabolic changes including loss of a critical amount of ATP and Ca^{2+} overload (Rovetto et al. 1975). To develop a model system for ischemic heart damage, we tested different hypoxia and reoxygenation protocols in EHM culture. 72 hrs of hypoxia resulted in high lactate accumulation, significant ATP depletion and loss of HIF-1 activity in monolayer cardiomyocytes. In EHM culture, contractile performance was not obviously disturbed after 72 hrs of hypoxia, but clearly diminished after additional 24 hrs of reoxygenation. In addition to reduced basal force of contraction, high calcium sensitivity (suggesting calcium overload) and less β-adrenergic response was observed. Extended hypoxia over 120 hrs resulted in similar damage as observed in the 72 hrs hypoxia 24 hrs reoxygenation experiment. These data identify a narrow time window for the simulation of hypoxia/reperfusion damage in EHM. An unanticipated observation was that EHM subjected to hypoxia/reoxygenation injury could be partially protected from fibroblasts, but not CPC-conditioned medium, suggesting a protective paracrine activity in fibroblasts.

RNAseq profiling identified enhanced anti-apoptotic and cell proliferation/growth enhancing effects in hFFs, which may explain the observed differential effect of conditions medium from hCPCs and hFFs. The suggested anti-inflammatory and

angiogenesis inducing activity in hCPCs may, in the absence of the respective target cells, not be functional in EHM. These data collectively suggest that complex multicellular models are needed to fully determine the biological activity of CPCs. Finally, our data supports the use of animal models to fully determine the likely comprehensive effects of cell based therapies.

4.7 CPCs protect EHM under chronic hypoxia

Cardiac progenitor cell based therapy, regardless of the delivery mode, requires the deposition and retention (at least transiently) of CPCs in or adjacent to damaged myocardium, which is typically inflamed and hypoxic (Li et al. 2016). In agreement with the concept of cell context specific efficacy of CPCs, we developed EHM with the most abundant cardiac cell populations, i.e., cardiomyocyte and fibroblasts, supplemented with CPCs. Finally, these EHM tri-cultures were composed of 65% cardiomyocyte, 28% foreskin fibroblasts and 7% hCPCs to simulate a native heart cell composition. Interestingly, EHM tri-cultures were protected from chronic (120 hrs) hypoxic injury. In line with the finding in H/R injury model, hCPCs did not enhance survival of cardiomyocytes, but helped to maintain strucutural and functional integrity, suggesting that hCPCs played a critical role in the adaptation to chronic hypoxia. Thus far, we propose that CPCs under chronic hypoxia support a myocardial hibernation state (Holley et al. 2015). The underlying mechanisms, especially with respect to mitochondria function and metabolism, need to be studied in more detail. Whether a modification of hCPCs, such as enforced miR133a expression, would enhance the therapeutic efficacy as to a protection from cell death remains to be studied.

4.8 Live cell imaging of cardiomyocyte oxygenation

To gain further insight into the mechanisms underlying hypoxic damage and protection from hypoxia, including hypoxia/reoxygenation injury, it is important to on the one hand establish a human model and on the other hand visualize cardiomyocyte specific oxygenation. We first demonstrated that a recently established hypoxia sensor, ODD-Luc can be integrated and utilized to visualize and identify the endogenous biological response to hypoxia in mouse embryonic stem

cell-derived cardiomyocytes (Hesse et al. 2014). Having the first evidence of applicability of ODD-Luc cardiomyocytes for imaging hypoxia in tissue level in a mouse EHM model, we next developed a human model that involves a human embryonic stem cell (hESC) line genetically modified to express ODD-Luc fusion protein. The preliminary data in human system first showed that cardiomyocytes differentiated from hESCs successfully express ODD-Luc with protein stabilization and thus enhanced Luc-signal under hypoxia. This indicates that it should be feasible to develop a human ODD-Luc EHM model for more detailed studies of the mechanisms underlying hypoxia associated myocardial damage as well as protection from hypoxic injury.

5 Conclusion and Perspectives

Engineered Heart Muscle (EHM) was established as model system for the evaluation of the biological activity of cardiac progenitor cells (CPCs) from mouse and human. Color-coding of cardiomyocytes and non-myocytes in EHM allowed for cell type specific morphological and molecular analyses. Interestingly, fibroblasts and CPCs, despite being distinct cell entities based on their molecular properties, supported functional assembly of EHM in a similar way. Moreover, fibroblasts, but not CPCs, appear to be protective in a H/R injury model. Conversely, CPCs were critical and supportive for the maintanence of cardiac function in EHM subjected to chronic hypoxia. This effect in the presence of cardiomyocytes and fibroblasts appeared cell context dependent. Genetic manipulation of CPCs by forced expression of miR-133a was established as a model system for enhanced biological activity. The ODD-Luc model will be instrumental not only for *in vitro* studies, but also to trace EHM survival after implantation *in vivo*.

Bibliography

1. Achilli F, Malafronte C, Lenatti L, Gentile F, Dadone V, Gibelli G, Maggiolini S, Squadroni L, Di Leo C, Burba I, Pesce M, Mircoli L, Capogrossi MC, Di Lelio A, Camisasca P, Morabito A, Colombo G, Pompilio G (2010) Granulocyte colony-stimulating factor attenuates left ventricular remodelling after acute anterior STEMI: results of the single-blind, randomized, placebo-controlled multicentre STem cEll Mobilization in Acute Myocardial Infarction (STEM-AMI) Trial. *Eur J Heart Fail*. 12:1111-21.

2. Ali SR, Hippenmeyer S, Saadat LV, Luo L, Weissman IL, Ardehali R (2014) Existing cardiomyocytes generate cardiomyocytes at a low rate after birth in mice. *Proc Natl Acad Sci U S A*. 111:8850-5.

3. Assmus B, Fischer-Rasokat U, Honold J, Seeger FH, Fichtlscherer S, Tonn T, Seifried E, Schachinger V, Dimmeler S, Zeiher AM (2007) Transcoronary transplantation of functionally competent BMCs is associated with a decrease in natriuretic peptide serum levels and improved survival of patients with chronic postinfarction heart failure: results of the TOPCARE-CHD Registry. *Circ Res*. 100:1234-41.

4. Bartunek J, Behfar A, Dolatabadi D, Vanderheyden M, Ostojic M, Dens J, El Nakadi B, Banovic M, Beleslin B, Vrolix M, Legrand V, Vrints C, Vanoverschelde JL, Crespo-Diaz R, Homsy C, Tendera M, Waldman S, Wijns W, Terzic A (2013) Cardiopoietic stem cell therapy in heart failure: the C-CURE (Cardiopoietic stem Cell therapy in heart failURE) multicenter randomized trial with lineage-specified biologics. *J Am Coll Cardiol*. 61:2329-38.

5. Bearzi C, Rota M, Hosoda T, Tillmanns J, Nascimbene A, De Angelis A, Yasuzawa-Amano S, Trofimova I, Siggins RW, Lecapitaine N, Cascapera S, Beltrami AP, D'Alessandro DA, Zias E, Quaini F, Urbanek K, Michler RE, Bolli R, Kajstura J, Leri A, Anversa P (2007) Human cardiac stem cells. *Proc Natl Acad Sci U S A*. 104:14068-73.

6. Beltrami AP, Barlucchi L, Torella D, Baker M, Limana F, Chimenti S, Kasahara H, Rota M, Musso E, Urbanek K, Leri A, Kajstura J, Nadal-Ginard B, Anversa P (2003) Adult cardiac stem cells are multipotent and support myocardial regeneration. *Cell*. 114:763-76.

7. Bergmann O, Bhardwaj RD, Bernard S, Zdunek S, Barnabe-Heider F, Walsh S, Zupicich J, Alkass K, Buchholz BA, Druid H, Jovinge S, Frisen J (2009) Evidence for cardiomyocyte renewal in humans. *Science*. 324:98-102.

8. Bergmann O, Zdunek S, Felker A, Salehpour M, Alkass K, Bernard S, Sjostrom SL, Szewczykowska M, Jackowska T, Dos Remedios C, Malm T, Andra M, Jashari R, Nyengaard JR, Possnert G, Jovinge S, Druid H, Frisen J (2015) Dynamics of Cell Generation and Turnover in the Human Heart. *Cell*. 161:1566-75.

9. Bernex F, De Sepulveda P, Kress C, Elbaz C, Delouis C, Panthier JJ (1996) Spatial and temporal patterns of c-kit-expressing cells in WlacZ/+ and WlacZ/WlacZ mouse embryos. *Development*. 122:3023-33.

10. Bersell K, Arab S, Haring B, Kuhn B (2009) Neuregulin1/ErbB4 Signaling Induces Cardiomyocyte Proliferation and Repair of Heart Injury. *Cell*. 138:257-270.

11. Bolli R, Chugh AR, D'Amario D, Loughran JH, Stoddard MF, Ikram S, Beache GM, Wagner SG, Leri A, Hosoda T, Sanada F, Elmore JB, Goichberg P, Cappetta D, Solankhi NK, Fahsah I, Rokosh DG, Slaughter MS, Kajstura J, Anversa P (2011) Cardiac stem cells in patients with ischaemic cardiomyopathy (SCIPIO): initial results of a randomised phase 1 trial. *Lancet*. 378:1847-57.

12. Bolli R, Tang XL, Sanganalmath SK, Rimoldi O, Mosna F, Abdel-Latif A, Jneid H, Rota M, Leri A, Kajstura J (2013) Intracoronary delivery of autologous cardiac stem cells improves cardiac function in a porcine model of chronic ischemic cardiomyopathy. *Circulation*. 128:122-31.

13. Chen CW, Okada M, Proto JD, Gao X, Sekiya N, Beckman SA, Corselli M, Crisan M, Saparov A, Tobita K, Peault B, Huard J (2013) Human pericytes for ischemic heart repair. *Stem Cells*. 31:305-16.

14. Chimenti I, Smith RR, Li TS, Gerstenblith G, Messina E, Giacomello A, Marban E (2010) Relative roles of direct regeneration versus paracrine effects of human cardiosphere-derived cells transplanted into infarcted mice. *Circ Res*. 106:971-80.

15. Cho HJ, Lee HJ, Song MK, Seo JY, Bae YH, Kim JY, Lee HY, Lee W, Koo BK, Oh BH, Park YB, Kim HS (2013) Vascular calcifying progenitor cells possess bidirectional differentiation potentials. *PLoS Biol*. 11:e1001534.

16. Chong JJ, Chandrakanthan V, Xaymardan M, Asli NS, Li J, Ahmed I, Heffernan C, Menon MK, Scarlett CJ, Rashidianfar A, Biben C, Zoellner H, Colvin EK, Pimanda JE, Biankin AV, Zhou B, Pu WT, Prall OW, Harvey RP (2011) Adult cardiac-resident MSC-like stem cells with a proepicardial origin. *Cell Stem Cell*. 9:527-40.

17. Chong JJ, Reinecke H, Iwata M, Torok-Storb B, Stempien-Otero A, Murry CE (2013) Progenitor cells identified by PDGFR-alpha expression in the developing and diseased human heart. *Stem Cells Dev*. 22:1932-43.

18. Chong JJ, Forte E, Harvey RP (2014) Developmental origins and lineage descendants of endogenous adult cardiac progenitor cells. *Stem Cell Res*. 13:592-614.

19. Christalla P, Hudson JE, Zimmermann W-H (2012) The Cardiogenic Niche as a Fundamental Building Block of Engineered Myocardium. *Cells Tissues Organs*. 195:82-93.

20. Chugh AR, Beache GM, Loughran JH, Mewton N, Elmore JB, Kajstura J, Pappas P, Tatooles A, Stoddard MF, Lima JA, Slaughter MS, Anversa P, Bolli R (2012) Administration of cardiac stem cells in patients with ischemic cardiomyopathy: the SCIPIO trial: surgical aspects and interim analysis of myocardial function and viability by magnetic resonance. *Circulation*. 126:S54-64.

21. Crisan M, Yap S, Casteilla L, Chen CW, Corselli M, Park TS, Andriolo G, Sun B, Zheng B, Zhang L, Norotte C, Teng PN, Traas J, Schugar R, Deasy BM, Badylak S, Buhring HJ, Giacobino JP, Lazzari L, Huard J, Peault B (2008) A perivascular

origin for mesenchymal stem cells in multiple human organs. *Cell Stem Cell*. 3:301-13.

22. Crisan M, Corselli M, Chen WC, Peault B (2012) Perivascular cells for regenerative medicine. *J Cell Mol Med*. 16:2851-60.

23. Davis DR, Zhang Y, Smith RR, Cheng K, Terrovitis J, Malliaras K, Li TS, White A, Makkar R, Marban E (2009) Validation of the cardiosphere method to culture cardiac progenitor cells from myocardial tissue. *PLoS One*. 4:e7195.

24. Duff SE, Li C, Garland JM, Kumar S (2003) CD105 is important for angiogenesis: evidence and potential applications. *FASEB J*. 17:984-92.

25. Ellison Georgina M, Vicinanza C, Smith Andrew J, Aquila I, Leone A, Waring Cheryl D, Henning Beverley J, Stirparo Giuliano G, Papait R, Scarfò M, Agosti V, Viglietto G, Condorelli G, Indolfi C, Ottolenghi S, Torella D, Nadal-Ginard B (2013) Adult c-kitpos Cardiac Stem Cells Are Necessary and Sufficient for Functional Cardiac Regeneration and Repair. *Cell*. 154:827-842.

26. Engel FB, Hsieh PCH, Lee RT, Keating MT (2006) FGF1/p38 MAP kinase inhibitor therapy induces cardiomyocyte mitosis, reduces scarring, and rescues function after myocardial infarction. *P Natl Acad Sci USA*. 103:15546-15551.

27. Ferreira-Martins J, Ogorek B, Cappetta D, Matsuda A, Signore S, D'Amario D, Kostyla J, Steadman E, Ide-Iwata N, Sanada F, Iaffaldano G, Ottolenghi S, Hosoda T, Leri A, Kajstura J, Anversa P, Rota M (2012) Cardiomyogenesis in the developing heart is regulated by c-kit-positive cardiac stem cells. *Circ Res*. 110:701-15.

28. Fischer KM, Cottage CT, Wu W, Din S, Gude NA, Avitabile D, Quijada P, Collins BL, Fransioli J, Sussman MA (2009) Enhancement of myocardial regeneration through genetic engineering of cardiac progenitor cells expressing Pim-1 kinase. *Circulation*. 120:2077-87.

29. Freire AG, Nascimento DS, Forte G, Valente M, Resende TP, Pagliari S, Abreu C, Carvalho I, Di Nardo P, Pinto-do OP (2014) Stable phenotype and function of immortalized Lin-Sca-1+ cardiac progenitor cells in long-term culture: a step closer to standardization. *Stem Cells Dev*. 23:1012-26.

30. Furtado MB, Costa MW, Pranoto EA, Salimova E, Pinto AR, Lam NT, Park A, Snider P, Chandran A, Harvey RP, Boyd R, Conway SJ, Pearson J, Kaye DM, Rosenthal NA (2014) Cardiogenic genes expressed in cardiac fibroblasts contribute to heart development and repair. *Circ Res*. 114:1422-34.

31. Gerbin KA, Murry CE (2015) The winding road to regenerating the human heart. *Cardiovasc Pathol*. 24:133-40.

32. Godier-Furnemont AF, Tiburcy M, Wagner E, Dewenter M, Lammle S, El-Armouche A, Lehnart SE, Vunjak-Novakovic G, Zimmermann WH (2015) Physiologic force-frequency response in engineered heart muscle by electromechanical stimulation. *Biomaterials*. 60:82-91.

33. Goumans MJ, de Boer TP, Smits AM, van Laake LW, van Vliet P, Metz CH, Korfage TH, Kats KP, Hochstenbach R, Pasterkamp G, Verhaar MC, van der Heyden MA, de Kleijn D, Mummery CL, van Veen TA, Sluijter JP, Doevendans PA (2007) TGF-beta1 induces efficient differentiation of human cardiomyocyte progenitor cells into functional cardiomyocytes in vitro. *Stem Cell Res*. 1:138-49.

34. Hassink RJ, Pasumarthi KB, Nakajima H, Rubart M, Soonpaa MH, de la Riviere AB, Doevendans PA, Field LJ (2008) Cardiomyocyte cell cycle activation improves cardiac function after myocardial infarction. *Cardiovascular Research*. 78:18-25.

35. Hesse AR, Levent E, Zieseniss A, Tiburcy M, Zimmermann WH, Katschinski DM (2014) Lights on for HIF-1alpha: genetically enhanced mouse cardiomyocytes for heart tissue imaging. *Cell Physiol Biochem*. 34:455-62.

36. Holley CT, Long EK, Lindsey ME, McFalls EO, Kelly RF (2015) Recovery of hibernating myocardium: what is the role of surgical revascularization? *J Card Surg*. 30:224-31.

37. Houtgraaf JH, den Dekker WK, van Dalen BM, Springeling T, de Jong R, van Geuns RJ, Geleijnse ML, Fernandez-Aviles F, Zijlsta F, Serruys PW, Duckers HJ (2012) First experience in humans using adipose tissue-derived regenerative cells in the treatment of patients with ST-segment elevation myocardial infarction. *J Am Coll Cardiol*. 59:539-40.

38. Hsieh PCH, Segers VFM, Davis ME, MacGillivray C, Gannon J, Molkentin JD, Robbins J, Lee RT (2007) Evidence from a genetic fate-mapping study that stem cells refresh adult mammalian cardiomyocytes after injury. *Nature Medicine*. 13:970-974.

39. Hu Y, Zhang Z, Torsney E, Afzal AR, Davison F, Metzler B, Xu Q (2004) Abundant progenitor cells in the adventitia contribute to atherosclerosis of vein grafts in ApoE-deficient mice. *J Clin Invest*. 113:1258-65.

40. Huang da W, Sherman BT, Lempicki RA (2009) Systematic and integrative analysis of large gene lists using DAVID bioinformatics resources. *Nat Protoc*. 4:44-57.

41. Hudson J, Titmarsh D, Hidalgo A, Wolvetang E, Cooper-White J (2012) Primitive Cardiac Cells from Human Embryonic Stem Cells. *Stem Cells and Development*. 21:1513-1523.

42. Ikuta K, Weissman IL (1992) Evidence that hematopoietic stem cells express mouse c-kit but do not depend on steel factor for their generation. *Proc Natl Acad Sci U S A*. 89:1502-6.

43. Irion S, Luche H, Gadue P, Fehling HJ, Kennedy M, Keller G (2007) Identification and targeting of the ROSA26 locus in human embryonic stem cells. *Nat Biotechnol*. 25:1477-82.

44. Ito CY, Li CY, Bernstein A, Dick JE, Stanford WL (2003) Hematopoietic stem cell and progenitor defects in Sca-1/Ly-6A-null mice. *Blood*. 101:517-23.

45. Izarra A, Moscoso I, Levent E, Cañón S, Cerrada I, Díez-Juan A, Blanca V, Núñez-Gil I-J, Valiente I, Ruíz-Sauri A, Sepúlveda P, Tiburcy M, Zimmermann W-H, Bernad A (2014) miR-133a Enhances the Protective Capacity of Cardiac Progenitors Cells after Myocardial Infarction. *Stem Cell Reports*. 3:1029-1042.

46. Jankowski RJ, Haluszczak C, Trucco M, Huard J (2001) Flow cytometric characterization of myogenic cell populations obtained via the preplate technique: potential for rapid isolation of muscle-derived stem cells. *Hum Gene Ther*. 12:619-28.

47. Kalogeris T, Baines CP, Krenz M, Korthuis RJ (2012) Cell biology of ischemia/reperfusion injury. *Int Rev Cell Mol Biol*. 298:229-317.

48. Keith MC, Bolli R (2015) "String theory" of c-kit(pos) cardiac cells: a new paradigm regarding the nature of these cells that may reconcile apparently discrepant results. *Circ Res*. 116:1216-30.

49. Kennedy-Lydon T, Rosenthal N (2015) Cardiac regeneration: epicardial mediated repair. *Proc Biol Sci*. 282.

50. Kim D, Pertea G, Trapnell C, Pimentel H, Kelley R, Salzberg SL (2013) TopHat2: accurate alignment of transcriptomes in the presence of insertions, deletions and gene fusions. *Genome Biol*. 14:R36.

51. Klug MG, Soonpaa MH, Koh GY, Field LJ (1996) Genetically selected cardiomyocytes from differentiating embronic stem cells form stable intracardiac grafts. *J Clin Invest*. 98:216-24.

52. Kovacic JC, Boehm M (2009) Resident vascular progenitor cells: an emerging role for non-terminally differentiated vessel-resident cells in vascular biology. *Stem Cell Res*. 2:2-15.

53. Kramann R, Schneider RK, DiRocco DP, Machado F, Fleig S, Bondzie PA, Henderson JM, Ebert BL, Humphreys BD (2015) Perivascular Gli1+ progenitors are key contributors to injury-induced organ fibrosis. *Cell Stem Cell*. 16:51-66.

54. Kubo H, Berretta RM, Jaleel N, Angert D, Houser SR (2009) c-Kit+ bone marrow stem cells differentiate into functional cardiac myocytes. *Clin Transl Sci*. 2:26-32.

55. Kuhn B, del Monte F, Hajjar RJ, Chang YS, Lebeche D, Arab S, Keating MT (2007) Periostin induces proliferation of differentiated cardiomyocytes and promotes cardiac repair. *Nature Medicine*. 13:962-969.

56. Laflamme MA, Murry CE (2011) Heart regeneration. *Nature*. 473:326-35.

57. Lauden L, Boukouaci W, Borlado LR, Lopez IP, Sepulveda P, Tamouza R, Charron D, Al-Daccak R (2013) Allogenicity of human cardiac stem/progenitor cells orchestrated by programmed death ligand 1. *Circ Res*. 112:451-64.

58. Lennartsson J, Ronnstrand L (2012) Stem cell factor receptor/c-Kit: from basic science to clinical implications. *Physiol Rev*. 92:1619-49.

59. Li TS, Cheng K, Malliaras K, Smith RR, Zhang Y, Sun B, Matsushita N, Blusztajn A, Terrovitis J, Kusuoka H, Marban L, Marban E (2012) Direct comparison of different stem cell types and subpopulations reveals superior paracrine potency and myocardial repair efficacy with cardiosphere-derived cells. *J Am Coll Cardiol*. 59:942-53.

60. Li X, Tamama K, Xie X, Guan J (2016) Improving Cell Engraftment in Cardiac Stem Cell Therapy. *Stem Cells Int*. 2016:7168797.

61. Liang J, Wu YL, Chen BJ, Zhang W, Tanaka Y, Sugiyama H (2013) The C-kit receptor-mediated signal transduction and tumor-related diseases. *Int J Biol Sci*. 9:435-43.

62. Liaw NY, Zimmermann WH (2016) Mechanical stimulation in the engineering of heart muscle. *Adv Drug Deliv Rev*. 96:156-60.

63. Limana F, Zacheo A, Mocini D, Mangoni A, Borsellino G, Diamantini A, De Mori R, Battistini L, Vigna E, Santini M, Loiaconi V, Pompilio G, Germani A, Capogrossi MC (2007) Identification of myocardial and vascular precursor cells in human and mouse epicardium. *Circ Res*. 101:1255-65.

64. Limana F, Bertolami C, Mangoni A, Di Carlo A, Avitabile D, Mocini D, Iannelli P, De Mori R, Marchetti C, Pozzoli O, Gentili C, Zacheo A, Germani A, Capogrossi MC (2010) Myocardial infarction induces embryonic reprogramming of epicardial c-kit(+) cells: role of the pericardial fluid. *J Mol Cell Cardiol*. 48:609-18.

65. Liu ML, Nagai T, Tokunaga M, Iwanaga K, Matsuura K, Takahashi T, Kanda M, Kondo N, Naito AT, Komuro I, Kobayashi Y (2014) Anti-inflammatory peptides from cardiac progenitors ameliorate dysfunction after myocardial infarction. *J Am Heart Assoc*. 3:e001101.

66. Livak KJ, Schmittgen TD (2001) Analysis of relative gene expression data using real-time quantitative PCR and the 2(-Delta Delta C(T)) Method. *Methods*. 25:402-8.

67. Louch WE, Koivumaki JT, Tavi P (2015) Calcium signalling in developing cardiomyocytes: implications for model systems and disease. *J Physiol*. 593:1047-63.

68. Lunde K, Solheim S, Aakhus S, Arnesen H, Abdelnoor M, Egeland T, Endresen K, Ilebekk A, Mangschau A, Fjeld JG, Smith HJ, Taraldsrud E, Grogaard HK, Bjornerheim R, Brekke M, Muller C, Hopp E, Ragnarsson A, Brinchmann JE, Forfang K (2006) Intracoronary injection of mononuclear bone marrow cells in acute myocardial infarction. *N Engl J Med*. 355:1199-209.

69. Makkar RR, Smith RR, Cheng K, Malliaras K, Thomson LE, Berman D, Czer LS, Marban L, Mendizabal A, Johnston PV, Russell SD, Schuleri KH, Lardo AC, Gerstenblith G, Marban E (2012) Intracoronary cardiosphere-derived cells for heart regeneration after myocardial infarction (CADUCEUS): a prospective, randomised phase 1 trial. *Lancet*. 379:895-904.

70. Malliaras K, Zhang Y, Seinfeld J, Galang G, Tseliou E, Cheng K, Sun B, Aminzadeh M, Marban E (2013) Cardiomyocyte proliferation and progenitor cell recruitment underlie therapeutic regeneration after myocardial infarction in the adult mouse heart. *EMBO Mol Med*. 5:191-209.

71. Martin CM, Meeson AP, Robertson SM, Hawke TJ, Richardson JA, Bates S, Goetsch SC, Gallardo TD, Garry DJ (2004) Persistent expression of the ATP-binding cassette transporter, Abcg2, identifies cardiac SP cells in the developing and adult heart. *Dev Biol*. 265:262-75.

72. Matsuura K, Nagai T, Nishigaki N, Oyama T, Nishi J, Wada H, Sano M, Toko H, Akazawa H, Sato T, Nakaya H, Kasanuki H, Komuro I (2004) Adult cardiac Sca-1-positive cells differentiate into beating cardiomyocytes. *J Biol Chem*. 279:11384-91.

73. Meder B, Katus HA, Rottbauer W (2008) Right into the heart of microRNA-133a. *Genes Dev*. 22:3227-31.

74. Menasche P, Alfieri O, Janssens S, McKenna W, Reichenspurner H, Trinquart L, Vilquin JT, Marolleau JP, Seymour B, Larghero J, Lake S, Chatellier G, Solomon S, Desnos M, Hagege AA (2008) The Myoblast Autologous Grafting in Ischemic Cardiomyopathy (MAGIC) trial: first randomized placebo-controlled study of myoblast transplantation. *Circulation*. 117:1189-200.

75. Messina E, De Angelis L, Frati G, Morrone S, Chimenti S, Fiordaliso F, Salio M, Battaglia M, Latronico MV, Coletta M, Vivarelli E, Frati L, Cossu G, Giacomello A (2004) Isolation and expansion of adult cardiac stem cells from human and murine heart. *Circ Res*. 95:911-21.

76. Meyer GP, Wollert KC, Lotz J, Pirr J, Rager U, Lippolt P, Hahn A, Fichtner S, Schaefer A, Arseniev L, Ganser A, Drexler H (2009) Intracoronary bone marrow cell transfer after myocardial infarction: 5-year follow-up from the randomized-controlled BOOST trial. *Eur Heart J*. 30:2978-84.

77. Mill JG, Stefanon I, dos Santos L, Baldo MP (2011) Remodeling in the ischemic heart: the stepwise progression for heart. *Brazilian Journal of Medical and Biological Research*. 44:890-898.

78. Miura M, Miura Y, Padilla-Nash HM, Molinolo AA, Fu B, Patel V, Seo BM, Sonoyama W, Zheng JJ, Baker CC, Chen W, Ried T, Shi S (2006) Accumulated chromosomal instability in murine bone marrow mesenchymal stem cells leads to malignant transformation. *Stem Cells*. 24:1095-103.

79. Miyamoto S, Kawaguchi N, Ellison GM, Matsuoka R, Shin'oka T, Kurosawa H (2010) Characterization of long-term cultured c-kit+ cardiac stem cells derived from adult rat hearts. *Stem Cells Dev*. 19:105-16.

80. Moroz E, Carlin S, Dyomina K, Burke S, Thaler HT, Blasberg R, Serganova I (2009) Real-time imaging of HIF-1alpha stabilization and degradation. *PLoS One*. 4:e5077.

81. Mushtaq M, DiFede DL, Golpanian S, Khan A, Gomes SA, Mendizabal A, Heldman AW, Hare JM (2014) Rationale and design of the Percutaneous Stem Cell Injection Delivery Effects on Neomyogenesis in Dilated Cardiomyopathy (the POSEIDON-DCM study): a phase I/II, randomized pilot study of the comparative

safety and efficacy of transendocardial injection of autologous mesenchymal stem cell vs. allogeneic mesenchymal stem cells in patients with non-ischemic dilated cardiomyopathy. *J Cardiovasc Transl Res*. 7:769-80.

82. Nagy A, Rossant J, Nagy R, Abramow-Newerly W, Roder JC (1993) Derivation of completely cell culture-derived mice from early-passage embryonic stem cells. *Proc Natl Acad Sci U S A*. 90:8424-8.

83. Naito H, Melnychenko I, Didie M, Schneiderbanger K, Schubert P, Rosenkranz S, Eschenhagen T, Zimmermann WH (2006) Optimizing engineered heart tissue for therapeutic applications as surrogate heart muscle. *Circulation*. 114:I72-8.

84. Noack C, Zafiriou MP, Schaeffer HJ, Renger A, Pavlova E, Dietz R, Zimmermann WH, Bergmann MW, Zelarayan LC (2012) Krueppel-like factor 15 regulates Wnt/beta-catenin transcription and controls cardiac progenitor cell fate in the postnatal heart. *EMBO Mol Med*. 4:992-1007.

85. Noseda M, Harada M, McSweeney S, Leja T, Belian E, Stuckey DJ, Abreu Paiva MS, Habib J, Macaulay I, de Smith AJ, al-Beidh F, Sampson R, Lumbers RT, Rao P, Harding SE, Blakemore AI, Jacobsen SE, Barahona M, Schneider MD (2015) PDGFRalpha demarcates the cardiogenic clonogenic Sca1+ stem/progenitor cell in adult murine myocardium. *Nat Commun*. 6:6930.

86. Oh H, Bradfute SB, Gallardo TD, Nakamura T, Gaussin V, Mishina Y, Pocius J, Michael LH, Behringer RR, Garry DJ, Entman ML, Schneider MD (2003) Cardiac progenitor cells from adult myocardium: homing, differentiation, and fusion after infarction. *Proc Natl Acad Sci U S A*. 100:12313-8.

87. Pavo N, Charwat S, Nyolczas N, Jakab A, Murlasits Z, Bergler-Klein J, Nikfardjam M, Benedek I, Benedek T, Pavo IJ, Gersh BJ, Huber K, Maurer G, Gyongyosi M (2014) Cell therapy for human ischemic heart diseases: critical review and summary of the clinical experiences. *J Mol Cell Cardiol*. 75:12-24.

88. Perin EC, Willerson JT, Pepine CJ, Henry TD, Ellis SG, Zhao DX, Silva GV, Lai D, Thomas JD, Kronenberg MW, Martin AD, Anderson RD, Traverse JH, Penn MS, Anwaruddin S, Hatzopoulos AK, Gee AP, Taylor DA, Cogle CR, Smith D, Westbrook L, Chen J, Handberg E, Olson RE, Geither C, Bowman S, Francescon J,

Baraniuk S, Piller LB, Simpson LM, Loghin C, Aguilar D, Richman S, Zierold C, Bettencourt J, Sayre SL, Vojvodic RW, Skarlatos SI, Gordon DJ, Ebert RF, Kwak M, Moye LA, Simari RD (2012) Effect of transendocardial delivery of autologous bone marrow mononuclear cells on functional capacity, left ventricular function, and perfusion in chronic heart failure: the FOCUS-CCTRN trial. *JAMA*. 307:1717-26.

89. Pfister O, Mouquet F, Jain M, Summer R, Helmes M, Fine A, Colucci WS, Liao R (2005) CD31- but Not CD31+ cardiac side population cells exhibit functional cardiomyogenic differentiation. *Circ Res*. 97:52-61.

90. Porrello ER, Mahmoud AI, Simpson E, Hill JA, Richardson JA, Olson EN, Sadek HA (2011) Transient regenerative potential of the neonatal mouse heart. *Science*. 331:1078-80.

91. Portal L, Martin V, Assaly R, d'Anglemont de Tassigny A, Michineau S, Berdeaux A, Ghaleh B, Pons S (2013) A model of hypoxia-reoxygenation on isolated adult mouse cardiomyocytes: characterization, comparison with ischemia-reperfusion, and application to the cardioprotective effect of regular treadmill exercise. *J Cardiovasc Pharmacol Ther*. 18:367-75.

92. Raphael Rubin DSS. Rubin's Pathology. *Clinicopathologic Foundations of Medicine*. 2008.

93. Reubinoff BE, Pera MF, Fong CY, Trounson A, Bongso A (2000) Embryonic stem cell lines from human blastocysts: somatic differentiation in vitro. *Nat Biotechnol*. 18:399-404.

94. Roncalli J, Mouquet F, Piot C, Trochu JN, Le Corvoisier P, Neuder Y, Le Tourneau T, Agostini D, Gaxotte V, Sportouch C, Galinier M, Crochet D, Teiger E, Richard MJ, Polge AS, Beregi JP, Manrique A, Carrie D, Susen S, Klein B, Parini A, Lamirault G, Croisille P, Rouard H, Bourin P, Nguyen JM, Delasalle B, Vanzetto G, Van Belle E, Lemarchand P (2011) Intracoronary autologous mononucleated bone marrow cell infusion for acute myocardial infarction: results of the randomized multicenter BONAMI trial. *Eur Heart J*. 32:1748-57.

95. Rota M, Padin-Iruegas ME, Misao Y, De Angelis A, Maestroni S, Ferreira-Martins J, Fiumana E, Rastaldo R, Arcarese ML, Mitchell TS, Boni A, Bolli R,

Urbanek K, Hosoda T, Anversa P, Leri A, Kajstura J (2008) Local activation or implantation of cardiac progenitor cells rescues scarred infarcted myocardium improving cardiac function. *Circ Res*. 103:107-16.

96. Rovetto MJ, Lamberton WF, Neely JR (1975) Mechanisms of glycolytic inhibition in ischemic rat hearts. *Circ Res*. 37:742-51.

97. Rubio D, Garcia-Castro J, Martin MC, de la Fuente R, Cigudosa JC, Lloyd AC, Bernad A (2005) Spontaneous human adult stem cell transformation. *Cancer Res*. 65:3035-9.

98. Sacchetti B, Funari A, Michienzi S, Di Cesare S, Piersanti S, Saggio I, Tagliafico E, Ferrari S, Robey PG, Riminucci M, Bianco P (2007) Self-renewing osteoprogenitors in bone marrow sinusoids can organize a hematopoietic microenvironment. *Cell*. 131:324-36.

99. Sagoo MS, Mehta JS, Hau S, Irion LD, Curry A, Bonshek RE, Tuft SJ (2007) Microsporidium stromal keratitis: in vivo confocal findings. *Cornea*. 26:870-3.

100. Sainz J, Al Haj Zen A, Caligiuri G, Demerens C, Urbain D, Lemitre M, Lafont A (2006) Isolation of "side population" progenitor cells from healthy arteries of adult mice. *Arterioscler Thromb Vasc Biol*. 26:281-6.

101. Schofield CJ, Ratcliffe PJ (2004) Oxygen sensing by HIF hydroxylases. *Nature Reviews Molecular Cell Biology*. 5:343-354.

102. Senyo SE, Steinhauser ML, Pizzimenti CL, Yang VK, Cai L, Wang M, Wu TD, Guerquin-Kern JL, Lechene CP, Lee RT (2013) Mammalian heart renewal by pre-existing cardiomyocytes. *Nature*. 493:433-6.

103. Smart N, Bollini S, Dube KN, Vieira JM, Zhou B, Davidson S, Yellon D, Riegler J, Price AN, Lythgoe MF, Pu WT, Riley PR (2011) De novo cardiomyocytes from within the activated adult heart after injury. *Nature*. 474:640-4.

104. Smith CL, Baek ST, Sung CY, Tallquist MD (2011) Epicardial-derived cell epithelial-to-mesenchymal transition and fate specification require PDGF receptor signaling. *Circ Res*. 108:e15-26.

105. Smits AM, van Vliet P, Metz CH, Korfage T, Sluijter JP, Doevendans PA, Goumans MJ (2009) Human cardiomyocyte progenitor cells differentiate into functional mature cardiomyocytes: an in vitro model for studying human cardiac physiology and pathophysiology. *Nat Protoc*. 4:232-43.

106. Soong PL, Tiburcy M, Zimmermann W-H (2012) Cardiac Differentiation of Human Embryonic Stem Cells and their Assembly into Engineered Heart Muscle. *Curr Protoc Cell Biol*. 55:23.8.1-23.8.21.

107. Stefanova I, Horejsi V, Ansotegui IJ, Knapp W, Stockinger H (1991) GPI-anchored cell-surface molecules complexed to protein tyrosine kinases. *Science*. 254:1016-9.

108. Sultana N, Zhang L, Yan J, Chen J, Cai W, Razzaque S, Jeong D, Sheng W, Bu L, Xu M, Huang GY, Hajjar RJ, Zhou B, Moon A, Cai CL (2015) Resident c-kit(+) cells in the heart are not cardiac stem cells. *Nat Commun*. 6:8701.

109. Suzuki G (2015) Translational research of adult stem cell therapy. *World J Cardiol*. 7:707-18.

110. Takamiya M, Haider KH, Ashraf M (2011) Identification and characterization of a novel multipotent sub-population of Sca-1(+) cardiac progenitor cells for myocardial regeneration. *PLoS One*. 6:e25265.

111. Takehara N, Nagata M, Ogata T, Nakamura T, Matoba S, Gojo S, Sawada T, Yaku H, Matsubara H. The ALCADIA (Autologous Human Cardiac-derived Stem Cell To Treat Ischemic Cardiomyopathy) trial. 2012.

112. Tallini YN, Greene KS, Craven M, Spealman A, Breitbach M, Smith J, Fisher PJ, Steffey M, Hesse M, Doran RM, Woods A, Singh B, Yen A, Fleischmann BK, Kotlikoff MI (2009) c-kit expression identifies cardiovascular precursors in the neonatal heart. *Proc Natl Acad Sci U S A*. 106:1808-13.

113. Tang XL, Rokosh G, Sanganalmath SK, Yuan F, Sato H, Mu J, Dai S, Li C, Chen N, Peng Y, Dawn B, Hunt G, Leri A, Kajstura J, Tiwari S, Shirk G, Anversa P, Bolli R (2010) Intracoronary administration of cardiac progenitor cells alleviates left ventricular dysfunction in rats with a 30-day-old infarction. *Circulation*. 121:293-305.

114. Tang XL, Li Q, Rokosh G, Sanganalmath SK, Chen N, Ou Q, Stowers H, Hunt G, Bolli R (2016) Long-Term Outcome of Administration of c-kitPOS Cardiac Progenitor Cells After Acute Myocardial Infarction: Transplanted Cells Do not Become Cardiomyocytes, but Structural and Functional Improvement and Proliferation of Endogenous Cells Persist for at Least One Year. *Circ Res*. 118:1091-105.

115. Taniguchi N, Nakamura T, Sawada T, Matsubara K, Furukawa K, Hadase M, Nakahara Y, Matsubara H (2010) Erythropoietin prevention trial of coronary restenosis and cardiac remodeling after ST-elevated acute myocardial infarction (EPOC-AMI): a pilot, randomized, placebo-controlled study. *Circ J*. 74:2365-71.

116. Tateishi K, Ashihara E, Takehara N, Nomura T, Honsho S, Nakagami T, Morikawa S, Takahashi T, Ueyama T, Matsubara H, Oh H (2007) Clonally amplified cardiac stem cells are regulated by Sca-1 signaling for efficient cardiovascular regeneration. *J Cell Sci*. 120:1791-800.

117. Terrovitis JV, Smith RR, Marban E (2010) Assessment and optimization of cell engraftment after transplantation into the heart. *Circ Res*. 106:479-94.

118. Tiburcy M, Didie M, Boy O, Christalla P, Doker S, Naito H, Karikkineth BC, El-Armouche A, Grimm M, Nose M, Eschenhagen T, Zieseniss A, Katschinski DM, Hamdani N, Linke WA, Yin X, Mayr M, Zimmermann WH (2011) Terminal Differentiation, Advanced Organotypic Maturation, and Modeling of Hypertrophic Growth in Engineered Heart Tissue. *Circulation Research*. 109:1105-1114.

119. Tiburcy M, Meyer T, Soong PL, Zimmermann WH (2014) Collagen-based engineered heart muscle. *Methods Mol Biol*. 1181:167-76.

120. Tillmanns J, Rota M, Hosoda T, Misao Y, Esposito G, Gonzalez A, Vitale S, Parolin C, Yasuzawa-Amano S, Muraski J, De Angelis A, Lecapitaine N, Siggins RW, Loredo M, Bearzi C, Bolli R, Urbanek K, Leri A, Kajstura J, Anversa P (2008) Formation of large coronary arteries by cardiac progenitor cells. *Proc Natl Acad Sci U S A*. 105:1668-73.

121. Tohyama S, Hattori F, Sano M, Hishiki T, Nagahata Y, Matsuura T, Hashimoto H, Suzuki T, Yamashita H, Satoh Y, Egashira T, Seki T, Muraoka N, Yamakawa H,

Ohgino Y, Tanaka T, Yoichi M, Yuasa S, Murata M, Suematsu M, Fukuda K (2013) Distinct metabolic flow enables large-scale purification of mouse and human pluripotent stem cell-derived cardiomyocytes. *Cell Stem Cell*. 12:127-37.

122. Tomita Y, Matsumura K, Wakamatsu Y, Matsuzaki Y, Shibuya I, Kawaguchi H, Ieda M, Kanakubo S, Shimazaki T, Ogawa S, Osumi N, Okano H, Fukuda K (2005) Cardiac neural crest cells contribute to the dormant multipotent stem cell in the mammalian heart. *J Cell Biol*. 170:1135-46.

123. Torella D, Indolfi C, Goldspink DF, Ellison GM (2008) Cardiac stem cell-based myocardial regeneration: towards a translational approach. *Cardiovasc Hematol Agents Med Chem*. 6:53-9.

124. Tossios P, Krausgrill B, Schmidt M, Fischer T, Halbach M, Fries JW, Fahnenstich S, Frommolt P, Heppelmann I, Schmidt A, Schomacker K, Fischer JH, Bloch W, Mehlhorn U, Schwinger RH, Muller-Ehmsen J (2008) Role of balloon occlusion for mononuclear bone marrow cell deposition after intracoronary injection in pigs with reperfused myocardial infarction. *Eur Heart J*. 29:1911-21.

125. Trapnell C, Roberts A, Goff L, Pertea G, Kim D, Kelley DR, Pimentel H, Salzberg SL, Rinn JL, Pachter L (2012) Differential gene and transcript expression analysis of RNA-seq experiments with TopHat and Cufflinks. *Nat Protoc*. 7:562-78.

126. Uchida S, De Gaspari P, Kostin S, Jenniches K, Kilic A, Izumiya Y, Shiojima I, Grosse Kreymborg K, Renz H, Walsh K, Braun T (2013) Sca1-derived cells are a source of myocardial renewal in the murine adult heart. *Stem Cell Reports*. 1:397-410.

127. Urbanek K, Quaini F, Tasca G, Torella D, Castaldo C, Nadal-Ginard B, Leri A, Kajstura J, Quaini E, Anversa P (2003) Intense myocyte formation from cardiac stem cells in human cardiac hypertrophy. *Proc Natl Acad Sci U S A*. 100:10440-5.

128. Valente M, Nascimento DS, Cumano A, Pinto-do OP (2014) Sca-1+ cardiac progenitor cells and heart-making: a critical synopsis. *Stem Cells Dev*. 23:2263-73.

129. van Berlo JH, Kanisicak O, Maillet M, Vagnozzi RJ, Karch J, Lin S-CJ, Middleton RC, Marbán E, Molkentin JD (2014) c-kit+ cells minimally contribute cardiomyocytes to the heart. *Nature*. 509:337-341.

130. van de Rijn M, Heimfeld S, Spangrude GJ, Weissman IL (1989) Mouse hematopoietic stem-cell antigen Sca-1 is a member of the Ly-6 antigen family. *Proc Natl Acad Sci U S A*. 86:4634-8.

131. van der Spoel TI, Jansen of Lorkeers SJ, Agostoni P, van Belle E, Gyongyosi M, Sluijter JP, Cramer MJ, Doevendans PA, Chamuleau SA (2011) Human relevance of pre-clinical studies in stem cell therapy: systematic review and meta-analysis of large animal models of ischaemic heart disease. *Cardiovasc Res*. 91:649-58.

132. Viola RJ, Provenzale JM, Li F, Li CY, Yuan H, Tashjian J, Dewhirst MW (2008) In vivo bioluminescence imaging monitoring of hypoxia-inducible factor 1alpha, a promoter that protects cells, in response to chemotherapy. *AJR Am J Roentgenol*. 191:1779-84.

133. Volz KS, Jacobs AH, Chen HI, Poduri A, McKay AS, Riordan DP, Kofler N, Kitajewski J, Weissman I, Red-Horse K (2015) Pericytes are progenitors for coronary artery smooth muscle. *Elife*. 4.

134. Wang X, Hu Q, Nakamura Y, Lee J, Zhang G, From AH, Zhang J (2006) The role of the sca-1+/CD31- cardiac progenitor cell population in postinfarction left ventricular remodeling. *Stem Cells*. 24:1779-88.

135. Warejcka DJ, Harvey R, Taylor BJ, Young HE, Lucas PA (1996) A population of cells isolated from rat heart capable of differentiating into several mesodermal phenotypes. *J Surg Res*. 62:233-42.

136. Wilson A, Oser GM, Jaworski M, Blanco-Bose WE, Laurenti E, Adolphe C, Essers MA, Macdonald HR, Trumpp A (2007) Dormant and self-renewing hematopoietic stem cells and their niches. *Ann N Y Acad Sci*. 1106:64-75.

137. Wong SP, Rowley JE, Redpath AN, Tilman JD, Fellous TG, Johnson JR (2015) Pericytes, mesenchymal stem cells and their contributions to tissue repair. *Pharmacol Ther*. 151:107-20.

138. Yancy CW, Jessup M, Bozkurt B, Butler J, Casey DE, Jr., Drazner MH, Fonarow GC, Geraci SA, Horwich T, Januzzi JL, Johnson MR, Kasper EK, Levy WC, Masoudi FA, McBride PE, McMurray JJ, Mitchell JE, Peterson PN, Riegel B, Sam F, Stevenson LW, Tang WH, Tsai EJ, Wilkoff BL (2013) 2013 ACCF/AHA guideline for the management of heart failure: a report of the American College of Cardiology Foundation/American Heart Association Task Force on practice guidelines. *Circulation*. 128:e240-327.

139. Ye J, Boyle A, Shih H, Sievers RE, Zhang Y, Prasad M, Su H, Zhou Y, Grossman W, Bernstein HS, Yeghiazarians Y (2012) Sca-1+ cardiosphere-derived cells are enriched for Isl1-expressing cardiac precursors and improve cardiac function after myocardial injury. *PLoS One*. 7:e30329.

140. Zangi L, Lui KO, von Gise A, Ma Q, Ebina W, Ptaszek LM, Spater D, Xu H, Tabebordbar M, Gorbatov R, Sena B, Nahrendorf M, Briscoe DM, Li RA, Wagers AJ, Rossi DJ, Pu WT, Chien KR (2013) Modified mRNA directs the fate of heart progenitor cells and induces vascular regeneration after myocardial infarction. *Nat Biotechnol*. 31:898-907.

141. Zaruba MM, Soonpaa M, Reuter S, Field LJ (2010) Cardiomyogenic Potential of C-Kit+-Expressing Cells Derived From Neonatal and Adult Mouse Hearts. *Circulation*. 121:1992-2000.

142. Zimmermann WH, Fink C, Kralisch D, Remmers U, Weil J, Eschenhagen T (2000) Three-dimensional engineered heart tissue from neonatal rat cardiac myocytes. *Biotechnol Bioeng*. 68:106-14.

143. Zimmermann WH, Schneiderbanger K, Schubert P, Didie M, Munzel F, Heubach JF, Kostin S, Neuhuber WL, Eschenhagen T (2002) Tissue engineering of a differentiated cardiac muscle construct. *Circ Res*. 90:223-30.

Appendix

A1. Reagents and medium

Reagents and medium for cell culture:

IGF-1 stock solution

Reconstitute IGF-1 (Recombinant Human IGF-1, #AF-100-11, Peprotech) in sterile 1x PBS with 0.1% human recombinant serum albumin (HSA) (#A9731, Sigma-Aldrich) according to manufacturer's protocol to obtain a stock concentration of 100 µg/ml; aliquots were stored at -20 °C until further use.

bFGF stock solution (Peprotech)

Reconstitute bFGF (Recombinant Human FGF-basic [154 a.a], #AF-100-18B, Peprotech) in sterile 1x PBS with 0.1% HSA (#A9731, Sigma-Aldrich) according to manufacturer's protocol to obtain a stock concentration of 10 µg/m; aliquots were stored at -20 °C until further use.

bFGF stock solution (Miltenyi Biotech)

Reconstitute bFGF (Human FGF-2 premium grade, #130-093-841, Miltenyi Biotech) in sterile 1x PBS with 0.1% HSA (#A9731, Sigma-Aldrich) according to manufacturer's protocol to obtain a stock concentration of 10 µg/ml; aliquots were stored at -20 °C until further use.

VEGF-A stock solution

Reconstitute VEGF-A (Animal-Free Recombinant Human VEGF [165], #AF-100-20, Peprotech) in sterile 1x PBS with 0.1% HSA (#A9731, Sigma-Aldrich) according to manufacturer's protocol to obtain a stock concentration of 5 µg/ml; aliquots were stored at -20 °C until further use.

TGF-β1 stock solution

Reconstitute TGF-β1 (Recombinant Human TGF-β1 [CHO cell derived], #AF-100-21C, Peprotech) in sterile 1x PBS with 0.1% HAS (#A9731, Sigma-Aldrich) according to manufacturer's protocol to obtain a stock concentration of 5 µg/ml; aliquots were stored at -20 °C until further use.

EGF stock solution

Reconstitute EGF (Animal-Free Recombinant Human EGF, #AF-100-18B, Peprotech) in sterile 1x PBS with 0.1% HSA (#A9731, Sigma-Aldrich) according to manufacturer's protocol to obtain a stock concentration of 10 µg/ml; aliquots were stored at -20 °C until further use.

BMP-4 stock solution

Reconstitute BMP-4 (Recombinant Human BMP-4, #314-BP, R&D Systems) in sterile 1x PBS with 0.1% HSA (#A9731, Sigma-Aldrich) according to manufacturer's protocol to obtain a stock concentration of 10 µg/ml; aliquots were stored at -20 °C until further use.

Activin A stock solution

Reconstitute Activin A (Recombinant Human/Mouse/Rat Activin A Protein, #338-AC, R&D Systems) in sterie 1x PBS with 0.1% HSA (#A9731, Sigma-Aldrich) according to manufacturer's protocol to obtain a stock concentration of 10 µg/ml; aliquots were stored at -20 °C until further use.

CHIR stock solution

Reconstitute CHIR (Stemolecule^{TM} CHIR99021, #04-0004, Stemgent) in DMSO according to manufacturer's protocol to obtain a stock concentration of 10 mmol/L; aliquots were stored at -20 °C until further use.

IWP-4 stock solution

Reconstitute IWP-4 (Stemolecule™ Wnt Inhibitor IWP-4, #04-0036, Stemgent) in DMSO according to manufacturer's protocol to obtain a stock concentration of 5 mmol/L; aliquots were stored at -20 °C until further use.

Nucleoside Mix (100x)

Dissolve 80 mg Adenosine (final con. 30 µmol/L, #A4036, Sigma), 85 mg Guanosine (final con. 30 µmol/L, #G6264, Sigma), 73 mg Cytidine (final con. 30 µmol/L, #4654, Sigma), 73 mg Uridine (final con. 30 µmol/L, #U-3003, Sigma) and 24 mg Thymidine (final con. 10 µmol/L, #T1895, Sigma) in 1x PBS, sterile filter; aliquots were stored at -20 °C until further use.

Ascorbic acid stock solution

Dissolve 0.87 g L-ascorbic acid 2-phosphate sesquimagnesium salt hydrate (#A8960, Sigma-Aldrich) in 10 ml of ddH_2O to obtain 300 mmol/L stock concentration, sterile filter; aliquots were stored at -20 °C until further use.

CMR supplement (50x)

Albumin Human (#A9731, Sigma-Aldrich)	1.25 g
Triiodothyronine (T3),	10 µg
Transferrin	25 mg
Sodium Selenite	80 µg

> adjust with Aq. dest. water up to 50 mL
> keep aliquots at -20 °C.

10x DMEM

Dissolve 1.34 g DMEM powder (DMEM, powder, high glucose, #52100-039, Gibco) in 10 ml of ddH_2O, sterile filter and keep at 4 °C.

10x RPMI

Dissolve 1.04 g RPMI powder (RPMI 1640 medium, powder, #52800-035, Gibco) in 10 ml of ddH_2O, sterile filter and keep at 4 °C.

Rat EHM medium

Iscove's medium (#F0465, Biochrom)	500 ml
Horse serum (#16050, Gibco)	58 ml
Chich embryo extract	11.6 ml
Penicilin (Pen)/Streptomycin (Strep) (100x, Pen: 10,000 U/mL and Strep: 10,000 µg/mL, #15140-122, Gibco)	5.8 ml

mESC medium

DMEM, high glucose, HEPES (#42430-025, Gibco)	500 ml
Fetal Bovine Serum (FBS) (#10270, Gibco)	92 ml
L-Glutamine (200 mmol/L, #25030-024, Gibco)	6.2 ml
Pen/Strep (100x, #15140-122, Gibco)	6.2 ml
MEM Non-Essential Amino Acids Solution (NEAA) (100x, #111450-035, Gibco)	6.2 ml
Sodium Pyruvate (100 mmol/L, #11360-039, Gibco)	6.2 ml
Nucleoside mix (100x)	6.2 ml
Leukemia Inhibitory factor (LIF) (1000 Units/ml, #ESG1106, Esgro)	62 µl
2-β-mercaptoethanol (31350-010, Sigma)	4.34 µl

mESC differentiation (diff.) medium / mEHM medium

Iscove's medium (#F0465, Biochrom)	500 ml
FBS (#10270, Gibco)	120 ml
L-Glutamine (200 mmol/L, #25030-024, Gibco)	6.2 ml
Pen/Strep (100x, #15140-122, Gibco)	6.2 ml
MEM-NEAA (100x, #111450-035, Gibco)	6.2 ml
L-Ascorbic acid 2-phosphate sesquimagnesium salt hydrate (Ascorbic acid for cell culture, #A8960, Sigma)	54 mg (final concentration [con]: 300 µmol/L)
2-β-mercaptoethanol (31350-010, Sigma)	4.34 µl

mCPC medium (incomplete)

DMEM/F-12 medium (#31300-038, Gibco)	500 ml
FBS (#10270, Gibco)	50 ml
Pen/Strep (100x, #15140-122, Gibco)	5.5 ml
L-Glutamine (200 mmol/L, #25030-024, Gibco)	5.5 ml
Insulin-Transferrin-Selenium-Ethanolamine (ITS-X) (100x, # 51500-056, Gibco)	5.5 ml
LIF (1000 Units/ml, #ESG1106, Esgro)	50 µl

mCPC medium

mCPC medium (incomplete)	50 ml
EGF stock solution	200 µl (final con: 40 ng/mL)
bFGF stock solution	100 µl (final con: 20 ng/mL)

mEF medium

DMEM medium (#61965-026, Gibco)	500 ml
FBS (#10270, Gibco)	50 ml
Pen/Strep (100x, #15140-122, Gibco)	5.5 ml
MEM-NEAA (100x, #111450-035, Gibco)	5.5 ml

hCM medium

RPMI medium 1640, GlutaMAX™ (#61870-010, Gibco)	500 ml
Pen/Strep (100x, #15140-122, Gibco)	5.2 ml
Sodium Pyruvate (100 mM, #11360-039, Gibco)	5.2 ml
Ascorbic acid stock solution (300 mmol/L)	333 µl
B-27® Supplement (50x, #17504-044, Gibco)	10 ml

hEHM medium (incomplete)

Iscove's medium (#F0465, Biochrom)	500 ml
L-Glutamine (200 mmol/L, #25030-024, Gibco)	5.5 ml
Pen/Strep (100x, #15140-122, Gibco)	5.5 ml
MEM-NEAA (100x, #111450-035, Gibco)	5.5. ml
Ascorbic acid stock solution (300 mmol/L)	500 µl

hEHM medium

hEHM medium (incomplete)	50 ml
B-27® Supplement, minus insulin (50x, #A18956-01, Gibco)	2 ml
IGF-1 stock solution	50 µl (final con: 100 ng/mL)
bFGF stock solution	50 µl (final con: 10 ng/mL)
VEGF-A stock solution	50 µl (final con: 5 ng/mL)

hEHM consolidation medium

hEHM medium	50 ml
TGF-β stock solution	50 µl (final con: 5 ng/mL)

hFF medium

DMEM, high glucose, HEPES (#42430-025, Gibco)	500 ml
FBS (#10270, Gibco)	75 ml
Pen/Strep (100x, #15140-122, Gibco)	5.8 ml

DMEM SF-B27 medium

DMEM, low glucose, GlutaMAX ™, Pyruvate (#21885-025, Gibco)	500 ml
Pen/Strep (100x, #15140-122, Gibco)	5 ml
MEM-NEAA (100x, #111450-035, Gibco)	5 ml
B-27® Supplement, minus insulin (50x, #A18956-01, Gibco)	20 ml

DMEM SF-CMR medium

DMEM, low glucose, GlutaMAX ™, Pyruvate (#21885-025, Gibco)	500 ml
Pen/Strep (100x, #15140-122, Gibco)	5 ml
MEM-NEAA (100x, #111450-035, Gibco)	5 ml
CMR supplement (50x)	10 ml

2x Rat EHM DMEM

10x DMEM	1 ml
Horse serum ((#16050, Gibco)	1 ml
Chick embryo extract	0.2 ml
Pen/Strep (100x, #15140-122, Gibco)	0.1 ml
ddH_2O	2.7 ml

2x Mouse EHM DMEM

10x DMEM	1 ml
FBS (#10270, Gibco)	2 ml
Pen/Strep (100x, #15140-122, Gibco)	0.2 ml
ddH_2O	1.8 ml

2x Human EHM RPMI

10x RPMI	2 ml
B-27® Supplement, minus insulin (50x, #A18956-01, Gibco)	0.8 ml
Pen/Strep (100x, #15140-122, Gibco)	0.2 ml
ddH_2O	7 ml

hESC medium

KO DMEM medium (#10829, Invitrogen)	39.5 ml
KSR (Knockout Serum Replacement) (#10828, Invitrogen)	10 ml
MEM-NEAA (100x, #111450-035, Gibco)	0.5 ml
L-Glutamine (200 mmol/L, #25030-024, Gibco)	0.5 ml
Pen/Strep (100x, #15140-122, Gibco)	0.5 ml
bFGF stock solution (Miltenyi Biotech)	50 µl (final con: 10 ng/mL)

hFF conditioned medium

hESC medium	50 ml
bFGF stock solution (Miltenyi Biotech)	25 µl (final con: 5 ng/mL)
> add onto hFFs for 48 hours	

hESC conditioned medium

hESC medium	25 ml
hFF conditioned medium	25 ml
bFGF stock solution (Miltenyi Biotech)	50 µl (final con: 10 ng/mL)

Mesoderm induction medium

hCM medium	50 ml
CHIR stock solution	5 µl (final con: 1 µmol/mL)
BMP4 stock solution	25 µl (final con: 5 ng/mL)
Activin-A stock solution	45 µl (final con: 9 ng/mL)
bFGF stock solution (Miltenyi Biotech)	25 µl (final con: 5 ng/mL)

Cardiac specification medium

hCM medium	50 ml
IWP4 stock solution	50 µl (final con: 5 µmol/mL)

hCM selection medium

RPMI medium 1640, without D-Glucose, without L-Glutamine (#01-101-1A, Biological Industries)	49.15 ml
Pen/Strep (100x, #15140-122, Gibco)	0.5 ml
Sodium DL-Lactate solution 50% in H2O (#71723, Sigma-Aldrich)	0.25 ml
2-mercaptoethanol (50 mmol/L; 31350010; Invitrogen)	0.1 ml

hCPC-Conditioned medium (ConM)

hCPCs were plated and cultured in T-25 culture flask in hFF-medium with the seeding density of 1 x 10^6 cells/flask. hFF medium was replaced with DMEM SF-CMR medium when hCPCs reached 90-100% confluency. DMEM SF-CMR medium from hCPCs was collected every second day for 7 days and immediately frozen and stored at -80 °C. hCPC conditioned medium (ConM) was prepared freshly, diluted 1:1 with fresh DMEM SF-CMR medium prior to use.

hFF-Conditioned medium (ConM)

hFFs were plated and cultured in T-25 culture flask in hFF-medium with the seeding density of 1 x 10^6 cells/flask. hFF medium was replaced with DMEM SF-CMR medium when hFFs reached 90-100% confluency. DMEM SF-CMR medium from hFFs was collected every second day for 7 days and immediately frozen and stored

at -80 °C. hFF-ConM was prepared freshly, diluted 1:1 with fresh DMEM SF-CMR medium prior to use.

Collagenase digestion solution

Dissolve 500 mg collagenase (Collagenase from Clostridium histolyticum for general use, Type I, # C0130, Sigma-Aldrich) in 250 ml of 1x PBS containing Ca^{+2} and Mg^{+2} with 20% FBS (#10270, Gibco), sterile filter and keep aliquots at -20 °C.

Dnase stock solution

Dissolve Dnase I (DNase I, Bovine Pancreas, #260913, Calbiochem) in ddH_2O to obtain a stock concentration of 1 mg/mL, keep aliquots at -20 °C.

EDTA solution

Add 500 µl of 0.5 M EDTA solution (EDTA solution pH 8.0 (0.5 M) for molecular biology (#A4892, AppliChem) to 500 ml of 1x PBS containing 0.45 g NaCl. Sterile filter, keep aliquots at 4 °C.

EB digestion protocol

Collagenase digestion solution	10 ml
Dnase stock solution	200 µl

hCM digestion solution

Accutase cell detachment solution, (#SCR005, Milipore)	97.75 ml
Trypsin (2.5%) (#15090-046, Gibco)	0.25 ml
Dnase stock solution	2 ml

Reagents for isometric force measurement:

$CaCl_2$ stock solution (2.25 mol/L)

$CaCl_2$ x $2H_2O$ (Mw: 147.02 g/mol)	165.57 g
ddH_2O	500 ml

MgCl2 stock solution (1.05 mol/L)

$MgCl_2$ x $6H_2O$ (Mw: 203.01 g/mol)	106.83 g
ddH_2O	500 ml

Stock I solution (0.2 mmol/L Calcium)

NaCl	175 g
KCl	10 g
$CaCl_2$ stock solution (2.25 mol/L)	2.22 ml
$MgCl_2$ stock solution (1.05 mol/L)	25 ml
ddH_2O	up to 1 L

Stock II solution

$NaHCO_3$	50 g
ddH_2O	1 L

Stock III solution

NaH_2PO_4	5.8 g
ddH_2O	1 L

> keep all the stock solutions at 4 °C.

Tyrode solution

Stock I solution (0.2 mmol/L Calcium)	200 ml
Stock II solution	190 ml
Stock III solution	50 ml
D-Glucose	5 g
Ascorbic acid	500 mg
ddH_2O	up to 5 L

>Prepare the Tyrode solution prior to contraction force measurement.

Reagents for western blot:

Solutions for cell lysis:

Protease inhibitor stock solution (10x)

Dissolve 1 tablet of protease inhibitor (Protease inhibitor, cOmplete ULTRA Tablets, Mini, EASYpack, #05892970001, Roche) in 1.5 ml of ddH_2O, keep in aliquots at -20 C.

Phosphatase inhibitor stock solution (10x)

Dissolve 1 tablet of phosphatase inhibitor (Phosphatase inhibitor, PhosSTOP EASYpack, #04906837001, Roche) in 1 ml of ddH_2O, keep aliquots at -20 °C.

Cell lysis buffer (incomplete)

Tris-HCl (pH 8.0)	10 mmol/L
NaCl	400 mmol/L
EDTA	1 mmol/L

> keep at 4 °C.

Cell lysis buffer

Cell lysis buffer (incomplete)	750 µl
Protease inhibitor stock solution (10x)	150 µl
Phosphatase inhibitor stock solution (10x)	100 µl

Solutions for SDS-gel electrophoresis:

0.5 mol/L Tris-HCl pH 6.8

Tris-HCl	30.28 g
ddH_2O	500 ml

> adjust to pH 6.8.

1.5 mol/L Tris-HCl pH 8.8

Tris-HCl	90.85 g
ddH_2O	500 ml

> adjust to pH 8.8.

Laemmli loading buffer (6x)

0.5 mol/L Tris-HCl pH 6.8	3 ml
Bromphenol blue 0.5%	0.75 ml
SDS	1.2 g
Glycerin 100%	1.5 ml
2-β-Mercaptoethanol	150 µl
ddH_2O	up to 10 ml

> keep aliquots at -20 °C.

Seperating gel (12%, 2 gels)

ddH_2O	3.3 ml
Acrylamide 30%	4 ml
1.5 mol/L Tris-HCl pH 8.8	2.5 ml
SDS 10%	100 µl
APS 10%	100 µl
TEMED	4 µl

Stacking gel (2 gels)

ddH_2O	2.8 ml
Acrylamide 30%	0.85 ml
0.5 mol/L Tris-HCl pH 6.8	1.25 ml
SDS 10%	50 µl
APS 10%	50 µl
TEMED	5 µl

Running buffer (10X, pH 8.3-8.7)

Tris-Base	30.3 g
Glycine	144.1 g
ddH_2O	1 L

Solutions for immunoblotting:

Transfer buffer (10x)

Tris-Base	60.5 g
Glycine	288 g
ddH_2O	up to 2 L

Transfer buffer (1x)

Transfer buffer (10x)	100 ml
Methanol	200 ml
ddH_2O	up to 1 L

Blocking buffer

Prepare 5% of milk powder (milk, non-fatty dried, Carl Roth) solution in 1x PBS.

Reagents for Agarose gel electrophoresis:

TAE buffer (50x)

Tris-Base	242.2 g
0.5 M EDTA pH 8.0	18.6 g
Acetic acid	57.1 g
ddH_2O	up to 1 L

> adjust to pH 8.5.

TAE buffer (1x)

TAE buffer (50x)	3 ml
ddH_2O	up to 150 ml

Agarose gel (1.5%)

TAE buffer (1x)	100 ml
Agarose UltraPureTM (AppliChem)	1.5 g

> Let the agarose gel cool down, pipette 0.2 µg/ml ethidium bromide (EtBR; Ethidium bromide solution, #46067, Sigma-Aldrich) into the gel and directly pour into the casting tray placed with a comb inside.

Reagents for Immunostaining:

Permeabilizing blocking buffer for Immunocyto/histostaining and Flow cytometry

Goat serum	26.3 ml
Bovine serum albumin (BSA) (#A3311, Sigma)	5.26 g
Triton x-100	2.63 ml
1x PBS	up to 500 ml

Non-permeabilizing blocking buffer for Flow cytometry

Prepare 1x PBS containing 5% FBS (#10270, Gibco) and keep at 4 °C until use.

A2. Primers

Gene		Sequence (5' —> 3')	Fragment size (bp)	Ensembl code
murine *Kit*	fwd	GAGCAAAGGTGTACCACTCC	162	ENSMUSG00000005672
	rev	GAACTCTTGCCCACATCGTT		
murine *Nkx2-5*	fwd	CGACAGCGGCAGGACCAGAC	133	ENSMUSG00000015579
	rev	CGTAGGCGGGAGCGTAGGC		
murine *Ly6a (Sca-1)*	fwd	GCAGCAGTTATTGTGCATTCTC	226	ENSMUSG00000075602
	rev	AAGGTCTGCAGGAGGACTGA		
murine *Ddr2*	fwd	CCGAAAGCTTCCAGAGTTTG	249	ENSMUSG00000026674
	rev	TTCTCCCAGCTTCTCCTTGA		
murine *Gapdh*	fwd	ATGTTCCAGTATGACTCCACTCACG	170	ENSMUSG00000057666
	rev	GAAGACACCAGTAGACTCCACGACA		
human *KIT*	fwd	TTGTTAGAGATCCTGCCAAGC	209	ENSG00000157404
	rev	GTAGGCGCGTTTCACACTTT		
human *PECAM1*	fwd	GGTGGAAGGAGTGCCCAG T	114	ENSG00000261371
	rev	GTGAAGTGTATTGGGGCCTTT		
human *ACTA2*	fwd	GGAAAAGATCTGGCACCACTC	196	ENSG00000107796
	rev	GCGTCCAGAGGCATAGAGAG		
human *NKX2-5*	fwd	GACCCTAGAGCCGAAAAGAA	227	ENSG00000183072
	rev	GTGGACGTGAGTTTCAGCAC		
human *ACTC1*	fwd	CCGGGAGAAGATGACTCAGA	170	ENSG00000159251
	rev	GCAAAGCGTAGCCCTCATAG		
human *TNNI3*	fwd	CTCACTGACCCTCCAAACG	206	ENSG00000129991
	rev	AATTTTCTCGAGGCGGAGA		
human *GATA4*	fwd	CTAAGACACCAGCAGCTCCTTC	146	ENSG00000136574
	rev	GTGCCCGTAGTGAGATGACAG		
human *FGF2*	fwd	CGACCCTCACATCAAGCTACA	219	ENSG00000138685
	rev	CGTTTCAGTGCCACAACATACCA		
human *VEGFA*	fwd	CACGAAGTGGTGAAGTTCATGG	121	ENSG00000112715

	rev	CACAGGATGGCTTGAAGATGT		
human *HGF*	fwd	CCTATGCAGAGGGACAAAGGA	133	ENSG00000019991
	rev	GCACATTGGTCTGCAGTATTCA		
human *IGF1*	fwd	ATTTCAACAAGCCCACAGGGTA	511	ENSG00000017427
	rev	AGGGGTGCGCAATACATCT		
human *PDGF*	fwd	GAGAAGCATCGAGGAAGCTG	109	ENSG00000197461
	rev	GGGCCAGATCAGGAAGTTG		
human *GAPDH*	fwd	CCT CAA GAT CAT CAG CAA TGC C	189	ENSG00000111640
	rev	ATG TTC TGG AGA GCC CCG C		
tdRFP	fwd	AGAGTTCATGCGCTTCAAGGT	121	
	rev	GCTTCTTGTAGT CGGGGATG		

A3. Antibodies and dyes

				Dilution amount		
Primary antibody	**Species**	**Manufacturer**	**Cat. #**	**Flow cytometry**	**Whole mount**	**WB**
Anti-CD117-PE	rat	Miltenyi Biotec	130-091-730	1:33	–	–
Anti-CD140a (PDGFRα)-PE	rat	eBioscience	12-1401	1:500	–	–
Anti-CD105-APC	rat	Miltenyi Biotec	130-092-930	1:11	–	–
Anti-Sca-1-PE	rat	Miltenyi Biotec	130-102-832	1:33	–	–
Anti-CD117-BV421	mouse	BD Horizon™	562434	1:20	–	–
Anti-CD31-FITC	mouse	BD Pharmingen	557508	1:20	–	–
Anti-CD31-BV510	mouse	BD Horizon™	563454	1:20	–	–
Anti-CD90-BUV395,	mouse	BD Horizon™	563804	1:20	–	–
Anti-CD105-PerCp-Cy 5.5	mouse	BD Horizon™	560819	1:20	–	–
Anti-CD45-FITC	mouse	BD Pharmingen	555482	1:20	–	–
Anti-α-Actinin (Sarcomeric)	mouse	Sigma-Aldrich	A7811	1:4000	1:1000	–
Anti-Ki67	rabbit	Thermoscientific	RM-9106-S0	1:50	1:200	–
Anti-active caspase-3	rabbit	Promega	G748	–	1:250	–
Anti-GFP	rabbit	Abcam	ab290	–	1:500	–
Anti-HIF-1α	mouse	BD Transduction	610959	–	–	1:1000
Anti-β-actin	mouse	Sigma-Aldrich	A2228	–	–	1:5000

				Dilution amount		
Secondary antibody	**Species**	**Manufacturer**	**Cat. #**	**Flow cytometry**	**Whole mount**	**WB**
anti-mouse-Alexa Fluor 488	goat	Invitrogen	A11001	1:1000	1:1000	–
anti-mouse-Alexa Fluor 546	goat	Invitrogen	A11003	1:1000	1:1000	–
anti-mouse-Alexa Fluor 633	goat	Invitrogen	A-21050	1:1000	1:1000	–
Anti-mouse-IgG-HRP conjugated	mouse	Dako	P0260	–	–	1:10000

			Dilution amount	
Dye	**Manufacturer**	**Cat. #**	**Flow cytometry**	**Whole mount**
Hoechst, 1 mg/ml	BD Biosciences	33342	1:1000	1:1000
Sytox Red Dead Cell Stain-633	Molecular Probes	S34859	1:1000	1:1000

A4. Life organisms

Animals:

Species	Background	Source
Mus musculus	NMRI (CD1)	Animal facility, UMG
Musmusculus	FVB.129S6-*Gt(ROSA26)Sor*$^{tm2(HIF1A/Luc)\ Kael}$/J: HIF-1α-ODD-Luc knock-in in ROSA26 locus, expression enhanced by fusion to a CMV promoter element	The Jackson laboratory
Rattus norvegicus	Wistar	Animal facility, UMG

Cell lines:

Cell line	Genetic background	Source
mESCs-αMHC-NeoR	mESC-R1 line (Nagy et al. 1993) with random integration of neoR gene under transcriptional control by cardiomyocyte specific αMHC promoter element	Institute of Pharmacology and Toxicology
mESCs-HIF-1α-ODD-Luc/αMHC-neoR	Transgenic ROSA26 ODD-Luc/+ mice derived mESCs ubiquitiously expressing HIF-1α-ODD-Luc fusion protein and neomycin resistance (neoR) under transciptional control by αMHC promoter element)	Isolation and transgenic modification of the stem cell line by Andreas Schraut (Institute of Pharmacology and Toxicology)
mCPCs (GFP^+)	Mouse cardiac progenitor cells isolated from adult mouse heart with retrovirus transduction of EGFP	Kindly provided by Mark Sussman (Fischer et al. 2009)
hCPCs (GFP^+)	Human cardiac progenitor cells isolated from atrial appendage of adult human heart with lentiviral transduction of EGFP	Kindly provided by Coretherapix Laboratory (Lauden et al. 2013)
hFFs (GFP^+)	Human foreskin fibroblasts with lentiviral transduction of EGFP	wild type hFFs; ATCC, #SCRC-1041
hES2 RFP	HES2 line (Embryonic Stem cell International) (Reubinoff et al. 2000) with tdRFP knock-in in ROSA26 locus	Kind gift by Gordon Keller (Irion et al. 2007)
hES2-HIF-1α-ODD-Luc	HES2 line with random integration of HIF-1α-ODD-Luc fusion protein under Cytomegalovirus (CMV) promoter element	Trangenic modification of the stem cell line by Dr. Claudia Noack and Krasimira Sharkova
Other cell types	**Genetic background**	**Source**
mEFs	NMRI mice	See section 2.2.3
mCM	Mouse cardiomyocytes from mESC-HIF-1α-ODD-Luc/αMHC-neoR	See section 2.1.2
hCM	Human cardiomyocytes from hES2 RFP	See section 2.1.3
ODD-Luc hCM	Human cardiomyocytes from hES2 RFP-HIF-1α-ODD-Luc	See section 2.7.5

A5. Human CPC specific differentially expressed genes

Table 17. Differentially expressed plasma membrane genes in hCPCs compared to hCFs and hFFs.

Gene symbol	Gene Name
HTR1D	5-hydroxytryptamine (serotonin) receptor 1D
HTR1F	5-hydroxytryptamine (serotonin) receptor 1F
HTR7	5-hydroxytryptamine (serotonin) receptor 7 (adenylate cyclase-coupled)
PALM2-AKAP2, AKAP2	A kinase (PRKA) anchor protein 2; paralemmin 2; PALM2-AKAP2 readthrough transcript
ADAM29	ADAM metallopeptidase domain 29
ART1	ADP-ribosyltransferase 1
ABCC9	ATP-binding cassette, sub-family C (CFTR/MRP), member 9
ABCD2	ATP-binding cassette, sub-family D (ALD), member 2
ATP2B2	ATPase, Ca++ transporting, plasma membrane 2
ATP6V1B1	ATPase, H+ transporting, lysosomal 56/58kDa, V1 subunit B1
ATP4A	ATPase, H+/K+ exchanging, alpha polypeptide
CD22	CD22 molecule
CASS4	Cas scaffolding protein family member 4
DSCAM	Down syndrome cell adhesion molecule
EGFLAM	EGF-like, fibronectin type III and laminin G domains
EHD1	EH-domain containing 1
EHD2	EH-domain containing 2
EPHB6	EPH receptor B6
FCER1G	Fc fragment of IgE, high affinity I, receptor for; gamma polypeptide
GPR34	G protein-coupled receptor 34
GPR37	G protein-coupled receptor 37 (endothelin receptor type B-like)
GPR39	G protein-coupled receptor 39
GPR4	G protein-coupled receptor 4
GPR65	G protein-coupled receptor 65
INADL	InaD-like (Drosophila)
LIMS1	LIM and senescent cell antigen-like domains 1
MICB	MHC class I polypeptide-related sequence B
NOX4	NADPH oxidase 4
NCKAP1L	NCK-associated protein 1-like
NOTCH4	Notch homolog 4 (Drosophila)
RAB13	RAB13, member RAS oncogene family; similar to hCG24991
RAB17	RAB17, member RAS oncogene family
RAB3A	RAB3A, member RAS oncogene family
RAB43	RAB43, member RAS oncogene family; hypothetical LOC100131426
RHD	Rh blood group, D antigen
ARHGDIA	Rho GDP dissociation inhibitor (GDI) alpha
ARHGAP26	Rho GTPase activating protein 26

ARHGEF2	Rho/Rac guanine nucleotide exchange factor (GEF) 2
SHKBP1	SH3KBP1 binding protein 1
TCIRG1	T-cell, immune regulator 1, ATPase, H+ transporting, lysosomal V0 subunit A3
B4GALT1	UDP-Gal:betaGlcNAc beta 1,4- galactosyltransferase, polypeptide 1
VSIG2	V-set and immunoglobulin domain containing 2
ADI1	acireductone dioxygenase 1
AFAP1	actin filament associated protein 1
ACVRL1	activin A receptor type II-like 1
ARC	activity-regulated cytoskeleton-associated protein
ADCY3	adenylate cyclase 3
ALK	anaplastic lymphoma receptor tyrosine kinase
ANK1	ankyrin 1, erythrocytic
ARSA	arylsulfatase A
ASGR1	asialoglycoprotein receptor 1
ROS1	c-ros oncogene 1 , receptor tyrosine kinase
CDH4	cadherin 4, type 1, R-cadherin (retinal)
CDH24	cadherin-like 24
CABP1	calcium binding protein 1
CACNA1D	calcium channel, voltage-dependent, L type, alpha 1D subunit
CACNA1B	calcium channel, voltage-dependent, N type, alpha 1B subunit
CA2	carbonic anhydrase II
CADM1	cell adhesion molecule 1
CCR10	chemokine (C-C motif) receptor 10
CCR7	chemokine (C-C motif) receptor 7
CHRM4	cholinergic receptor, muscarinic 4
CHRNA1	cholinergic receptor, nicotinic, alpha 1 (muscle)
CHRNA9	cholinergic receptor, nicotinic, alpha 9
CSPG5	chondroitin sulfate proteoglycan 5 (neuroglycan C)
CLTCL1	clathrin, heavy chain-like 1
CLDN2	claudin 2
CLDN24	claudin-24-like
F2RL3	coagulation factor II (thrombin) receptor-like 3
COL13A1	collagen, type XIII, alpha 1
COL23A1	collagen, type XXIII, alpha 1
COL25A1	collagen, type XXV, alpha 1
CPLX4	complexin 4
CNTNAP1	contactin associated protein 1
CTTNBP2	cortactin binding protein 2
DDN	dendrin
DRD4	dopamine receptor D4
EDA	ectodysplasin A
ESAM	endothelial cell adhesion molecule
EFNB1	ephrin-B1
EPB41L3	erythrocyte membrane protein band 4.1-like 3
ESR1	estrogen receptor 1

FGA	fibrinogen alpha chain
FLT4	fms-related tyrosine kinase 4
FUT1	fucosyltransferase 1 (galactoside 2-alpha-L-fucosyltransferase, H blood group)
GABBR1	gamma-aminobutyric acid (GABA) B receptor, 1
GABRR2	gamma-aminobutyric acid (GABA) receptor, rho 2
GJB2	gap junction protein, beta 2, 26kDa
GJC2	gap junction protein, gamma 2, 47kDa
GRIN2C	glutamate receptor, ionotropic, N-methyl D-aspartate 2C
GRIK2	glutamate receptor, ionotropic, kainate 2
GRM2	glutamate receptor, metabotropic 2
GRM6	glutamate receptor, metabotropic 6
ENPEP	glutamyl aminopeptidase (aminopeptidase A)
GLRA3	glycine receptor, alpha 3
GHR	growth hormone receptor
GNG2	guanine nucleotide binding protein (G protein), gamma 2
GNG4	guanine nucleotide binding protein (G protein), gamma 4
GNGT2	guanine nucleotide binding protein (G protein), gamma transducing activity polypeptide 2
GBP2	guanylate binding protein 2, interferon-inducible
HBEGF	heparin-binding EGF-like growth factor
HRH2	histamine receptor H2
HAS1	hyaluronan synthase 1
IGSF9	immunoglobulin superfamily, member 9
INPP5E	inositol polyphosphate-5-phosphatase, 72 kDa
IGF1R	insulin-like growth factor 1 receptor
ITGA2B	integrin, alpha 2b (platelet glycoprotein IIb of IIb/IIIa complex, antigen CD41)
ITGA5	integrin, alpha 5 (fibronectin receptor, alpha polypeptide)
ITGA8	integrin, alpha 8
ITGAX	integrin, alpha X (complement component 3 receptor 4 subunit)
ITGB2	integrin, beta 2 (complement component 3 receptor 3 and 4 subunit)
IL12RB2	interleukin 12 receptor, beta 2
IL15	interleukin 15
IL6	interleukin 6 (interferon, beta 2)
KLHL17	kelch-like 17 (Drosophila)
LZTS1	leucine zipper, putative tumor suppressor 1
LILRB3	leukocyte immunoglobulin-like receptor, subfamily B (with TM and ITIM domains), member 3
LTK	leukocyte receptor tyrosine kinase
LIN7A	lin-7 homolog A (C. elegans)
LRP1	low density lipoprotein-related protein 1 (alpha-2-macroglobulin receptor)
LRP2	low density lipoprotein-related protein 2
LHCGR	luteinizing hormone/choriogonadotropin receptor
LAG3	lymphocyte-activation gene 3
MSR1	macrophage scavenger receptor 1
HLA-DOA	major histocompatibility complex, class II, DO alpha
MMP14	matrix metallopeptidase 14 (membrane-inserted)
MMP25	matrix metallopeptidase 25

MTNR1A	melatonin receptor 1A
MPP2	membrane protein, palmitoylated 2 (MAGUK p55 subfamily member 2)
MPP7	membrane protein, palmitoylated 7 (MAGUK p55 subfamily member 7)
MAPK8IP3	mitogen-activated protein kinase 8 interacting protein 3
MUC1	mucin 1, cell surface associated
MYO7A	myosin VIIA
MYH6	myosin, heavy chain 6, cardiac muscle, alpha
MYH9	myosin, heavy chain 9, non-muscle
NRG1	neuregulin 1
NRXN1	neurexin 1
NCF2	neutrophil cytosolic factor 2
NEXN	nexilin (F actin binding protein)
OSM	oncostatin M
OPCML	opioid binding protein/cell adhesion molecule-like
PARD6B	par-6 partitioning defective 6 homolog beta (C. elegans)
PARVG	parvin, gamma
PTCH2	patched homolog 2 (Drosophila)
PHEX	phosphate regulating endopeptidase homolog, X-linked
PDE4A	phosphodiesterase 4A, cAMP-specific (phosphodiesterase E2 dunce homolog, Drosophila)
PLA2G4F	phospholipase A2, group IVF
PHKA1	phosphorylase kinase, alpha 1 pseudogene 1; phosphorylase kinase, alpha 1 (muscle)
PODXL	podocalyxin-like
PVRL2	poliovirus receptor-related 2 (herpesvirus entry mediator B)
PKD1	polycystic kidney disease 1 (autosomal dominant)
KCNN3	potassium intermediate/small conductance calcium-activated channel, subfamily N, member 3
KCNN4	potassium intermediate/small conductance calcium-activated channel, subfamily N, member 4
KCNJ1	potassium inwardly-rectifying channel, subfamily J, member 1
KCNJ14	potassium inwardly-rectifying channel, subfamily J, member 14
KCNJ2	potassium inwardly-rectifying channel, subfamily J, member 2
KCNMB4	potassium large conductance calcium-activated channel, subfamily M, beta member 4
KCNS2	potassium voltage-gated channel, delayed-rectifier, subfamily S, member 2
KCNG1	potassium voltage-gated channel, subfamily G, member 1
PRR7	proline rich 7 (synaptic)
PTGER1	prostaglandin E receptor 1 (subtype EP1), 42kDa
PTPN3	protein tyrosine phosphatase, non-receptor type 3
PTPRF	protein tyrosine phosphatase, receptor type, F
PTPRH	protein tyrosine phosphatase, receptor type, H
PCDH11X	protocadherin 11 X-linked
PCDH12	protocadherin 12
PCDHB15	protocadherin beta 15
P2RY1	purinergic receptor P2Y, G-protein coupled, 1
RHOF	ras homolog gene family, member F (in filopodia)
RHOG	ras homolog gene family, member G (rho G)
RAMP1	receptor (G protein-coupled) activity modifying protein 1
RAMP2	receptor (G protein-coupled) activity modifying protein 2

ROR2	receptor tyrosine kinase-like orphan receptor 2
RAPSN	receptor-associated protein of the synapse
RIMS3	regulating synaptic membrane exocytosis 3
RXFP3	relaxin/insulin-like family peptide receptor 3
ROM1	retinal outer segment membrane protein 1
SGCA	sarcoglycan, alpha (50kDa dystrophin-associated glycoprotein)
SELP	selectin P (granule membrane protein 140kDa, antigen CD62)
SIRPB1	signal-regulatory protein beta 1
SIT1	signaling threshold regulating transmembrane adaptor 1
MLLT4	similar to Afadin (Protein AF-6); myeloid/lymphoid or mixed-lineage leukemia (trithorax homolog, Drosophila); translocated to, 4
SLC1A5	solute carrier family 1 (neutral amino acid transporter), member 5
SLC12A7	solute carrier family 12 (potassium/chloride transporters), member 7
SLC12A1	solute carrier family 12 (sodium/potassium/chloride transporters), member 1
SLC13A5	solute carrier family 13 (sodium-dependent citrate transporter), member 5
SLC16A3	solute carrier family 16, member 3 (monocarboxylic acid transporter 4)
SLC16A7	solute carrier family 16, member 7 (monocarboxylic acid transporter 2)
SLC2A1	solute carrier family 2 (facilitated glucose transporter), member 1
SLC2A9	solute carrier family 2 (facilitated glucose transporter), member 9
SLC22A13	solute carrier family 22 (organic anion transporter), member 13
SLC22A5	solute carrier family 22 (organic cation/carnitine transporter), member 5
SLC25A4	solute carrier family 25 (mitochondrial carrier; adenine nucleotide translocator), member 4
SLC26A9	solute carrier family 26, member 9
SLC28A1	solute carrier family 28 (sodium-coupled nucleoside transporter), member 1
SLC6A13	solute carrier family 6 (neurotransmitter transporter, GABA), member 13
SLC7A1	solute carrier family 7 (cationic amino acid transporter, y+ system), member 1
SLC7A9	solute carrier family 7 (cationic amino acid transporter, y+ system), member 9
SLC8A1	solute carrier family 8 (sodium/calcium exchanger), member 1
SLC9A1	solute carrier family 9 (sodium/hydrogen exchanger), member 1
SLC9A3R2	solute carrier family 9 (sodium/hydrogen exchanger), member 3 regulator 2
SORBS3	sorbin and SH3 domain containing 3
S1PR3	sphingosine-1-phosphate receptor 3
STOM	stomatin
STX3	syntaxin 3
TLN1	talin 1
TNS4	tensin 4
TBXA2R	thromboxane A2 receptor
TPO	thyroid peroxidase
TRHR	thyrotropin-releasing hormone receptor
TFRC	transferrin receptor (p90, CD71)
TGFB1I1	transforming growth factor beta 1 induced transcript 1
TGFBR2	transforming growth factor, beta receptor II (70/80kDa)
TGM3	transglutaminase 3 (E polypeptide, protein-glutamine-gamma-glutamyltransferase)
TRPC5	transient receptor potential cation channel, subfamily C, member 5
TRPM2	transient receptor potential cation channel, subfamily M, member 2

TM4SF1	transmembrane 4 L six family member 1
TMPRSS9	transmembrane protease, serine 9
TMEM204	transmembrane protein 204
TNF	tumor necrosis factor (TNF superfamily, member 2)
TNFSF11	tumor necrosis factor (ligand) superfamily, member 11
TNFSF8	tumor necrosis factor (ligand) superfamily, member 8
VASP	vasodilator-stimulated phosphoprotein
VEPH1	ventricular zone expressed PH domain homolog 1 (zebrafish)
VAMP1	vesicle-associated membrane protein 1 (synaptobrevin 1)
XIRP1	xin actin-binding repeat containing 1
ZAP70	zeta-chain (TCR) associated protein kinase 70kDa
ZYX	zyxin

Table 18. Differentially expressed cell adhesion genes in hCPCs compared to hCFs and hFFs.

Gene symbol	Gene Name
ADAM22	ADAM metallopeptidase domain 22
AEBP1	AE binding protein 1
CD22	CD22 molecule
CUZD1	CUB and zona pellucida-like domains 1
CASS4	Cas scaffolding protein family member 4
CDON	Cdon homolog (mouse)
DSCAM	Down syndrome cell adhesion molecule
LIMS1	LIM and senescent cell antigen-like domains 1
RAB13	RAB13, member RAS oncogene family; similar to hCG24991
RADIL	Ras association and DIL domains
B4GALT1	UDP-Gal:betaGlcNAc beta 1,4- galactosyltransferase, polypeptide 1
WISP2	WNT1 inducible signaling pathway protein 2
AOC3	amine oxidase, copper containing 3 (vascular adhesion protein 1)
BMP1	bone morphogenetic protein 1
CDH16	cadherin 16, KSP-cadherin
CDH4	cadherin 4, type 1, R-cadherin (retinal)
CDH23	cadherin-like 23
CDH24	cadherin-like 24
CLSTN2	calsyntenin 2
CPXM1	carboxypeptidase X (M14 family), member 1
CTNNAL1	catenin (cadherin-associated protein), alpha-like 1
CADM1	cell adhesion molecule 1
CADM4	cell adhesion molecule 4
CLDN2	claudin 2
COL6A3	collagen, type VI, alpha 3
COL13A1	collagen, type XIII, alpha 1
COL20A1	collagen, type XX, alpha 1
COL27A1	collagen, type XXVII, alpha 1

CNTN3	contactin 3 (plasmacytoma associated)
CNTNAP1	contactin associated protein 1
CNTNAP2	contactin associated protein-like 2
CYR61	cysteine-rich, angiogenic inducer, 61
DPT	dermatopontin
DAB1	disabled homolog 1 (Drosophila)
EDA	ectodysplasin A
EMILIN1	elastin microfibril interfacer 1
ESAM	endothelial cell adhesion molecule
EFNB1	ephrin-B1
FBLN7	fibulin 7
FPR2	formyl peptide receptor 2
HES1	hairy and enhancer of split 1, (Drosophila)
HAS1	hyaluronan synthase 1
ITGA2B	integrin, alpha 2b (platelet glycoprotein IIb of IIb/IIIa complex, antigen CD41)
ITGA5	integrin, alpha 5 (fibronectin receptor, alpha polypeptide)
ITGA8	integrin, alpha 8
ITGAX	integrin, alpha X (complement component 3 receptor 4 subunit)
ITGB2	integrin, beta 2 (complement component 3 receptor 3 and 4 subunit)
IL32	interleukin 32
LAMA1	laminin, alpha 1
LAMA2	laminin, alpha 2
LSAMP	limbic system-associated membrane protein
MCAM	melanoma cell adhesion molecule
MTSS1	metastasis suppressor 1
MAG	myelin associated glycoprotein
MYH9	myosin, heavy chain 9, non-muscle
NPHP4	nephronophthisis 4
NRXN1	neurexin 1
NFASC	neurofascin homolog (chicken)
NLGN2	neuroligin 2
NLGN4Y	neuroligin 4, Y-linked
NRP2	neuropilin 2
NTM	neurotrimin
OPCML	opioid binding protein/cell adhesion molecule-like
PARVG	parvin, gamma
PVRL2	poliovirus receptor-related 2 (herpesvirus entry mediator B)
PKD1	polycystic kidney disease 1 (autosomal dominant)
PSTPIP1	proline-serine-threonine phosphatase interacting protein 1
PTPRF	protein tyrosine phosphatase, receptor type, F
PCDH11X	protocadherin 11 X-linked
PCDH12	protocadherin 12
PCDHB15	protocadherin beta 15
PCDHGA11	protocadherin gamma subfamily A, 11
PCDHGA5	protocadherin gamma subfamily A, 5

PCDHGA6	protocadherin gamma subfamily A, 6
PCDHGA7	protocadherin gamma subfamily A, 7
PCDHGA8	protocadherin gamma subfamily A, 8
PCDHGB2	protocadherin gamma subfamily B, 2
PCDHGB3	protocadherin gamma subfamily B, 3
PCDHGB4	protocadherin gamma subfamily B, 4
PCDHGB6	protocadherin gamma subfamily B, 6
PCDHGC5, PCDHGC3	protocadherin gamma subfamily C, 5
ROR2	receptor tyrosine kinase-like orphan receptor 2
RELN	reelin
ROM1	retinal outer segment membrane protein 1
RS1	retinoschisin 1
SCARF2	scavenger receptor class F, member 2
SELP	selectin P (granule membrane protein 140kDa, antigen CD62)
MLLT4	similar to Afadin (Protein AF-6); myeloid/lymphoid or mixed-lineage leukemia (trithorax homolog, Drosophila); translocated to, 4
SORBS3	sorbin and SH3 domain containing 3
SPACA4	sperm acrosome associated 4
SNED1	sushi, nidogen and EGF-like domains 1
THBS4	thrombospondin 4
TGFB1I1	transforming growth factor beta 1 induced transcript 1
TNF	tumor necrosis factor (TNF superfamily, member 2)
ZYX	zyxin

Table 19. Differentially expressed genes involved in actin cytoskeleton organization in hCPCs compared to hCFs and hFFs.

Gene symbol	Gene Name
CDC42BPG	CDC42 binding protein kinase gamma (DMPK-like)
CDC42EP2	CDC42 effector protein (Rho GTPase binding) 2
EHD2	EH-domain containing 2
NCK2	NCK adaptor protein 2
NUAK2	NUAK family, SNF1-like kinase, 2
PDLIM7	PDZ and LIM domain 7 (enigma)
ARHGAP26	Rho GTPase activating protein 26
ARHGEF2	Rho/Rac guanine nucleotide exchange factor (GEF) 2
WIPF1	WAS/WASL interacting protein family, member 1
ACTC1	actin, alpha, cardiac muscle 1
ACTN4	actinin, alpha 4
ALDOA	aldolase A, fructose-bisphosphate
CXCL1	chemokine (C-X-C motif) ligand 1 (melanoma growth stimulating activity, alpha)
DAAM2	dishevelled associated activator of morphogenesis 2
DBN1	drebrin 1
EPB41	erythrocyte membrane protein band 4.1 (elliptocytosis 1, RH-linked)

EPB41L3	erythrocyte membrane protein band 4.1-like 3
FSCN1	fascin homolog 1, actin-bundling protein (Strongylocentrotus purpuratus)
FLNA	filamin A, alpha (actin binding protein 280)
FLNB	filamin B, beta (actin binding protein 278)
FOXJ1	forkhead box J1
FMNL3	formin-like 3
GHRL	ghrelin/obestatin prepropeptide
GHSR	growth hormone secretagogue receptor
INF2	inverted formin, FH2 and WH2 domain containing
MTSS1	metastasis suppressor 1
MYO9B	myosin IXB
MYH6	myosin, heavy chain 6, cardiac muscle, alpha
MYH9	myosin, heavy chain 9, non-muscle
NPHP4	nephronophthisis 4
PLEK2	pleckstrin 2
RHOF	ras homolog gene family, member F (in filopodia)
RAC2	ras-related C3 botulinum toxin substrate 2 (rho family, small GTP binding protein Rac2)
SPTBN5	spectrin, beta, non-erythrocytic 5
TLN1	talin 1
TMSB10	thymosin beta 10
VASP	vasodilator-stimulated phosphoprotein
XIRP1	xin actin-binding repeat containing 1

Table 20. Differentially expressed extracellular region genes in hCPCs compared to hCFs and hFFs.

Gene symbol	Gene Name
AGPAT1	1-acylglycerol-3-phosphate O-acyltransferase 1 (lysophosphatidic acid acyltransferase, alpha)
ADAMTS3	ADAM metallopeptidase with thrombospondin type 1 motif, 3
ADAMTSL4	ADAMTS-like 4
ADAMTSL5	ADAMTS-like 5
C1QTNF2	C1q and tumor necrosis factor related protein 2
CD248	CD248 molecule, endosialin
CMTM4	CKLF-like MARVEL transmembrane domain containing 4
CMTM7	CKLF-like MARVEL transmembrane domain containing 7
TIMP1	TIMP metallopeptidase inhibitor 1
ACHE	acetylcholinesterase (Yt blood group)
AHSG	alpha-2-HS-glycoprotein
ANGPTL2	angiopoietin-like 2
ANGPTL3	angiopoietin-like 3
APOB	apolipoprotein B (including Ag(x) antigen)
APOC1	apolipoprotein C-I
BMP5	bone morphogenetic protein 5
BCAN	brevican
CDH13	cadherin 13, H-cadherin (heart)

CPB2	carboxypeptidase B2 (plasma)
CP	ceruloplasmin (ferroxidase)
CCL2	chemokine (C-C motif) ligand 2
CCL7	chemokine (C-C motif) ligand 7
CXCL5	chemokine (C-X-C motif) ligand 5
COL6A6	collagen type VI alpha 6
COL4A6	collagen, type IV, alpha 6
COL9A2	collagen, type IX, alpha 2
COL9A3	collagen, type IX, alpha 3
COL7A1	collagen, type VII, alpha 1
COL8A2	collagen, type VIII, alpha 2
COL14A1	collagen, type XIV, alpha 1
CSF2	colony stimulating factor 2 (granulocyte-macrophage)
CFD	complement factor D (adipsin)
CFI	complement factor I
CRISPLD2	cysteine-rich secretory protein LCCL domain containing 2
CRLF1	cytokine receptor-like factor 1
ELN	elastin
EMILIN3	elastin microfibril interfacer 3
EDN1	endothelin 1
ECM1	extracellular matrix protein 1
ECM2	extracellular matrix protein 2, female organ and adipocyte specific
FBN2	fibrillin 2
FGB	fibrinogen beta chain
FJX1	four jointed box 1 (Drosophila)
GSN	gelsolin (amyloidosis, Finnish type)
GPC1	glypican 1
GRN	granulin
GREM1	gremlin 1, cysteine knot superfamily, homolog (Xenopus laevis)
GDF7	growth differentiation factor 7
HAPLN3	hyaluronan and proteoglycan link protein 3
IGFBP1	insulin-like growth factor binding protein 1
IGFBP5	insulin-like growth factor binding protein 5
IBSP	integrin-binding sialoprotein
ICAM1	intercellular adhesion molecule 1
IL24	interleukin 24
IL33	interleukin 33
IL4	interleukin 4
LAMA4	laminin, alpha 4
LAMB3	laminin, beta 3
LEFTY1	left-right determination factor 1
LIF	leukemia inhibitory factor (cholinergic differentiation factor)
LOX	lysyl oxidase
LOXL4	lysyl oxidase-like 4
MGP	matrix Gla protein

MMP16	matrix metallopeptidase 16 (membrane-inserted)
METRN	meteorin, glial cell differentiation regulator
NPPB	natriuretic peptide precursor B
NENF	neuron derived neurotrophic factor
OSTN	osteocrin
OGN	osteoglycin
PDGFC	platelet derived growth factor C
PTN	pleiotrophin
PMCH	pro-melanin-concentrating hormone
PCSK5	proprotein convertase subtilisin/kexin type 5
PCSK6	proprotein convertase subtilisin/kexin type 6
PRSS36	protease, serine, 36
SELE	selectin E
SEMA3F	sema domain, immunoglobulin domain (Ig), short basic domain, secreted, (semaphorin) 3F
SERPINA1	serpin peptidase inhibitor, clade A (alpha-1 antiproteinase, antitrypsin), member 1
SPOCK3	sparc/osteonectin, cwcv and kazal-like domains proteoglycan (testican) 3
SFTPB	surfactant protein B
TNXB	tenascin XB; tenascin XA pseudogene
THSD4	thrombospondin, type I, domain containing 4
TGFB2	transforming growth factor, beta 2
TNFAIP2	tumor necrosis factor, alpha-induced protein 2
ERBB3	v-erb-b2 erythroblastic leukemia viral oncogene homolog 3 (avian)
VCAM1	vascular cell adhesion molecule 1
VEGFC	vascular endothelial growth factor C
VIT	vitrin
VTN	vitronectin
WNT16	wingless-type MMTV integration site family, member 16
WNT5A	wingless-type MMTV integration site family, member 5A
WNT7A	wingless-type MMTV integration site family, member 7A
WNT9A	wingless-type MMTV integration site family, member 9A
ZP3	zona pellucida glycoprotein 3 (sperm receptor)

A6. Growth factors and cytokines differentially expressed in hCPCs and hFFs

Table 21. hCPC specific up-regulated growth factors and cytokines compared to hFFs.

Gene symbol	Gene name
FGF1	Fibroblast Growth Factor 1 (Acidic)
IL15	Interleukin 15
PDGFA	Platelet-Derived Growth Factor Alpha Polypeptide
TYMP	Thymidine Phosphorylase
TNFSF9	Tumor Necrosis Factor (Ligand) Superfamily, Member 9
TGFB3	Transforming Growth Factor, Beta 3
ANGPT2	Angiopoietin 2
CFP	Complement Factor Properdin
IL17B	Interleukin 17B
TNFSF10	Tumor Necrosis Factor (Ligand) Superfamily, Member 10
IL13	Interleukin 13
TNF	Tumor Necrosis Factor
FGF8	Fibroblast Growth Factor 8 (Androgen-Induced)
IFNA8	Interferon, Alpha 8
BMP8A	Bone Morphogenetic Protein 8a
LHB	Luteinizing Hormone Beta Polypeptide
FGF16	Fibroblast Growth Factor 16
IL18BP	Interleukin 18 Binding Protein
CFHR3	Complement Factor H-Related 3
IL16	Interleukin 16
IL18	Interleukin 18
PDGFB	Platelet-Derived Growth Factor Beta Polypeptide
TNFSF8	Tumor Necrosis Factor (Ligand) Superfamily, Member 8
ERAP1	Endoplasmic Reticulum Aminopeptidase 1
MDK	Midkine (Neurite Growth-Promoting Factor 2)
IL32	Interleukin 32
GDNF	Glial Cell Derived Neurotrophic Factor
PGF	Placental Growth Factor
HBEGF	Heparin-Binding EGF-Like Growth Factor
BMP1	Bone Morphogenetic Protein 1
CXCL3	Chemokine (C-X-C Motif) Ligand 3
JAG1	Jagged 1
TGFB1	Transforming Growth Factor, Beta 1
IL1A	Interleukin 1, Alpha
CFH	Complement Factor H
IL1B	Interleukin 1, Beta
CXCL12	Chemokine (C-X-C Motif) Ligand 12
VEGFA	Vascular Endothelial Growth Factor A
IL6	Interleukin 6
CXCL8	Chemokine (C-X-C Motif) Ligand 8
CXCL1	Chemokine (C-X-C Motif) Ligand 1 (Melanoma Growth Stimulating Activity, Alpha)

Table 22. hFF specific up-regulated growth factors and cytokines compared to hCPCs.

Gene symbol	Gene name
FGF13	Fibroblast Growth Factor 13
IGF1	Insulin-Like Growth Factor 1 (Somatomedin C)
CCL4	Chemokine (C-C Motif) Ligand 4
CCL3L3	Chemokine (C-C Motif) Ligand 3-Like 3
IL19	Interleukin 19
NRG2	Neuregulin 2
FIGF	C-Fos Induced Growth Factor (Vascular Endothelial Growth Factor D)
GRP	Gastrin-Releasing Peptide
CRH	Corticotropin Releasing Hormone
EGF	Epidermal Growth Factor
CXCL11	Chemokine (C-X-C Motif) Ligand 11
TGFA	Transforming Growth Factor, Alpha
CYTL1	Cytokine-Like 1
CCL28	Chemokine (C-C Motif) Ligand 28
TNFSF18	umor Necrosis Factor (Ligand) Superfamily, Member 18
CXCL14	Chemokine (C-X-C Motif) Ligand 14
CCL3	Chemokine (C-C Motif) Ligand 3
PDGFD	Platelet Derived Growth Factor D
IL34	Interleukin 34
CSF2	Colony Stimulating Factor 2 (Granulocyte-Macrophage)
CXCL10	Chemokine (C-X-C Motif) Ligand 10
BMP2	Bone Morphogenetic Protein 2
HGF	Hepatocyte Growth Factor (Hepapoietin A; Scatter Factor)
SPP1	Secreted Phosphoprotein 1
NTF3	Neurotrophin 3
TM7SF2	Transmembrane 7 Superfamily Member 2
KITLG	KIT Ligand
EREG	Epiregulin
BDNF	Brain-Derived Neurotrophic Factor
ANGPT1	Angiopoietin 1
VEGFC	Vascular Endothelial Growth Factor C
CCL2	Chemokine (C-C Motif) Ligand 2
GDF15	Growth Differentiation Factor 15
CSF1	Colony Stimulating Factor 1 (Macrophage)
FGF2	Fibroblast Growth Factor 2 (Basic)
GRN	Granulin